Bi-polar Bi-directional DC-DC Converter Topologies for Renewable Energy Applications

Submitted in partial fulfilment of requirement
for the award of the degree of

Doctor of Philosophy

By

Patil Mounica

(Roll No: 717010)

Under the supervision of
Dr. S. Srinivasa Rao
Professor

DEPARTMENT OF ELECTRICAL ENGINEERING
NATIONAL INSTITUTE OF TECHNOLOGY
(An Institution of National Importance, Ministry of Education, Govt. of India)
Warangal-506 004, India
November–2021

Approval Sheet

This Thesis entitled "**Bi-polar Bi-directional DC-DC Converter Topologies for Renewable Energy Applications**" by **Patil Mounica, Roll No: 717010** is approved for the degree of Doctor of Philosophy

Examiners

_____

_____

Supervisor

Dr. S. Srinivasa Rao
Professor

Chairman

Dr. D M Vinod Kumar
Professor
Department of Electrical Engineering
NIT Warangal

Date: _____

DEPARTMENT OF ELECTRICAL ENGINEERING
NATIONAL INSTITUTE OF TECHNOLOGY
(An Institution of National Importance, Ministry of Education, Govt. of India)
Warangal – 506 004, India

Certificate

This is to certify that the thesis entitled **"Bi-polar Bi-directional DC-DC Converter Topologies for Renewable Energy Applications**", submitted by Ms. **Patil Mounica,** Roll No: **717010**, to the Department of Electrical Engineering, National Institute of Technology, Warangal in partial fulfilment of the requirements for the award of the degree of **Doctor of Philosophy** in Electrical Engineering is a record of bonafide research work carried out by her under my supervision and guidance. The contents of this thesis, in full or in parts have not been submitted simultaneously to any other institute or university for the award of any degree or diploma.

Station :
Date :

Dr. S. Srinivasa Rao
(Thesis Supervisor)
Professor
Department of Electrical Engineering
National Institute of Technology
Warangal – 506004

Declaration

This is to certify that the work presented in the thesis entitled "**Bi-polar Bi-directional DC-DC Converter Topologies for Renewable Energy Applications"** is a bonafide work done by me under the supervision of **Dr. S. Srinivasa Rao, Professor**, Department of Electrical Engineering, National Institute of Technology, Warangal, India and was not submitted elsewhere for the award of any degree.

I declare that this written submission represents my ideas in my own words and where others ideas or words have been included, I have adequately cited and referenced the original sources. I also declare that I have adhered to all principles of academic honesty and integrity and have not misrepresented or fabricated or falsified any idea/data/fact/source in my submission. I understand that any violation of the above will be a cause for disciplinary action by the institute and can also evoke penal action from the sources which have thus not been properly cited or from whom proper permission has not been taken when needed.

Patil Mounica
(Roll No: 717010)

Date:
Place: NIT Warangal

Acknowledgements

First and foremost, I would like to express my deep sense of gratitude to my thesis supervisor **Dr. S. Srinivasa Rao**, Professor in the Department of Electrical Engineering for his continuous monitoring, moral support, patience, encouragement and timely inputs throughout my research work. His commitment towards research work is always been a source of inspiration for rest of my life.

I would like to extend gratitude to my Doctoral Scrutiny Committee: Chairman **Dr. D. M. Vinod Kumar**, Professor, Department of Electrical Engineering and members **Dr. Bhagwan K Murthy**, Professor, Department of Electrical Engineering, **Dr. B. L. Narasimharaju**, Associate Professor, Department of Electrical Engineering and **Dr. S Ravi Chandra**, Associate Professor, Department of Computer Science & Engineering for their continuous monitoring, keen interest, insightful comments and encouragement.

My Sincere thanks to **Prof. N V Ramana Rao**, Director NIT Warangal for providing all the necessary facilities to carry out this research work.

I thank all the faculty members in the Department of Electrical Engineering for their support, encouragement and valuable suggestions during various stages of my work. I thank all the supporting staff in the Department of Electrical Engineering for their help, support and co-operation during my research work in the laboratory.

I thank my fellow scholar **Mr. Y. Bhaskar S S Gupta** for his constant support throughout this work and also I would like to thank all other fellow scholars especially, **Mr. Satish Reddy D, Mr. Ramesh D** and **Mr. S Madhu Babu** from Department of Electrical Engineering who are always ready to share their ideas and extend their support in tough times. I would like to thank all the members who are directly or indirectly involved and supported me in successful completion of this work.

Last but not the least, I would like to thank my parents, **P Himavantha Reddy** and **Anasuya**, my sister **Nikhita** and brother in-law **Abhinay** and my husband **Ch Rajeshwar Reddy** and sister in-law **N.P. Lakshmi** for their understanding, support and patience which are helped me in the successful completion of work.

Patil Mounica

List of Figures

List of Tables

List of Abbreviations

AC	Alternating Current
DC	Direct Current
PV	Photo Voltaic
IGBT	Insulated Gate Bipolar Transistor
GTO	Gate Turn-off Thyristor
NPC	Neutral Point-Clamped
EMI	Electromagnetic Interference
ZVS	Zero Voltage Switching
ZCS	Zero Current Switching
ZCT	Zero Current Transition
BDC	Bidirectional DC Converter
ACC	Active Clamp Circuits
VDR	Voltage Doubler Rectifier
MOSFET	Metal-Oxide Semiconductor Field Effect Transistors
CCM	Continuous Conduction Mode
PWM	Pulse Width Modulation
PPS	Pulse Width Phase Shift
DCSR	Direct Current Slew Rate
DAB	Double Active Bridge
PI	Proportional Integral

Abstract

In most renewable energy systems, energy storage is a concern for self-sufficiency and flexibility in energy management. It improves the electricity quality and reliability by storing extra energy during off-peak periods and releasing this energy whenever required. These energy storage system are required to responds as per the demand to ensure smooth operation during peak load time and outage. Therefore it is necessary to install a bidirectional converter between the energy storage system and point of common connection to the grid. To interact with a grid, this bidirectional converter must meet numerous characteristics, including bidirectional power flow capabilities, high efficiency, and high quality power conversion. Bi - directional DC-DC converters are primarily categorised into two types: isolated converters and non-isolated converters. Isolated converters, such as phase shifted full bridge converters, are popular because they may accomplish gentle switching over a large load range by using the transformer's leakage inductance. They do, however, have downsides such as large circulation currents, high voltage stress across the output diodes, and low efficiency when the output voltage is high. Non-isolated DC-DC converters achieve high voltage gain, reduced size, weight and volume due to absence of a high frequency transformer. Because of its simple layout, the basic buck–boost converter is suited for low power levels. However, the voltage gain of a typical buck–boost converter is limited and suffers from difficulties such as excessive reverse recovery, conduction losses, and high voltage stress on semiconductor components. To address these restrictions, many non-isolated bidirectional DC-DC converter (BDC) topologies have been developed, including cascaded BDC, coupled-inductor-based BDC, switched-capacitor-based BDC, interleaved BDC, and multilayer modular BDC.

When two or more conventional buck–boost converters are cascaded, a wide conversion ratio is attained while current ripple is minimised. However, because there are more power devices, diodes, inductors, and capacitors that do not have voltage stress reduction, its robustness suffers, limiting its application at high voltage. Coupled-inductor-based BDCs can deliver high output voltage while maintaining a low duty cycle and reducing voltage stress across the switches. Furthermore, the primary switch and output diodes may work with zero-current switching (ZCS). In general, the output diode in linked inductor converters faces significant challenges like voltage stress and leakage inductance, which causes high-voltage surges on the primary side during turn-off. As a result, coupling

inductor topologies are inappropriate for high-power applications. The switched-capacitor converter is more efficient and has a larger boost/buck ratio; nevertheless, it requires huge number of switches. Furthermore, high-current pulses arise as a result of capacitors with varying voltages being linked in parallel at each switching moment. This may limit the power output available for switched-capacitor converter applications. Interleaved BDCs operated in discontinuous current mode (DCM) are often utilised in high-power applications and to further reduce the converter's input current ripple. Furthermore, because the inductor current grows from zero, switching in every cycle can automatically achieve ZCS turn-on conditions. The presence of an additional transformer to obtain high voltage gain is the primary disadvantage of this converter. Modular multilevel BDCs are designed to fulfil the demands of high power, high voltage, and various input/output applications. The fundamental drawback of these configurations is the power device's hard-switching and the absence of power control strategy in many network connection scenarios. The switching loss increases with the number of modules, reducing its performance in high-power applications significantly.

In this research work four bipolar bidirectional DC-DC converter topologies are proposed for battery energy storage system for regulating the power flow for both low power and high power applications to achieve the high voltage gain along with reduced voltage stress, inherent voltage balance at the bipolar DC micro grid, low switching losses resulting in high efficiency. A soft switching technique with series connection of modular bidirectional DC converters, interleaved switched capacitor technique, half bridge converter with L-C resonant technique and coupled inductor and switched capacitor technique are implemented for achieving high voltage gain along with reduced voltage stress and reduced current ripple. Detailed mathematical analysis, modelling and simulation results are presented for all the proposed topologies for various operating conditions. To validate the proposed topologies, experiments are performed on the lab-scale prototype for all feasible operating conditions, and results are obtained for the converters with different load variations. Based on the analysis of both simulations and experimental results, it is observed that the proposed bipolar bidirectional DC-DC converter topologies accomplish a decrease in input and output current ripple and capacitor voltage ripple, reduction in voltage stress across the switching device, offer high voltage gain along with the DC-link voltage balance. Detailed analysis of the proposed converter topologies with the simulations and experimental results are presented in various chapters of the thesis.

Keyword: Bidirectional DC-DC converter, bipolar DC micro-grid, soft switching, switched capacitor, coupled inductors, energy storage system

CONTENTS

Chapter-1
Introduction

1.1. Introduction

Renewable energy has a huge potential scope to grow over a few decades due to advancements in the fabrication of solar panels, semiconductor technology, digital signal processing techniques and policies. The primary reason is the availability of renewable energy sources over a wide geographical area where as fossil fuel is limitedly available in few countries. The dramatic growth in the renewable energy share is expected by 2030 to ensure energy security. The growth in the renewable sector will eventually reduce air pollution and the premature mortality from the intoxication of the high carbon dioxide concentration [1]. Out of the various renewable energy sources, the solar photovoltaic energy systems are growing rapidly throughout the world. The installed capacity has reached 600 GW in 2020 [2]. With the massive improvement in materials used for development of solar cells and fabrication technologies, the cost of photovoltaic panels is reducing day by day. It is expected that, in every five years, the installed capacity will be double the prior. [3] At present, 2% of the total load demand in the world is supplied from solar energy [4]. Furthermore, cars driven by internal combustion engines have very low fuel economy, and the burning of hydrocarbon fuels in these vehicles emits a large amount of poisonous gas. Aside from the energy and heat producing industries, the large number of cars utilized in and across the world in the transportation sector is a main cause of air pollution [5].

To address this issue many countries have set targets to reduce the production and sale of petroleum fueled vehicles by incorporating electric vehicles. As a result the need for establishment of solar charging stations is growing. To ensure reliable electrical energy in the solar photovoltaic electrical energy generating stations with energy storage systems in the area of AC and DC micro-grids and electric vehicle charging stations, the need for effective and efficient energy management is required. To address this issue a bidirectional DC-DC converters at the battery energy storage system play a crucial role in unipolar DC grids and bipolar bidirectional DC-DC converters in bipolar DC micro-grids. Further the design of high voltage high power DC micro-grid systems require an appropriate DC-DC converters. The power semiconductor devices have some limitations with respect to voltage rating, control techniques and converter topologies and components required for fabrication of these bipolar bidirectional DC-DC Converters. The various issues related to these are explained in detail in this chapter.

Due to the constraint of semiconductor device voltage rating, switching frequency, and affordability multilevel converters were being frequently employed in high-voltage, high-power photovoltaic systems. Multilevel inverters reduces harmonic distortion, require a smaller output filter with higher power density. Another significant benefit seems to be voltage stress on the switches is minimized, allowing a high-voltage, high-power converter to be fabricated using lower voltage rating semiconductor components. Fig 1.1 depicts a typical bipolar power conversion system with renewable energy applications, which includes two-stage AC-DC and DC-DC converters linked by a high voltage DC-link [6].

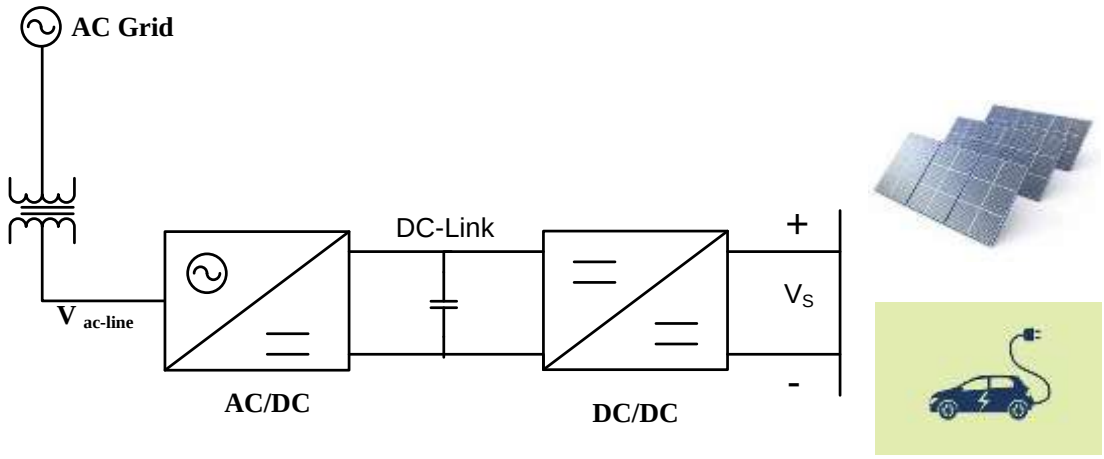

Fig. 1.1 Electrical power system using two stages and renewable energy systems [6]

Fig 1.2 depicts the state-of-the-art high power semiconductor device ratings. A single IGBT module can only take a few kilo volts of power. Other higher voltage rating devices, such as GTO, have the voltage and current ratings of up to 12kV and 1500A respectively. However their operating frequency is limited to 500 Hz. To achieve larger voltage requirements, the power semiconductor devices can be connected in series however the voltage unbalance issue arise between the devices due to parameter mismatches. As a consequence, it is difficult to meet the high-voltage, high-power density criterion [7]. The concept of bipolar converter topology with neutral point-clamped (NPC) three-level inverter was proposed by Nabae in [8]. Reduced voltage stress on switches, lower EMI, and less harmonic distortion are all advantages of this bipolar converter. A three-level NPC leg in DC-DC converters with galvanic isolation in their DC-DC converter applications using NPC architecture was proposed by Pinheiro and Barbi in [9].

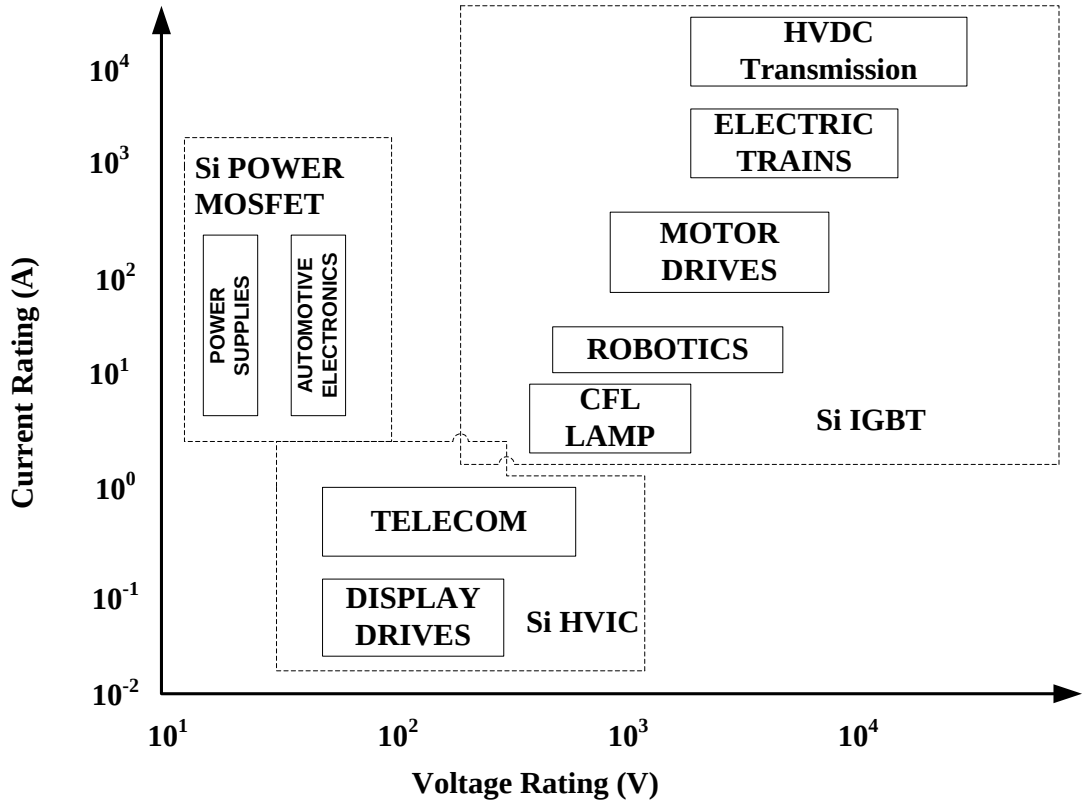

Fig 1.2 High voltage device rating at the cutting edge of technology [7]

A bidirectional flying capacitor converter to manage the charge and discharge current in a hybrid fuel cell power system was proposed by Ruan in [10], Utilization of bipolar boost converters for high power and high voltage applications, as well as the use of bipolar bidirectional DC-DC converters in renewable energy systems with bidirectional power flow was proposed in [11], [12]. A generalized bipolar converter topology is presented which can independently balance each DC voltage level without the additional circuits are proposed in [13]. A systematic technique for deriving a series of six non-isolated three-level DC/DC converters from typical buck and boost converters such as buck, boost, buck-boost, Cuk, SEPIC, and zeta was proposed by Ruan in [14].

Fig 1.3 shows a conventional DC micro-grid structure consists of a distributed generating unit, a battery storage unit, a load cell, and a grid-connected converter [15]. DC micro-grid technology focuses on ensuring the system's power balance by stabilizing the DC bus voltage. Incorporating energy storage technologies can enhance the device's voltage sag and the inrush current difficulties caused by load-switching, fluctuations in natural circumstances, and instantaneous failures in DC micro-grid systems, improving the

dependability and scheduling flexibility of the distributed generation grid link. Due to technical lag, packet delay, low bandwidth communication control lowers the system's long-distance reliability and DC micro-grid distribution. To mitigate the danger of high transmission control, each unit is separated into three control layers based on the normalized voltage of the DC bus and synchronized integration of individual units [16]. When compared to a uni-polar converter, the bi-polar converter has only half of the switches changes their state in every cycle, and the voltage stress on the switch is half of the bus voltage [17], [18].

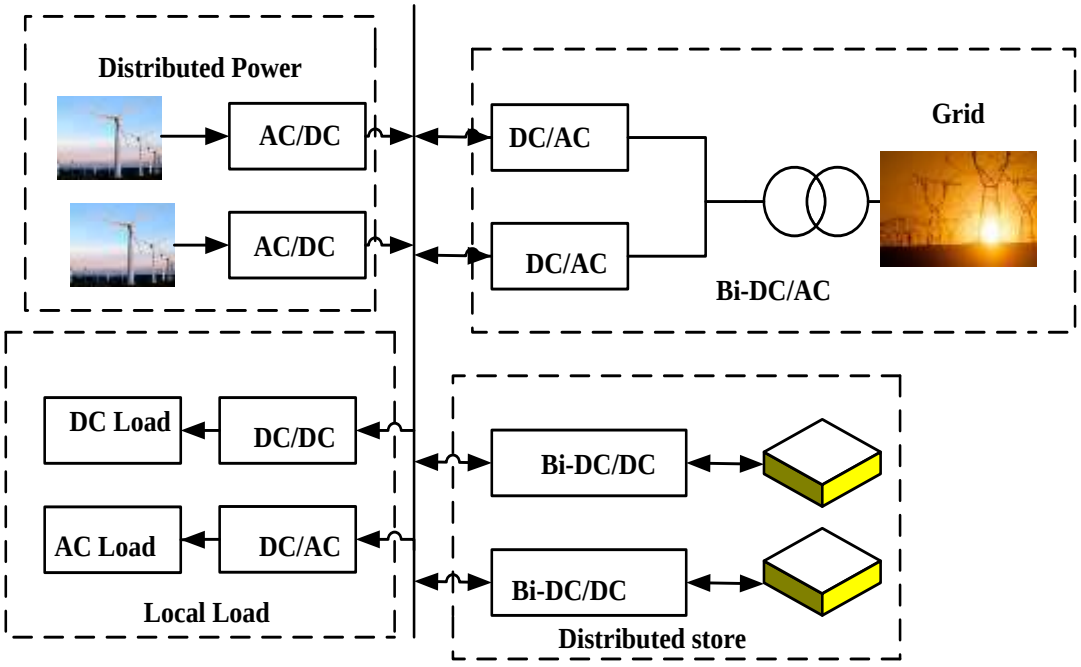

Fig 1.3 A conventional DC micro-grid structure [15]

Bi-DC/DC- Bidirectional DC-DC Converter

In bidirectional DC-DC converter plays a major role in the DC micro-grid system with battery energy storage. Many applications, necessitates a high-voltage and high-power bidirectional DC-DC converter. The standard uni-polar bidirectional DC-DC converter architecture, is not appropriate for high-voltage and high-power applications. Therefore a bi-polar topology with simple configuration, high efficiency, stability offer a modular structure. The isolated [19] – [22] and non-isolated [23] – [25] bi-polar bidirectional DC-DC converter configurations are most commonly used in DC micro-grids. When employing input parallel, output parallel (IPOP) configurations require a modular bidirectional DC/DC converters at battery end. However these configurations suffer with current sharing problems across the units. The voltage equalization concern must be resolved when using input series, output series (ISOS) configuration. Whereas while using input parallel, output series (IPOS)

or input series output parallel (ISOP), both current sharing and voltage equalization concerns play a crucial role [26], [27].

In order to control the DC bus voltage and also transfer of energy, converter at storage system need to be switched ON and OFF at regular intervals, which may exceed the maximum permitted number of charge-discharge cycles and cause reduction in service life. To achieve a lower voltage variation and power variation in the DC micro-grid and to supply low cost electric energy for a large grid, it is required to measure and assess the optimum solution through voltage fluctuation level assessment [28] - [31].

1.2. Literature Review

Several researchers have proposed various bidirectional DC-DC converters for energy storage systems for effective and efficient energy flow between grid and energy storage system by addressing various issues. To decrease stress on power devices with varying component counts, the converters operate at different power levels and employ different switching techniques. Detailed literature review on the various power electronic converter topologies is given below.

Bidirectional DC-DC converters

Because the operation of a renewable energy system fluctuates due to fluctuations in temperature, a bidirectional dc to dc converter is used as a vital component for linking storage devices between a renewable energy system's source and load for continuous power flow. A vast majority of bidirectional DC-DC converters (BDC) on the market are either current or voltage fed [32]. BDCs are classified as buck or boost depending on the location of an auxiliary battery storage. Battery technology is located on the high voltage side in the buck type and on the low voltage side in the boost type. Various DC-DC converters are being used to modify the input voltage depending on the desired application. In general, there are 2 kinds of BDCs: non-isolated and isolated. The boost kind and buck kind DC-DC converters are frequently used in transformer-less non-isolated energy conversion systems. To provide isolation between the source and the load side, a high frequency transformer-based system is a viable option. When an extremely high step-up or step-down ratio is desired, isolation is necessary. However, the non-isolated kind is far more appealing in terms

of efficiency, size, weight, and cost. As a result, in high-power or spaceship power system applications where weight and compactness are critical, the transformer-less variant is desirable.

1.2.1 Isolated Bidirectional DC-DC Converters

In low voltage and significantly higher current applications, such as solar, fuel cell, or battery energy storage systems, galvanically isolated DC–DC converters with a current-fed (CF) port are a formidable rival to traditional voltage-fed (VF) converters [33]-[36]. The constant input current of CF converters allows for more efficient functioning of such systems [37]-[39]. Furthermore, the intrinsic boost capability provides for reduced isolation transformer design requirements [40] and greater voltage regulation capability [41]. Other benefits include decreased RMS current stress in the switches and readily achieved high part load efficiency [42]-[44]. Although VF DC–DC converters have received significant attention in research and industrial applications over the last few decades, further enhancements and soft switching capabilities for CF converters are still being pursued [45],[46]. Clamping is required in galvanically isolated CF topologies to prevent voltage overrun throughout the switching devices. Many soft-switching CF-based DC–DC converters employ passive clamping devices or diodes in series with switching devices [47], resulting in considerable losses in situations with relatively large input currents.

Active clamp circuits (ACC) for full-bridge converters were presented in [48], along with shifting controllers; symmetrical control techniques have been proposed in [49]. The ACC is used to produce zero voltage switching (ZVS) conditions for primary transistor switches, as well as to alleviate the problem of voltage overshoot. In [50], a half-bridge function as a voltage doubler rectifier (VDR) circuit was suggested for significant step-up applications. The bidirectional full-bridge version, described in [51], employs the ACC and phase shift control, and achieves excellent peak efficiency in both directions of power flow.

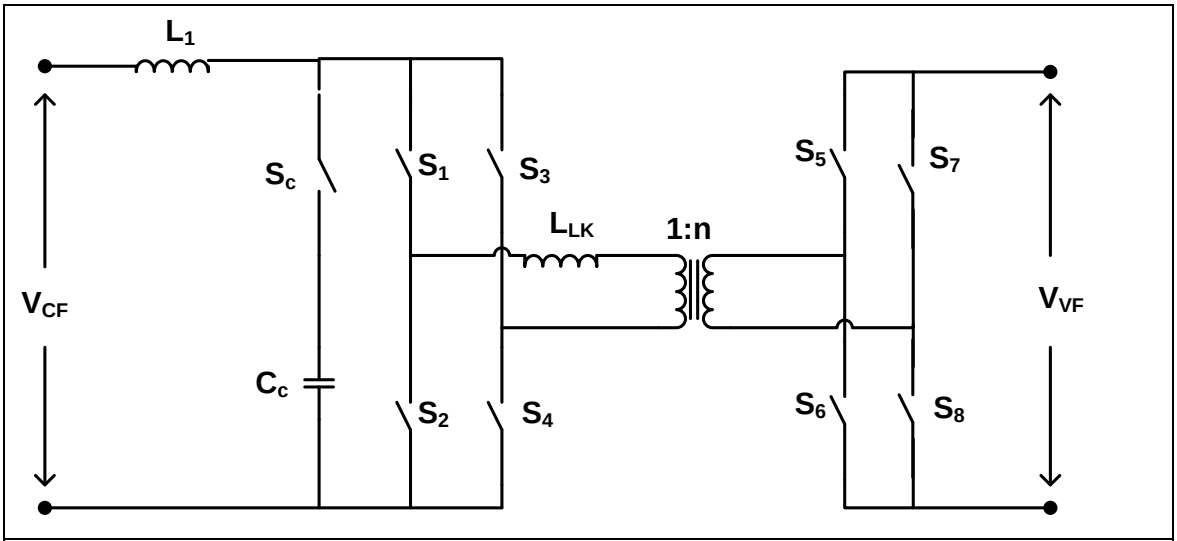

Fig.1.4.Conventional full-bridge bidirectional DC–DC converter. [48]

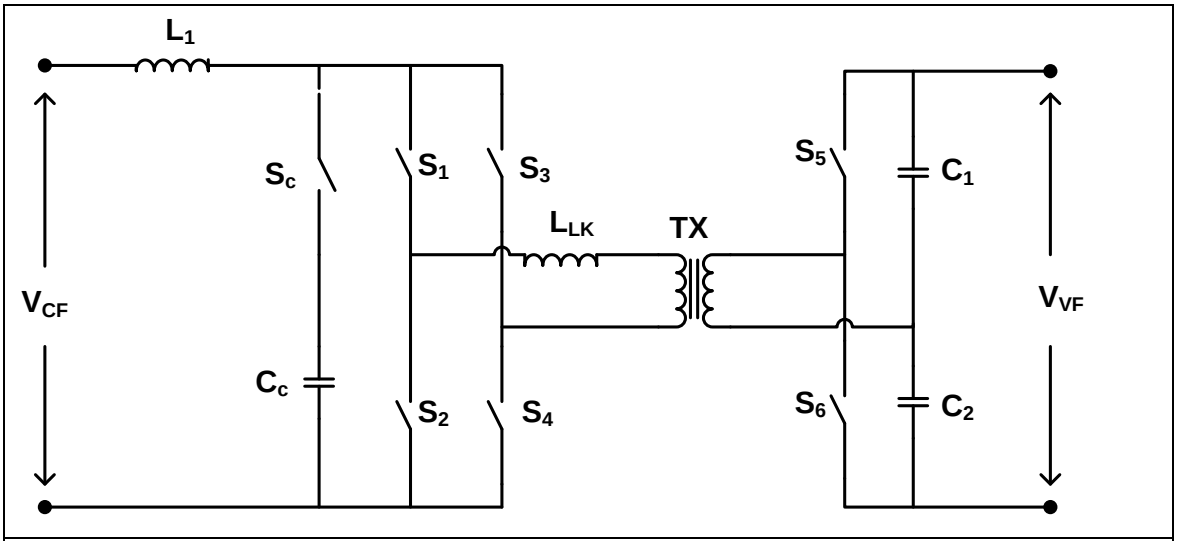

Fig.1.5.Bidirectional DC-DC converter topology: with an active clamp circuit [52]

In [52] introduces a bidirectional design with a half-bridge voltage source component. Because it cannot use the same phase-shift approach, it is recommended as hard-switched while working in buck mode. To solve the problem, partly soft switching employing duty cycle shift (DCS) control [53] in conjunction with synchronous rectification (SR) might be used. The ACC, on the other hand, enables the maximum current via the CF-side switching devices and a transformer to be greater than the input current, resulting in higher conduction losses [54]. Various approaches have been taken to solve this issue, though at the expense of increasing component count and complication [55],[56].

In [57], an unique snubber-less intermediate modulation-based (SMB) control strategy for the half-bridge CF converter was invented, which has been mainly added to a family of bidirectional converters [58] based on operating clamping by secondary side active switches, allowing ZVS of all switches to be achieved without extra clamping circuits. In [59], this method was used to a converter with a half-bridge on the voltage source side. To successfully regulate the topologies, the transformer's leakage inductance must be carefully structured (possibly by an external inductor). Furthermore, the topology switches have very large peak currents, particularly during load variation operations. In [60] describes a version of this approach that is based on the resonance effect between both the leakage inductance and the MOSFET's drain-to-source capacitance. The approach has been used effectively to several bidirectional converters [61]. The primary challenges are related to constituent parameter incompatibility, non-linearity for practical components, substantial oscillations, and the requirement for variable frequency management.

1.2.2 Non-Isolated Bidirectional DC-DC Converters

The non-isolated half-bridge BDC topology consists of a boost converter and a buck converter interconnected in anti-parallel [62]. To transmit power in both directions, it may function in either synchronous buck or boost mode. By changing the diode with an additional switch, the bidirectional topology [63] may be produced from the basic inverting buck-boost architecture. By cascading the buck converter and the boost converter, the topologies [64],[65] may be produced. This topology works throughout all four quadrants of the v-i diagram. It can do step-down and step-up operations in both directions. The most adaptable architecture is cascading buck-boost BDC. However, it has numerous disadvantages, including a rise in the number of power switches, which results in a more complicated control scheme and controller design, as well as increased turn-on losses due to the reverse recovery problem of transistor body diodes. By substituting the primary diode with a MOSFET, the bidirectional Cuk converter structure [66], [67] is developed from its standard unidirectional Cuk converter. Because of the reduced ripple in the input and output currents, the bidirectional Cuk converter is an excellent choice for applications such as battery equalization [68], ultra-capacitor-battery interface circuits [69], and bidirectional converter to control power flow and ensure the integrity of batteries. Inductors L_1 and L_2 can be connected together to reduce input and output current ripple. The voltage output could be

greater or lower than the input voltage in both the ways since the Cuk converter is basically a series-connected boost and buck topology with the capacitor C.

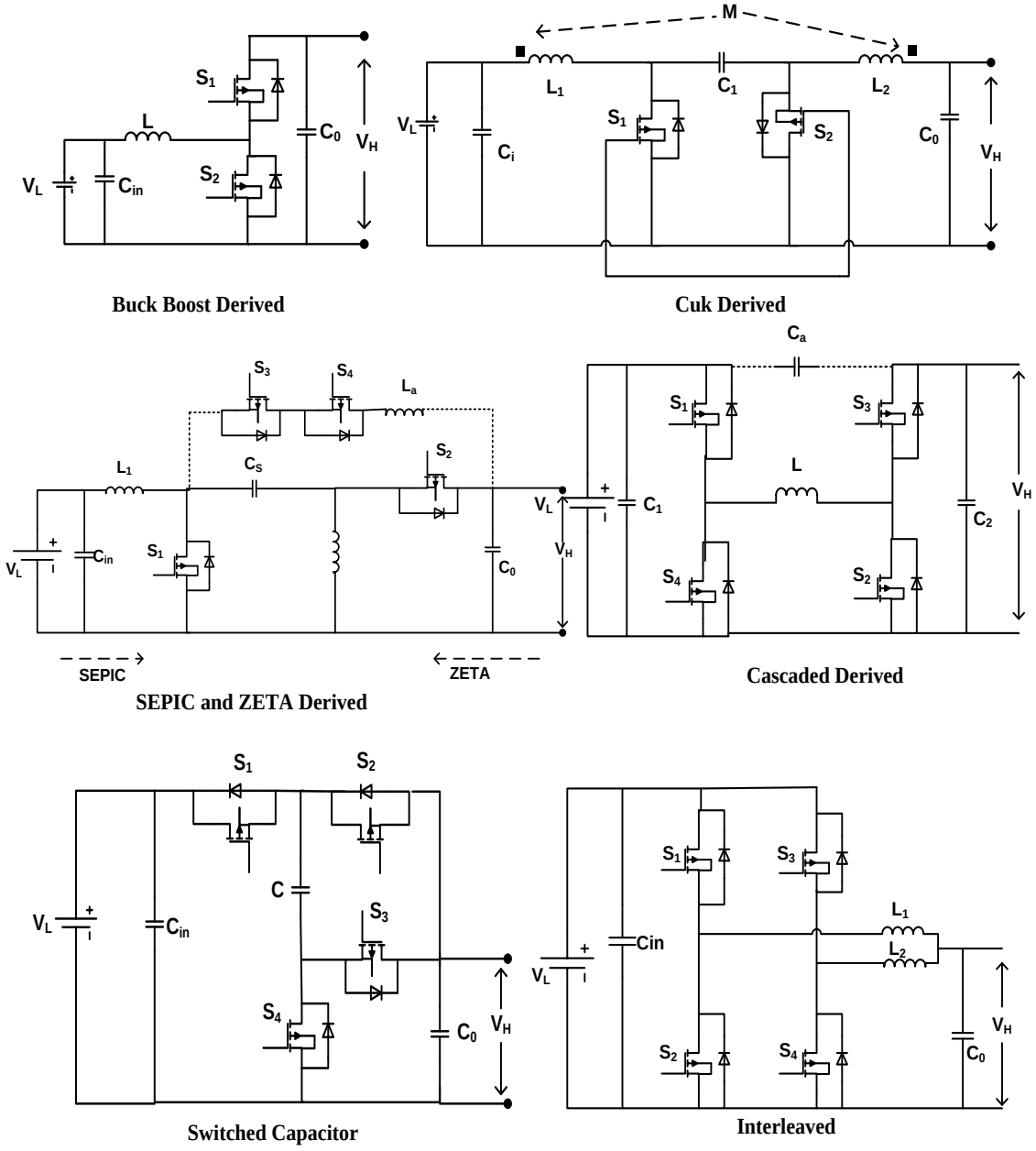

Fig.1.6 Non-isolated Bidirectional DC-DC Converter Topology

A bidirectional SEPIC/Zeta DC-DC converter's basic architecture design acts as a standard SEPIC converter for forward power flow and as a Zeta converter for backward power flow [70], [71]. It's essentially a Cuk converter reorganisation. The output voltage of a SEPIC/Zeta converter can be higher or lower in both directions, but the polarities of the dc bus stay constant. [72], [73] suggest an improved BDC that uses a linked inductor of the

same winding turns on the essential and auxiliary sides. Over a typical half-bridge bidirectional converter, the suggested converter provides benefits such as larger step-up and step-down gains and a significantly lower magnitude of switching current. The suggested BDC with tapping inductor in [74] provides a high step-up ratio, eliminating the active switch's severe duty cycle as well as the large peak currents in the active and passive switches. In addition, a reduced step-down ratio is attained. In several applications, the polarities of dc bus voltage is inverted with regard to a common ground. When it is necessary to implement the DC-DC converter using Integrated Circuit (IC) technology, switched capacitor (SC) BDCs [75] are usually utilized. Because no magnetic equipment is required in any of those converter, IC manufacturing prospects seem promising.

Many approaches for operating switches and switching patterns for power conversion have been presented, beginning with the notion of employing simple switched capacitor cells in filter design. Every capacitor in the converter is essentially charged from supply or second capacitor. Moreover, switched capacitor converters have poor regulation capabilities, its voltage conversion ratio is governed by the circuit architecture, and significant input current ripple that causes Electromagnetic Interference (EMI). The majority of these issues may be resolved by incorporating a current control system and a voltage control strategy, which will alter the capacitor's charging trajectory. It does, however, increase conversion complexity and expense. The main characteristics of all converters are high efficiency, dependability, and a simple control approach. Soft-switching technologies are becoming more widespread and are being employed in non-isolated BDCs due to the limited efficiency of hard-switching converters. Soft switching maximises efficiency by reducing power loss and allowing for downsizing and weight reduction. However, it complicates the design and makes controlling and tuning the controller parameters more difficult.

Half-bridge single-phase bidirectional converters incorporating additional ZVS/ZVS circuits are the most common types [76],[77]. Other types of converters, such as the Cuk converter, the SEPIC/Zeta converter, as well as the switched capacitor converter, may feature resonant circuit design with active clamps. The most frequent topology is an interleaving half bridge topology. This design provides high voltage gain, highly efficient, with minimal input current ripple while using smaller inductor and capacitor sizes, making

it less expensive than traditional BDCs. An interleaved converter's power inductors can be connected either directly or inversely. Inverse coupling decreases phase current ripple while increasing transient response.

Bi-polar Bidirectional DC-DC Converters

The bidirectional DC-DC converter provides an interface between both the energy storage units and the DC bus and must allow energy to flow in both directions. When the renewable energy sources exceeds the energy associated with the system, the bidirectional DC-DC converter charges the energy storage unit. When the generated energy is inadequate, the energy storage provides energy to the load and maintains the system's power balance. Various multi-input-single-output configurations are presented in [78]-[82]. Those converters are simple and efficient when compared to traditional topologies. Consequently, these converters cannot be used for bi-polar DC micro-grid applications since they require dual output with three output terminals. Furthermore, many of these converters consider output voltage control impossible in the event of an outage or non-operation from one of the input sources.

Several single-input multi-output converters have been suggested in [83]-[85]. Most of these converters feature lower switching devices, higher power density as well as efficiency, and are also suited for bipolar DC micro-grid applications. Most converters, therefore, cannot merge multiple renewable energy sources. Furthermore, most of these converters generate numerous independent outputs and thus cannot be used for bi-polar DC micro-grid applications that need two series-connected outputs. Because they contain series-connected outputs, the converters in [86], [87] are small, effective, and well-suited for bi-polar DC micro-grid applications. However, they are high-gain multi-output DC-DC converters with additional devices or circuits that are unnecessary for low-voltage bi-polar DC micro-grid applications.

Several multi-input-multi-output DC-DC converters are presented in [88]-[90]. Apart from [91], all other converts feature series-connected outputs and only one inductor. As a result, these converters are suitable for low-voltage bi-polar DC micro-grids and are reasonably small and efficient. Moreover, because the converter in [92] is bidirectional, it

is not suitable for integrating just renewable energy sources. Although converters in [93]-[95] are unidirectional, they employ a large switching devices to provide numerous outputs, significantly reducing efficiency. More inductors are used in the converter in [96]. Because of the reduced blocked voltages of the switching devices, traditional bidirectional bipolar DC-DC converters can minimize switching losses, and switching devices with a low rated on-state resistance may be used in high voltage and power bidirectional converter [97]. The disadvantage is that while running with a high voltage-gain, most switching devices reach a period of severe duty cycles.

As a result, a new type of transformer-less bidirectional DC-DC converter with a high voltage-gain and the ability to operate with non-extreme duty cycles which might be appropriate for hybrid vehicle applications. With shipboard electric distribution networks, a transformer-less bi-polar DC-DC Buck converter with a significant step-down conversion ratio is currently suggested [98]. Furthermore, the power switches' non-extreme duty cycles may be regulated by selecting appropriate double modulation waves. Furthermore, the switching devices with non-extreme duty cycles may be regulated by selecting appropriate double modulation waves. Similarly, [99] proposes a hybrid boost bi-polar DC-DC converter with a high step-up conversion ratio for solar systems, which can function with a 50V DC input and a 600V DC output.

1.2.3 Isolated Bi-polar Bidirectional DC-DC Converter

When compared to the two-level converter, the three-level converter works about half of the switches in one cycle, thus reducing switch voltage stress [100].The basic purpose of a high-frequency transformer is to attain galvanic isolation of both the DC bus and energy storage elements, thereby reducing electromagnetic interference (EMI); to modify the voltage conversion limit; to modify transformer leakage inductance and main switch parasitic capacitance resonance, so that soft switching with IGBT is easier, thereby improving converter efficiency. Fixed-frequency pulse width modulation (PWM) and frequency modulation (FM) modes are used in the isolated three-level bidirectional DC/DC topology modulation. Frequency modulation complicates the architecture consists of magnetic components, the controlling circuit, and the filtering circuit, and also the gain is substantially impacted by the load because when switching frequency deviates from the

nominal value. Fixed-frequency modulating reduces the complexity of resonant components. Because when switching frequency is identical to the resonant frequency, the load has no effect on the gain. Soft switching necessitates a suitable switching current and dead time, however the dead time is too long, increase the voltage and current fluctuations, and also the dead time must be restricted to an acceptable range.

The high-voltage side switching devices in [101] uses pulse width and amplitude modulation, as well as the resonant tank voltage amplitudes are modulated. To fulfil the needs of energy storage device voltage, high gain mode, medium gain mode, and low gain mode are employed. The high-voltage side network uses bi-polar modulating in the forward power transmission, while the low-voltage side component is in an uncontrollable rectification condition.

As illustrated in Fig 1.7, the high-voltage side switching devices in [102] create a bi-polar structure, whereas the low-voltage side switching devices adopt a buck/boost circuit parallel configuration. When transformer leakage current control is applied to a conventional pulse width phase shift modulation (PPS), and the peak current, voltage, and losses are minimized. ZVS soft switching is implemented in all switching devices. The transformer loss is considerably decreased, and overall efficiency is increased, thanks to the Direct Current Slew Rate (DCSR) control technology. The bi-polar half-bridge operates in an inverted condition when operated in the other way. The energy is transferred via the transformer and then across two half-bridge circuit design with the assistance of the support capacitor V_c to accomplish buck operation.

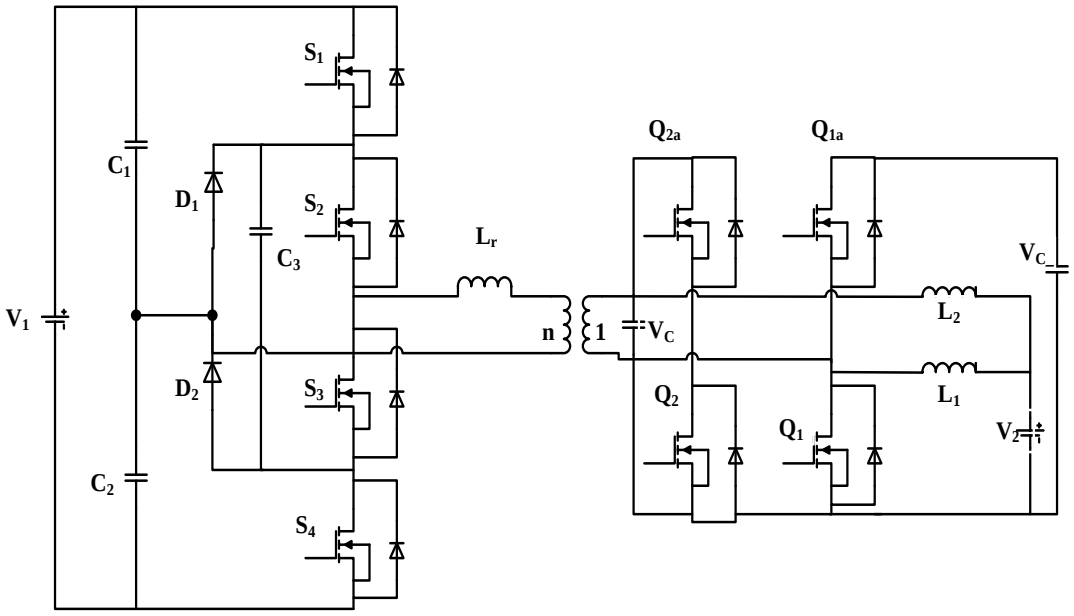

.Fig 1.7 Bi-polar Bidirectional DC Converter with phase shift [102]

In [103] employs phase shift control in a double active bridge (DAB) with capacitor inductance series resonance (CLLC). The active bridge operates in the inverter state in bidirectional operation, whereas the passive bridge operates in the rectified state. Some MOSFETs are capable of realizing the ZVS switch and analyzing the phase requirements needed to do so. On the basis of the bi-polar DAB circuit, [104] includes bus capacitor voltage balancing control, and the parameters modeling and development technique are simplified.

1.2.4 Non-isolated Bi-polar Bidirectional DC-DC Converter

The DC bus capacitor is used in [105] to produce a bi-polar state (buck/boost synchronized PWM modulator). dv/dt soft switching is used to minimize the current surge. The voltage gain is 2/D whenever the interconnected capacitive buck converter is combined with a switched capacitor circuit and a buck circuit; when the buck circuit is combined with n-1 switched capacitor networks, the voltage gain is up to n/D. As a result, it is appropriate for low-voltage, low-power battery storage and solar systems. [106] Cascades a uni-polar buck-boost converter to produce a bi-polar bidirectional DC-DC converter. PWM modulation with interleaved pulses is utilized. Moreover, the modulating approach simply allows the duty ratios of the top and bottom half bridges to be unpredictable, impacting the voltage balancing effect of the DC bus and necessitating an extra voltage balance control loop in boost mode, adding to the control structure's complexity. Despite the fact that the converter described in [107] lacks the high voltage gain capabilities of the converter presented in [105], the voltage and current stress are almost same, and the flying capacitor voltage is readily stabilized at half of the high voltage side. By extending the flying capacitor circuit, the bi-polar DC-DC converter may be easily expanded into a multi-level bidirectional DC-DC converter, further lowering the voltage stress on the switches. As a result, it is appropriate for greater voltage levels.

1.3. Motivation

Traditional DC micro-grids have offer many advantages that makes them attractive in electrical distribution network. They give the flexibility of connecting various renewable energy sources such as solar photovoltaic, wind energy etc with required power conversion

stages. DC micro-grids also have the capability of connecting to battery storage systems, fast charging electric vehicle stations. Some of the advantages of DC micro-grids that have made them popular are the absence of synchronisation issues and the capacity to ride through faults. Further due to increase in various loads which are operating with DC supply made further popular of DC micro-grids. Bipolar dc micro-grids are more dependable than unipolar dc micro-grids and provide three distinct voltage levels. Because the quantity of load and generated power varies over time, an effective voltage balancing approach is required in bipolar dc micro-grids. To equalize the voltage of the positive and negative buses and also requirement of bipolar bidirectional DC-DC converters for efficient transfer of energy in both directions with minimum number of components and simple control circuits is a challenging issue. Therefore an attempt was made in this research work to propose a bipolar bidirectional DC-DC converter topologies and their control strategies. Detailed mathematical analysis, modeling, simulation and experimental results are provided for the proposed bi-polar bidirectional DC-DC converter topologies to their merits.

1.4. Scope of the Thesis

The scope of this research work is to propose bipolar bidirectional DC-DC converter topologies which can operate for both low power and high power applications to achieve high voltage gain along with reduced voltage stress, low switching losses resulting in high efficiency and also inherent voltage balance at the poles of a DC micro-grid.

As a result, the following contributions to this thesis can be summarized:

1. To design and implement a bipolar bidirectional DC-DC converter topologies for battery energy storage system for regulating the power flow.
2. To design and implement a bipolar bidirectional DC-DC converter topologies for solar powered electric vehicle charging stations.
3. To develop a control scheme to achieve inherent voltage balance at the bipolar DC micro-grid.

The schematic diagram of bipolar grid employing bidirectional DC-DC converter is shown in Fig 1.8.

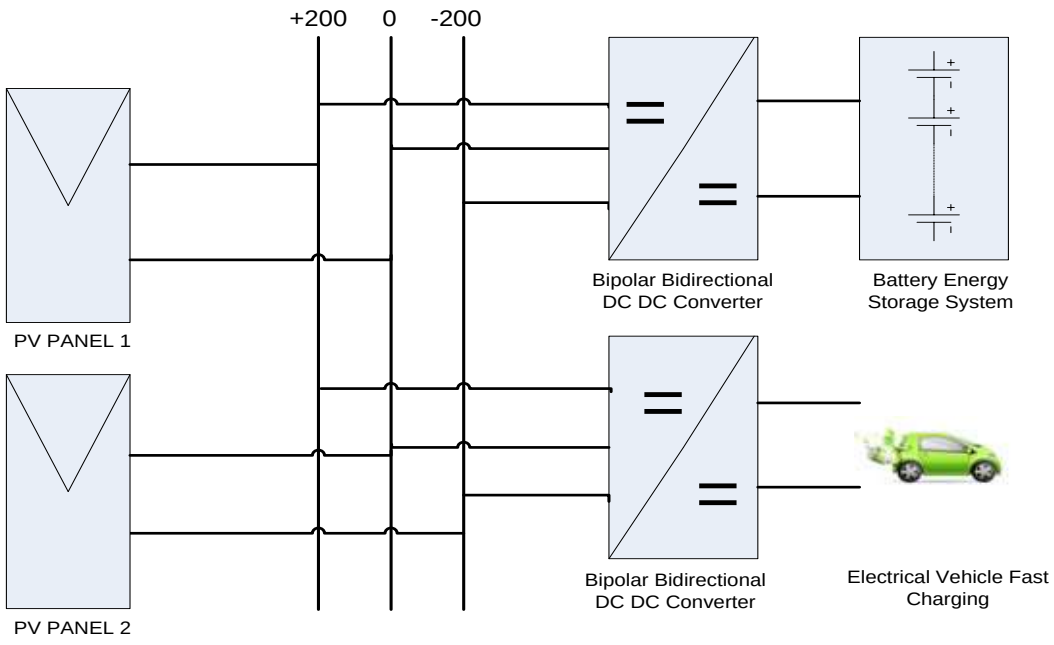

Fig.1.8 Block diagram of Bipolar Grid employing Bidirectional DC-DC Converter

In the first proposed topology, a soft switching technique for a non-isolated bipolar bidirectional DC–DC converter with series connection of modular bidirectional DC converters suitable for both small and medium scale bipolar DC micro-grids to achieve high voltage gain. The soft switching technique is implemented by turning-on all the power devices at zero current during discontinuous conduction and turning-off is achieved by using an auxiliary devices in the circuit. Soft switching, high efficiency, transformer less structure and inherent control for voltage balance make this converter employable in bipolar DC grids.

A non-isolated bipolar bidirectional DC-DC converter with an interleaved switching capacitor for bipolar DC micro-grids appropriate for both low and high power applications is developed in the second suggested topology to achieve high voltage gain. On the low voltage side, an interleaved structure is proposed to realize current sharing and decrease current ripple, while on the high voltage side, a switched capacitor architecture is presented to achieve high voltage gain.

In the third suggested architecture, a non-isolated soft switching bipolar bi-directional

DC-DC converter for bipolar DC micro-grids appropriate for both low and high power applications is built using a half bridge converter to obtain high voltage gain. Half bridge converter on the low voltage side and a series L-C half bridge resonant converter on the high voltage side to produce high voltage gain while minimizing voltage stress and switching losses, resulting in high efficiency.

A non-isolated bipolar bidirectional DC-DC converter with linked inductor and switched capacitor technology for bipolar DC micro-grids appropriate for both low and high power applications is developed in the fourth suggested architecture to achieve high voltage gain. The inclusion of the clamping circuit, which is utilized to reutilize the leakage inductance power, results in zero voltage switching for all switching devices. The PI controller is used to connect an energy storage system to the grid in order to achieve bidirectional power flow and voltage balancing at the grid level.

1.5. Organization of the Proposed Thesis

The **Chapter-1** gives the detailed literature study on bidirectional DC-DC converter topologies and bipolar bidirectional DC-DC converter topologies, key issues and their drawbacks presented and also motivation for the research work in the area of Bipolar Bidirectional DC-DC Converter Topologies is presented.

In Chapter-2, simulation results are presented for proposed bipolar BDC converter topology (proposed topology-1) for medium and high voltage DC micro-grids. Results are compared with the conventional topologies to show the merits of proposed topology.

In Chapter-3, the suggested bipolar BDC converter with interleaved switching capacitor (proposed topology-2) for bipolar DC micro-grids is simulated and tested. The suggested topology virtues are demonstrated by comparing their results to those of standard topologies.

In Chapter-4, simulation results are presented for the proposed bipolar BDC converter with coupled inductor (proposed topology-3) for bi-polar DC micro-grids with energy storage. Results are compared with the conventional topologies to show the merits of proposed topologies.

In Chapter-5, simulation and experimental results are provided for the suggested non-isolated soft switching bipolar BDC converter topology with high voltage gain (proposed topology-4) for bi-polar DC micro-grid. Results are compared with the conventional topologies to show the merits of proposed topologies.

Finally, **Chapter-6** highlights the various conclusions drawn at different stages of the work, the significant contribution of research work. Finally, conclusions and future scope for the work is suggested.

Chapter-2

Bipolar Bidirectional DC-DC Converter for Medium and High Voltage DC Micro Grids

2.1. Introduction

In this chapter, the bi-polar bidirectional DC-DC converter is proposed for medium and high voltage DC micro-grids. The proposed converter can work in both directions i.e., both modes of operations such as buck mode and boost mode and support soft-switching features with low voltage stress on the switching devices. All power switches are switched on spontaneously under zero current when working in the discontinuous conduction mode. All switches are turned off at zero current by introducing an extra zero-current-transition commutation circuit in each power module, which reduces turn-off loss. Detailed analysis and simulation results for the converter with three power modules are explained in detail below.

2.2. Bi-Polar Bidirectional DC-DC Converter

Schematic of the proposed bipolar bidirectional DC-DC converter is shown in Fig.2.1**.** It consists of three modules and each module consists of two switches, inductor and capacitor as main circuit, two auxiliary switches and resonant circuit consists of inductor and capacitor. First module consists of main switches (S_1, S_2), inductor L_1 and capacitor C_1 and two auxiliary switches (S_{A1}, S_{A2}), inductor L_{R1} and capacitor C_{R1} act as L-C resonance circuit. Similarly other two modules also have the same components. The current through the inductors L_1, L_2 and L_3 are represented by i_1, i_2 and i_3 respectively. High step up gain in boost mode or high step down gain in buck mode can be achieved by considering both positive and negative circuits as individual modular bidirectional DC-DC converter. The transmission of power flow and inherent voltage balance occurs by using L-C resonance circuit. In each module, the auxiliary cell utilizes the L-C resonance circuit to achieve soft switching in the switches and diodes. Operating in discontinuous conduction mode causes the switches to turn on naturally under ZCS conditions, and an auxiliary cell is inserted into the main power channel to lower the current to zero, resulting in a zero current transition turn-off situation. When the positive circuit functions as the boost mode and the negative circuit functions as the buck mode, then direction of power flow will be from low voltage side to high voltage side. When the positive circuit functions as buck mode and the negative circuit functions as the boost mode, then the direction of power flow is from high voltage

side to low voltage side. Detailed operation of bipolar modular bidirectional DC-DC converter is discussed in subsequent section.

2.2.1 Analysis of Bipolar Bidirectional DC-DC Converter

Steady-state analysis of proposed bi-polar bidirectional DC-DC converter shown in Fig.2.1 is discussed in detail for buck mode and boost mode of operation. For steady-state analysis, all the switching devices and the energy storage elements are considered as ideal and the current in inductor is discontinuous; the voltage across the capacitors is assumed constant.

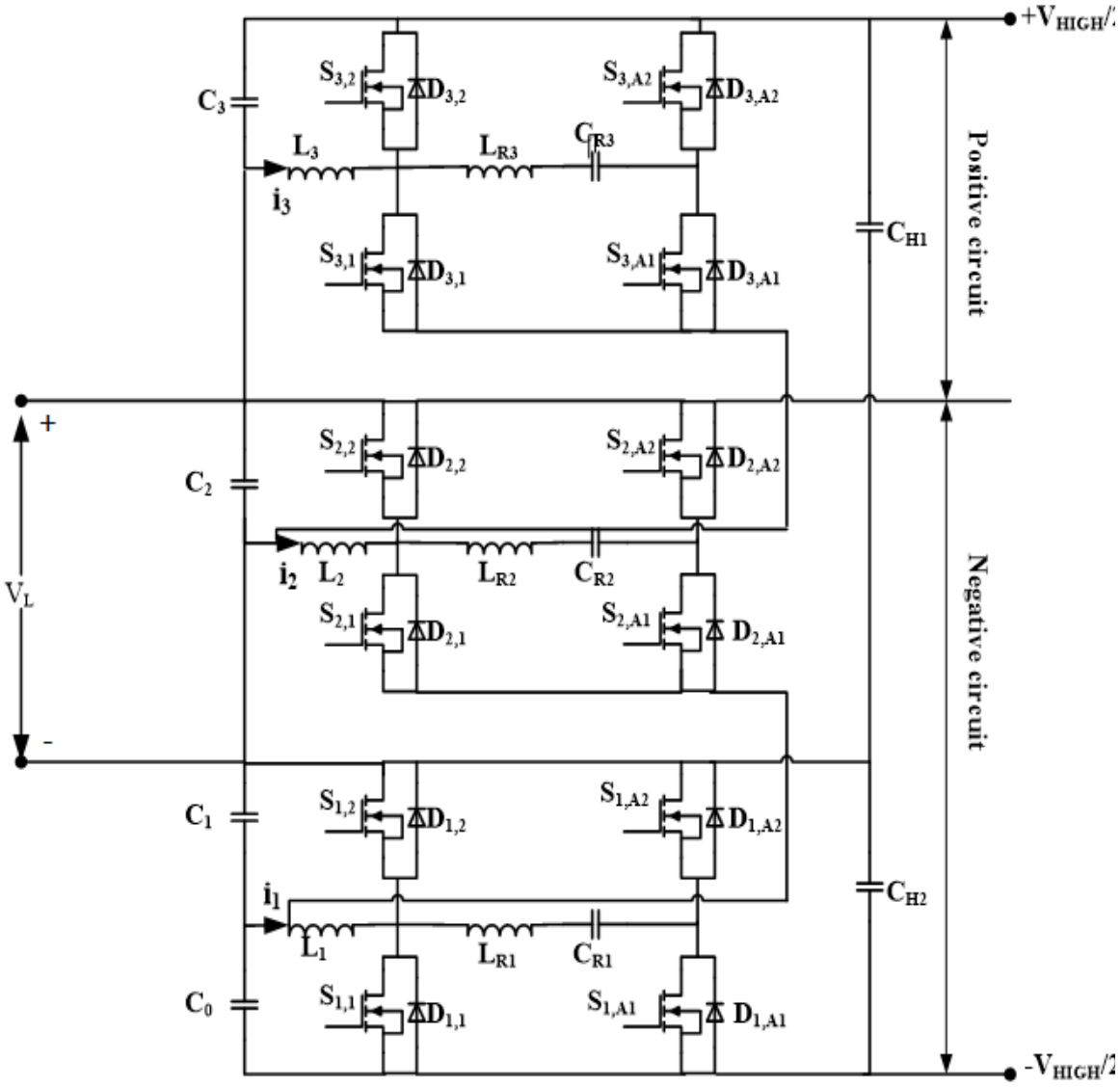

Fig. 2.1 Schematic of bipolar bidirectional DC-DC converter

2.2.1.1 Boost mode of Operation

In this mode of operation, output voltage is stepped up by controlling the switches S_1 and S_{A1} along with antiparallel diodes of switches S_1, S_{A1} and S_2. Resonant circuit components help to achieve the required voltage gain and voltage balance across the capacitors. One complete cycle of operation of the converter is divided into eight modes as discussed below:

Mode 1: In this mode of operation the Switch S_1 is ON, and S_{A1} is OFF, diode D_{A1} is ON. The direction of currents is shown in Fig 2.2. Inductor current i_1 starts increasing and L_{R1} and C_{R1} gives the resonant current and when this resonant current is equal to zero, the diode is clamped to the resonant capacitor voltage .

Mode 2: In this mode of operation switch S_1 is ON, the inductor current i_1 starts increasing when inductor current equals to current flowing through the switch, the voltage across the resonant capacitor is same as input capacitor voltage magnitude.

Mode 3: In this mode of operation the switch S_{A1} is ON under ZCS conditions as a result the resonant current starts increasing until it compensate the inductor current magnitude, allowing the current flowing through the switch to zero due to the resonance of L_{R1} and C_{R1}.

Mode 4: In this mode of operation the diode D_1 is ON and S_1 is OFF under zero current transition (ZCT) conditions and the flow of current through the switch is reversed. The resonant current is same as current flowing through the inductor due to resonance of L_{R1} and C_{R1} making D_1 is reverse bias

Mode 5: In this mode of operation the switch S_{A1} is ON. Capacitor C_{R1} is charged through inductors L_1 and L_{R1} which results in boosting of the output voltage.

Mode 6: In this mode of operation the switch S_{A1} is ON and D_2 is ON. The direction of currents is shown in Fig 2.2. The direction of current flow in inductors i.e i_1, i_{LR1} starts decreasing. The capacitor C_1 is charged by the inductor L_1.

Mode 7: In this mode of operation the switch S_1 is OFF and S_{A1} is OFF under ZCS conditions, D_2 and D_{A1} are ON. The inductor current i_{LR1} starts decreasing and reaches to zero due to resonance circuited formed by L_{R1} and C_{R1} making D_{A1} is block.

Mode 8: In this mode of operation of the switches S_1 and S_{A1} are OFF. The inductor current i_1 starts decreasing and reaches to zero making the S_1 turn ON under ZCS conditions for the next cycle. Inductor L_1 charges the capacitor C_1.

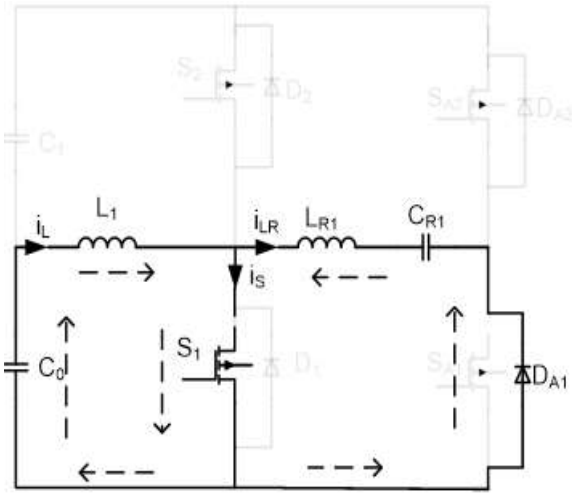

MODE 1

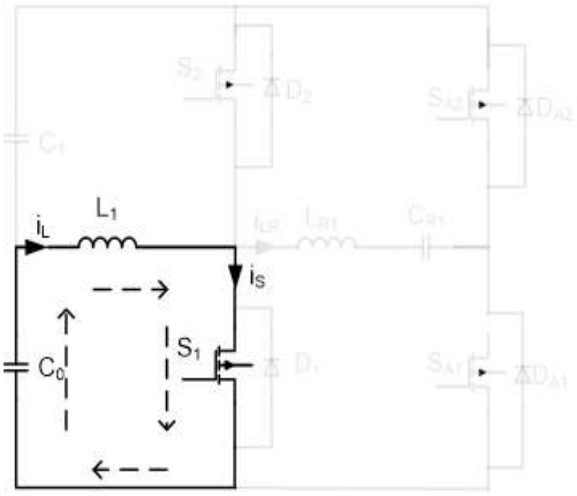

MODE 2

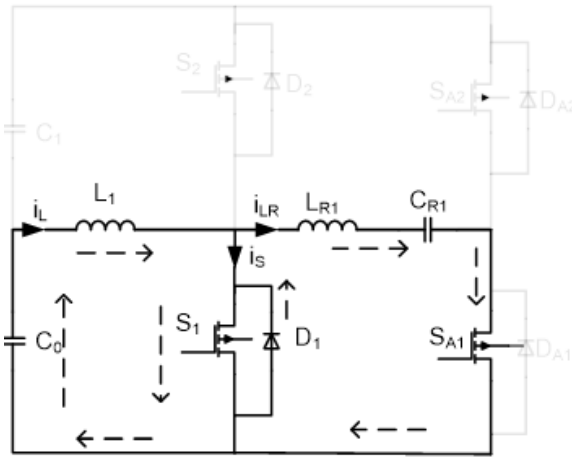

MODE 3

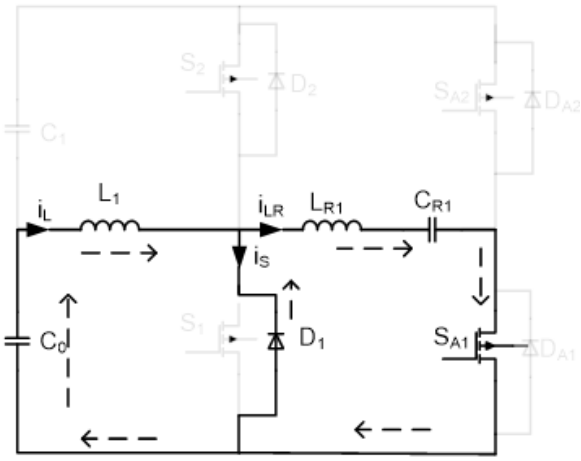

MODE 4

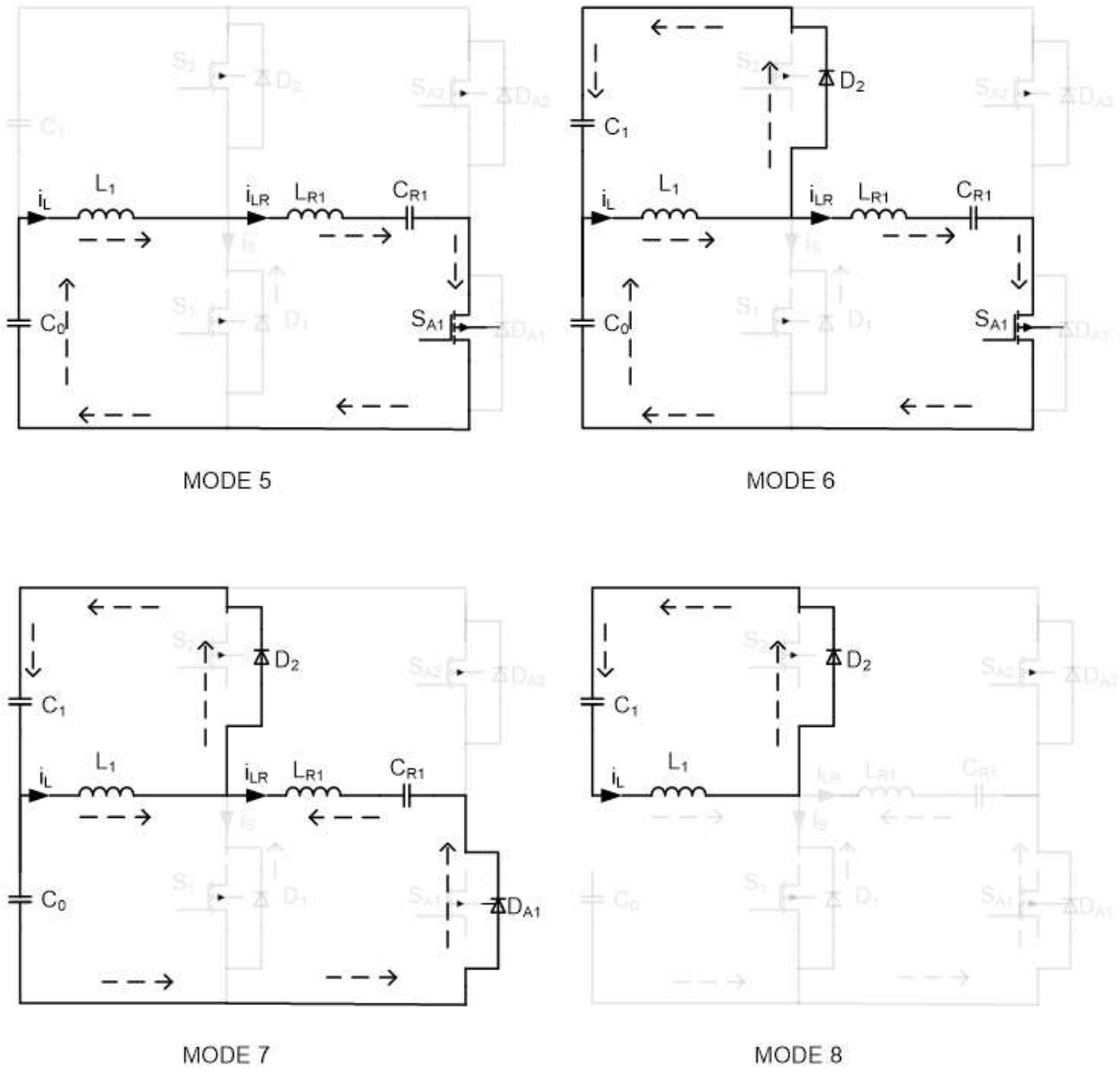

Fig.2.2 Modes of operation for the proposed DC-DC converter in boost mode

2.2.1.2 Buck mode of Operation

By controlling the switches S_2 and S_{A2} along with antiparallel diodes of switches S_2, S_{A2} and S_1 outputvoltage is stepped down (buck operation). The flow of power direction is from high voltage to low voltage side (C_0) in the buck mode.Converter operation for one cycle is divided into eight modes and Fig 2.3 represents the modes of operation in buck mode.

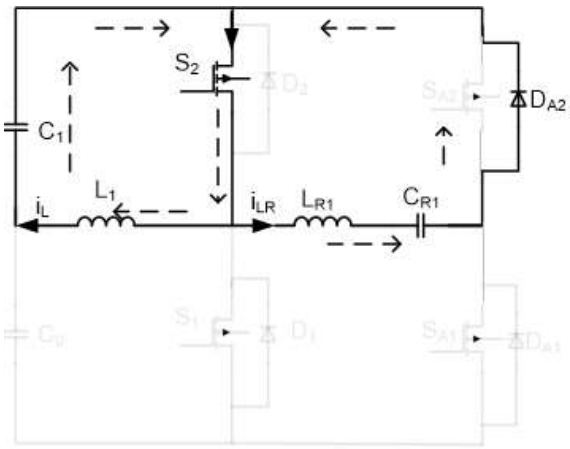

MODE 1

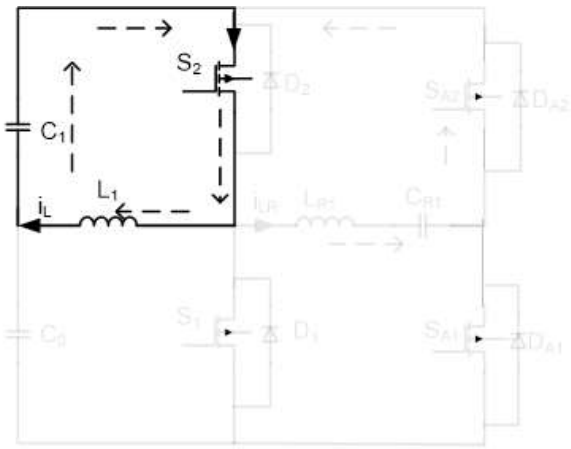

MODE 2

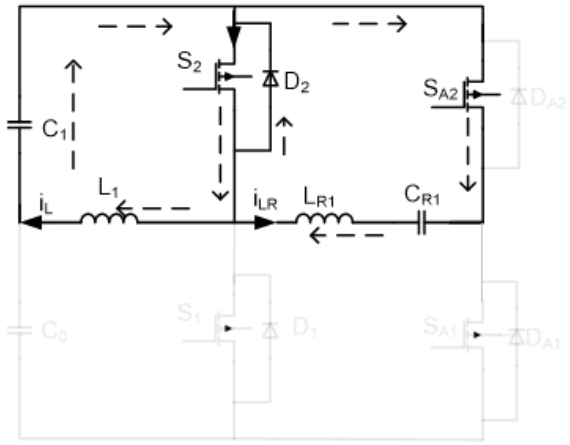

MODE 3

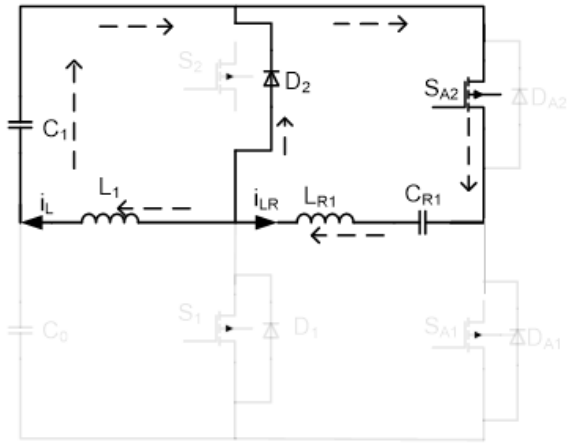

MODE 4

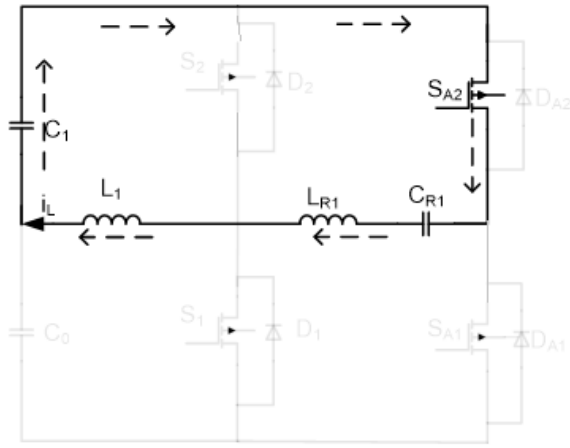

MODE 5

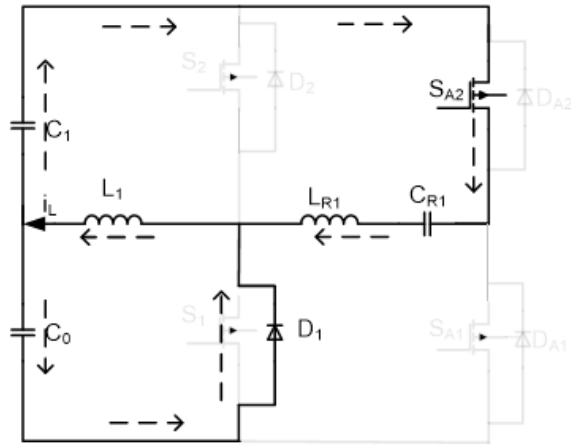

MODE 6

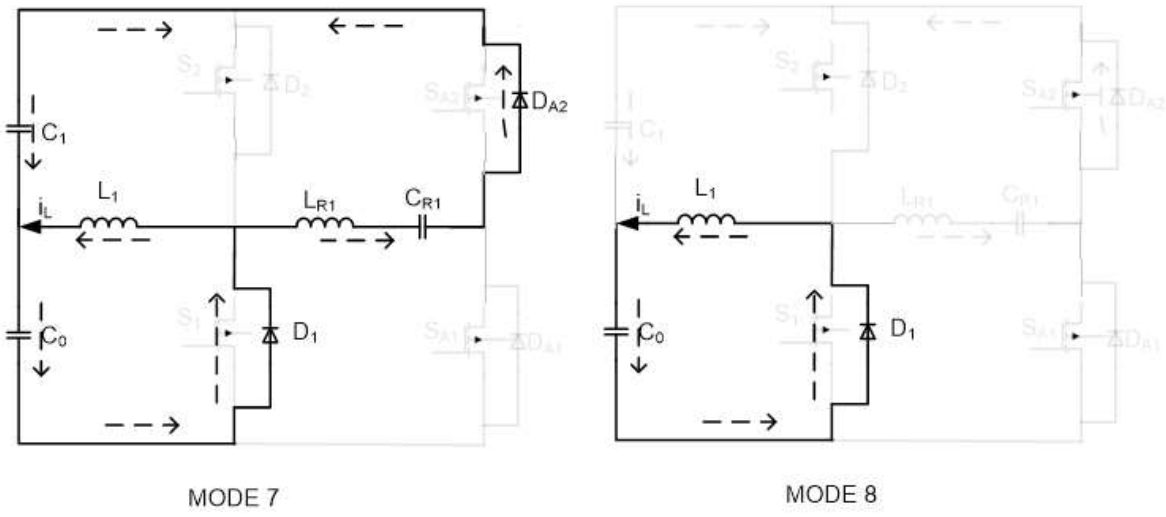

Fig 2.3 Operation for the proposed Convereter topology in buck mode

2.3 Design of Bipolar Bidirectional DC-DC Converter

Design of various circuit parameter such as inductors and capacitors for the main power circuit and also resonant circuit parameters for the 10 KW converter operating at a switching frequency of 20 KHz to obtain the voltage of 500 volts at buck operation and 2000 volts at boost operation for the proposed bipolar bidirectional DC-DC converter are discussed below. Converter specifications and parameters are listed in Table 2.1.

2.3.1 Design of Inductor

The conversion ratio in a bipolar modular bidirectional DC converter with 'x' power units is $X = V_H/V_L = x + 1$. The x^{th} power unit's power transfer may be written as (X-x) P/X, where i_x is the x^{th} power unit's inductor current. It is possible to deduce the following mathematical relationships:

$$L_x \frac{di_x}{dt} = V \tag{2.1}$$

$$t_{on} = \frac{D}{f} \tag{2.2}$$

Where V is the voltage of each power module, f represents the switching frequency, and D represents the duty cycle. From (2.1) and (2.2), the maximum inductor current i_{x-MAX} can be obtained by

$$i_{x-MAX} = \frac{V*D}{L_x*f} \quad (2.3)$$

Since the converter is operating in discontinuous conduction mode, the inductor current rises from zero, $\Delta i_x = i_{x\text{-}MAX}$. To determine the inductor's energy balance,

$$\frac{X-x}{X} * P = \frac{1}{2} * L_x * f * i_{x-MAX}^2 \quad (2.4)$$

From (2.3)and(2.4) , the inductor expression is derived as

$$L_x = \frac{X*V^2*D^2}{2*f*P*(X-x)} \quad (2.5)$$

For D=0.5, $$L_x = \frac{X*V^2}{8*f*P*(X-x)} \quad (2.6)$$

2.3.2 Design of Capacitor

The capacitor is one of the important component of the converter that allows energy to be stored and transferred to achieve buck and boost operation. The capacitors are connected in series to have the same capacitance so that the voltage balance may be reliably maintained. Because the power communicated by the capacitors is decreased down from the base capacitor C_0 to the top capacitor C_3, the voltage ripple at the base capacitor C_0 is considerable. The voltage ripple of capacitor C_0 is denoted as

$$\beta = \frac{\Delta V_{C0}}{V_{C0}} \quad (2.7)$$

$$\frac{1}{2} * C_0 * \left[\left(V + \frac{\beta}{2} * V\right)^2 - \left(V - \frac{\beta}{2} * V\right)^2\right] * f = \frac{(X-1)*P}{X} \quad (2.8)$$

From (2.7) and(2.8) ,

$$C_3 = C_0 = \frac{P*(X-1)}{X*f*\beta*V^2} \quad (2.9)$$

2.3.3 Design of Resonant circuit parameters

Boost or buck mode of operation can be considered to design the resonant circuit parameters. Here I have considered boost mode, from mode-1the current flowing through the switch is the sum of current flowing through the inductor and the resonant inductor and also the resonant capacitor voltage V_{CR} is clamped at $-V_{CR}$.

$$i_S = i_1 + i_{LR1} \tag{2.10}$$

$$V_{CR} = 2 * V - Z_1 * i_{1-MAX} \tag{2.11}$$

$$Z_1 = \sqrt{\frac{L_{R1}}{C_{R1}}} \tag{2.12}$$

From(2.11)and(2.12), $$V_{CR} = 2 * V - \sqrt{\frac{L_{R1}}{C_{R1}}} * i_{1-MAX} \tag{2.13}$$

$$i_{CR1-MAX} = \frac{V_{CR1}}{Z_1} = V_{CR1} * \sqrt{\frac{C_{R1}}{L_{R1}}} \tag{2.14}$$

Then, $i_{CRx-MAX} = n * i_{x-MAX}$ is selected. From (2.13) and (2.14), the equation is represented as

$$(1 + n) i_{k-MAX} = \frac{2V}{\sqrt{\frac{L_{R1}}{C_{R1}}}} \tag{2.15}$$

The equation may be written as, assuming T_{Rx} is the resonance time between C_{Rx} and L_{Rx}.

$$\frac{T_{Rx}}{2} = \pi * \sqrt{L_{Rx} * C_{Rx}} \tag{2.16}$$

From (2.15) *and* (2.16),

$$L_{Rx} = \frac{V^2 * T_{Rx}}{2 * \pi * (1+n) * L_x * f} \tag{2.17}$$

$$C_{Rx} = \frac{(1+n) * T_{Rx}}{8 * \pi * L_x * f} \tag{2.18}$$

2.3.3.1 Calculation of current stress in inductors

Since each module of the bipolar bidirectional DC deliver the same power as that of the unipolar bidirectional DC-DC converter, the power semiconductor switches in the bipolar bidirectional DC-DC converter experience less switching current stress than those in the unipolar converter. Reduction in the Current stress is calculated from the equations (2.3) and (2.6) as

$$i_{n-MAX} = \frac{(X-x) * P * 4}{X * V} \tag{2.19}$$

Table-2.1. Converter Specifications and Parameters.

Parameters	Values
Rated Power	10 kW
Capacitors values C_0, C_1,C_2,C_3	30µF
Filter Inductors L_1,L_2,L_3	200µH , 300µH , 600µH
Resonant inductors L_{R1},L_{R2},L_{R3}	4.84µH , 7.28µH, 14.5µH
Resonant capacitors C_{R1},C_{R2},C_{R3}	0.084µF, 0.056µF, 0.028µF
Switching Frequency	20kHz
Boost voltage V_H	2000 V
Buck voltage V_L	500V

2.4. Simulation Results

Simulation tests in Matlab/Simulk are carried out to assess the viability of the proposed bi-polar bi-directional DC-DC converter, and results are reported for both buck mode and boost mode of operation.

2.4.1 Results of Boost Mode of Operation

From the simulation results shown in Fig. 2.4, it is observed that primary switch $S_{1,1}$ is turned–on using ZCS and turned-off using ZCT. Before the gating signal was applied to $S_{1,1,}$ the switching current, in association with the inductor current i_1 and resonant current i_{LR1}, rises from zero, results in ZCS across switches. When the current was reversed and passed through the diode $D_{1,1}$, $S_{1,1}$ were turned off using ZCT. Figure 2.5 depicts the ZCS for auxiliary switch $S_{1,A1}$. When the current reverses and travels through the diode $D_{1,A1}$, ZCS is used to turn off the switch $S_{1,A1}$. As illustrated in Fig. 2.6, the diode $D_{1,2}$ conducts and commutates with zero current. As a result, the diode has no reverse-recovery losses. Fig 2.7 depicts the current flowing through the inductors and voltage across the resonant capacitor. The positive and negative pole voltage in the boost mode of operation is shown in Fig.2.8. From the simulation results, it is observed that the capacitor output voltages are inherently balanced without any control technique with the low ripple value.When V_H is constant at 2000V, for different power levels between 100W and 1600W, the efficiency of

boost operation for the proposed converter is shown in Fig 2.9.The maximum efficiency obtained is 96.8% at a load of 100 Ω.

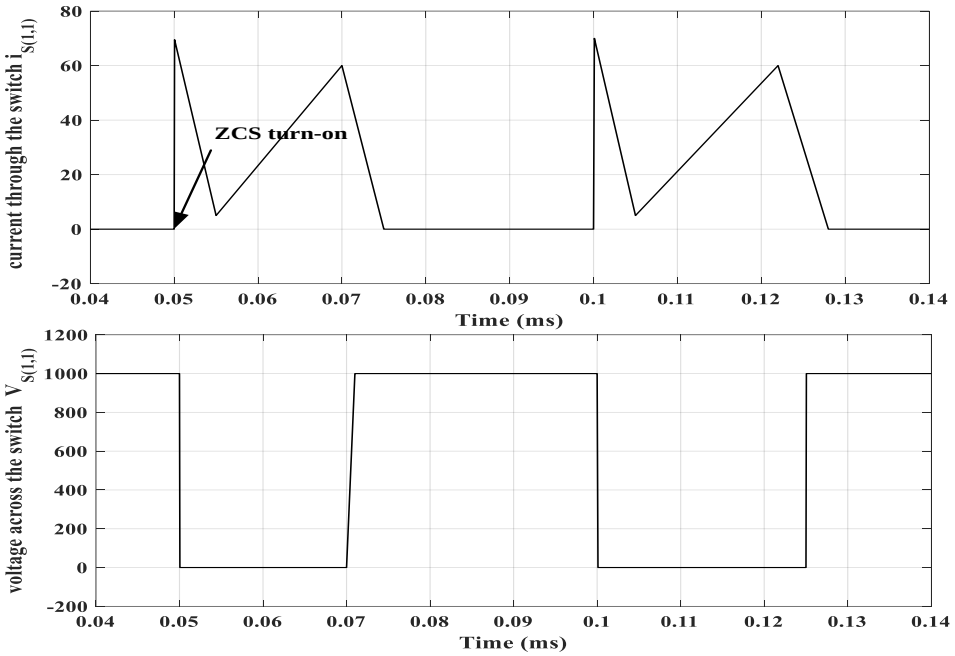

Fig 2.4 Current flowing through the switch and voltage across the switch $S_{1,1}$

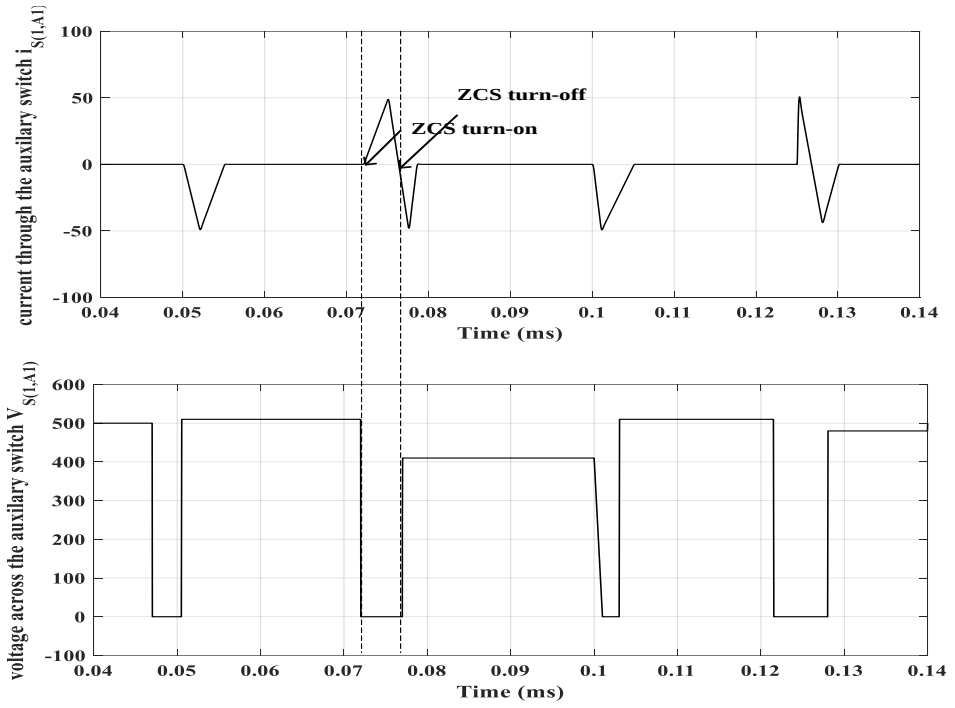

Fig 2.5 Current flowing through the auxiliary switch and voltage across the auxiliary switch $S_{1,A1}$.

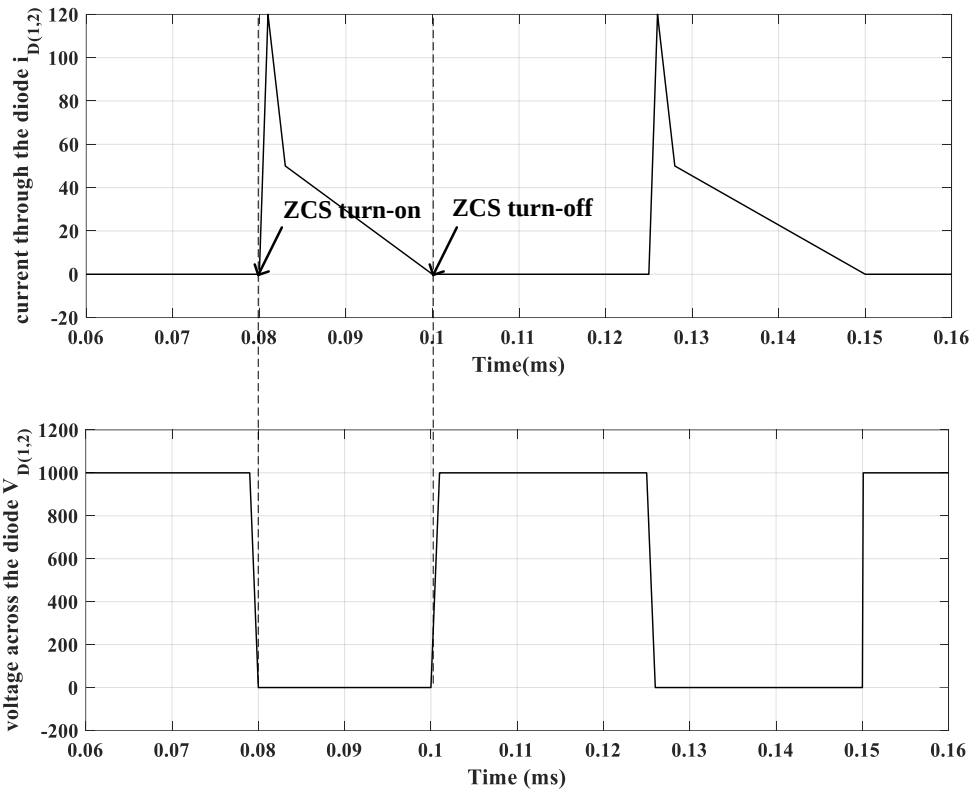

Fig 2.6 Current flowing through the diode and voltage across the diode $D_{1, A1}$.

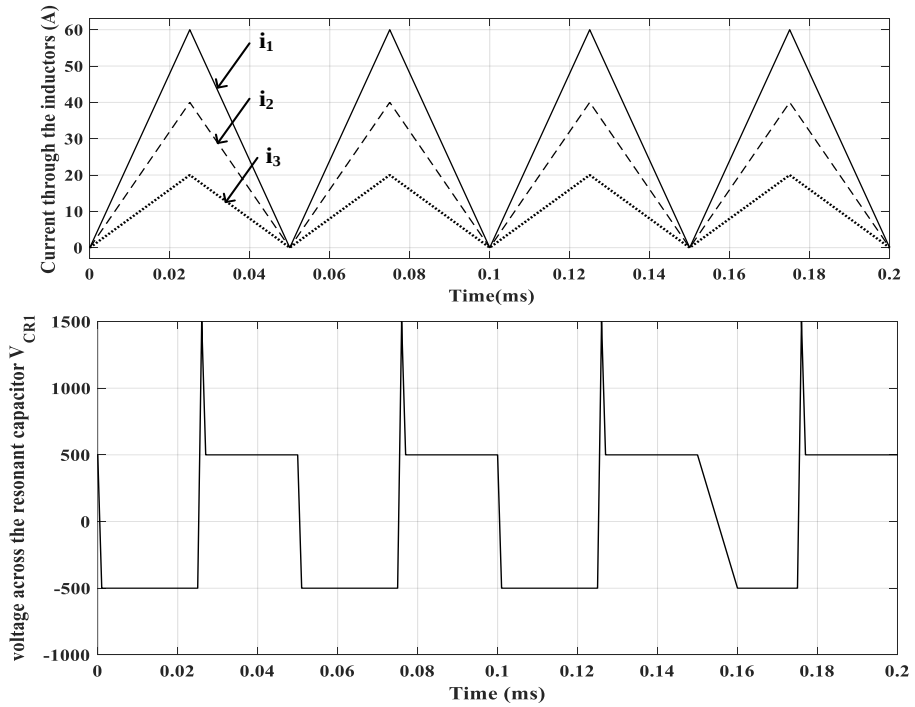

Fig 2.7 Current flowing through the inductors($L_{R1)}$ and voltage across the resonant capacitor C_{R1}

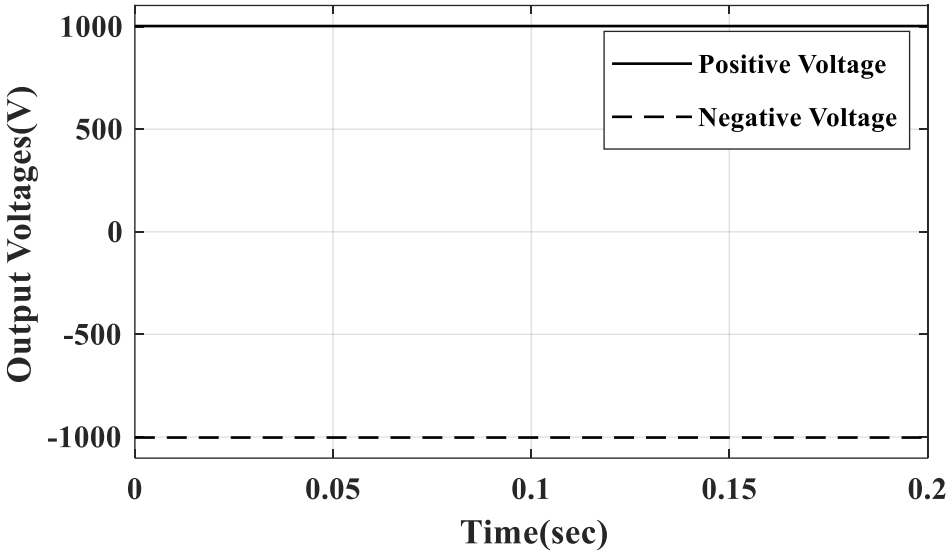

Fig.2.8 Output voltages.

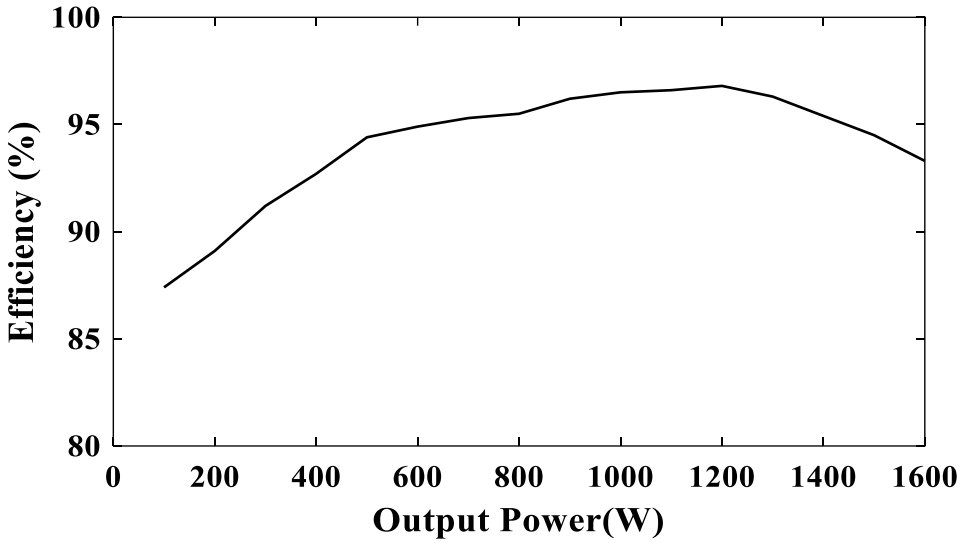

Fig. 2.9.Efficiency curve of the proposed bipolar bidirectional DC converter.

2.4.2 Results of Buck Mode of Operation

Buck mode of operation of the proposed converter for an input voltage of V_H=2000V, the current flowing through the switch and voltage across the switching device is shown in Fig 2.10. From the results it is observed that ZCS turn-on and ZCT turn-off is realized and also indicating the voltage stress across the switching device is 1000V which is

half of input voltage. From Fig 2.11, it is observed that the switch turn-on and turn-off is happening under zero current switching simultaneously. The current flowing through the auxiliary switch and voltage across the auxiliary switching device is shown in Fig 2.11 and also it is observed that voltage stress across the auxiliary switching device is 500V which is same as buck voltage. When the current is reversed and passing through the diode $D_{1, A2}$, the switch $S_{1, A2}$ is switched off with zero current switching. The diode $D_{2, 1}$ conducts and commutates with zero current, as shown in Fig. 2.12. The inductor currents and voltage across the resonant capacitor are shown in Fig 2.13. From the results it is observed that the converter operates in the discontinuous conduction mode and the maximum peak current decreases from 60A to 20A. Fig 2.14 shows the output voltage of the converter. When V_H is 2000V constant, and input power continually changing between 100W and 1600W, the efficiency of the converter in buck mode of operation is shown in Fig 2.15. The maximum efficiency is around 96.7% at a load of 2.5Ω.

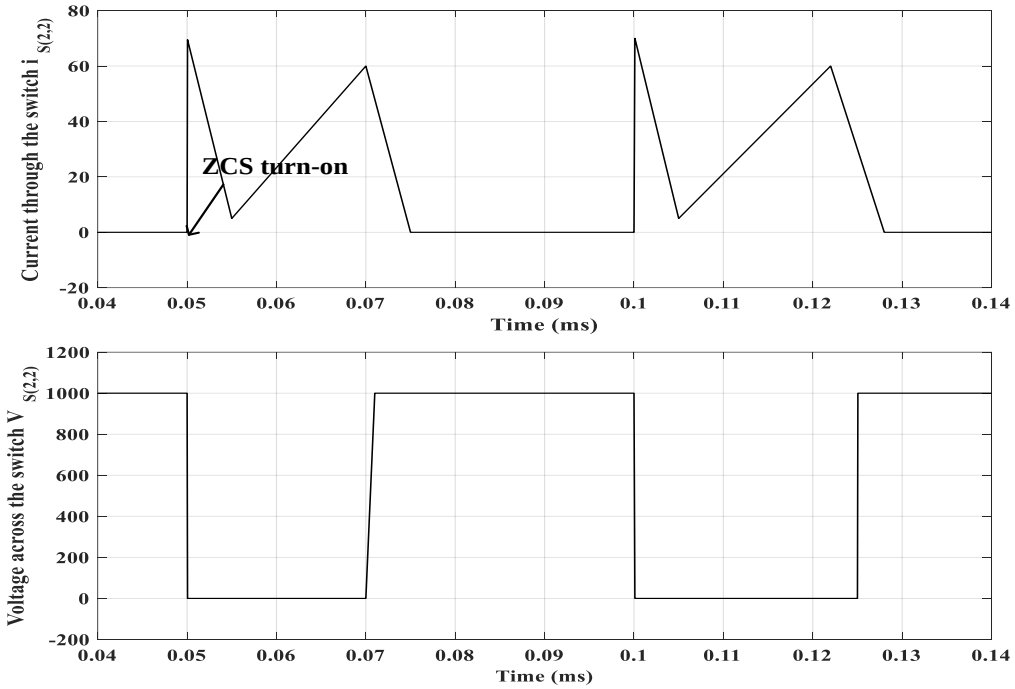

Fig 2.10 Current flowing through the switch and voltage across the switch $S_{2,2}$

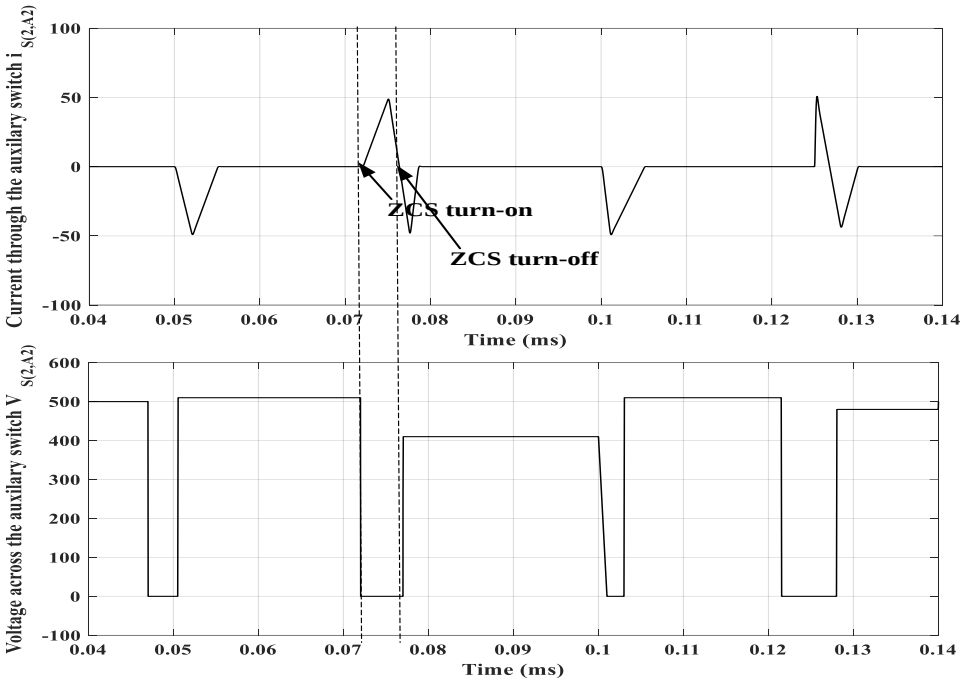

Fig 2.11Current flowing through the auxiliary switch and voltage across the auxiliary switch $S_{1, A1}$.

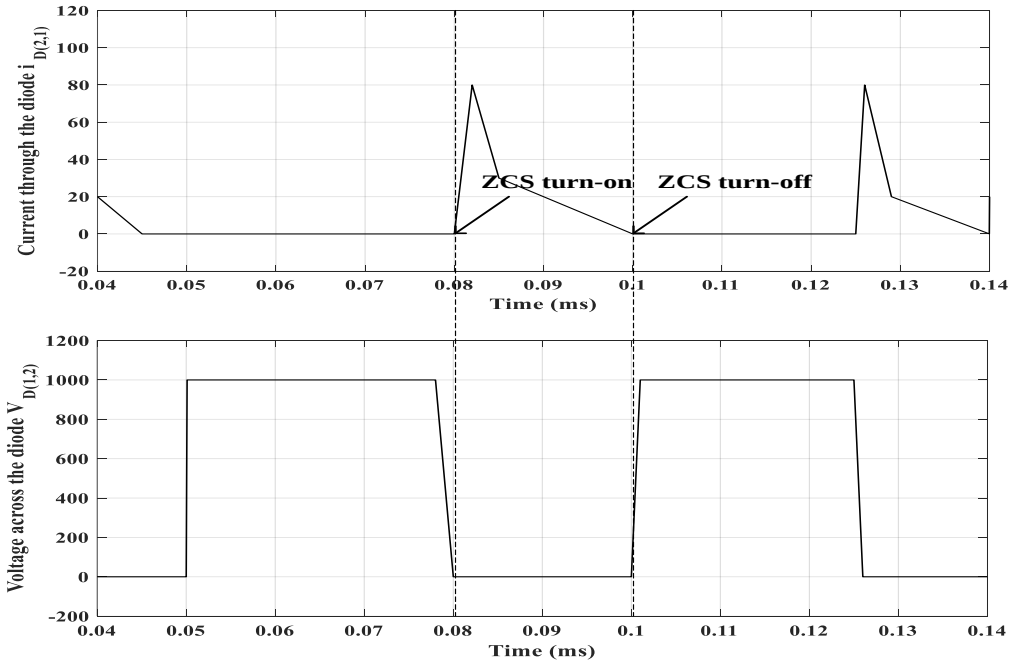

Fig 2.12Current flowing through the diode and voltage across the diode $D_{1,A1}$.

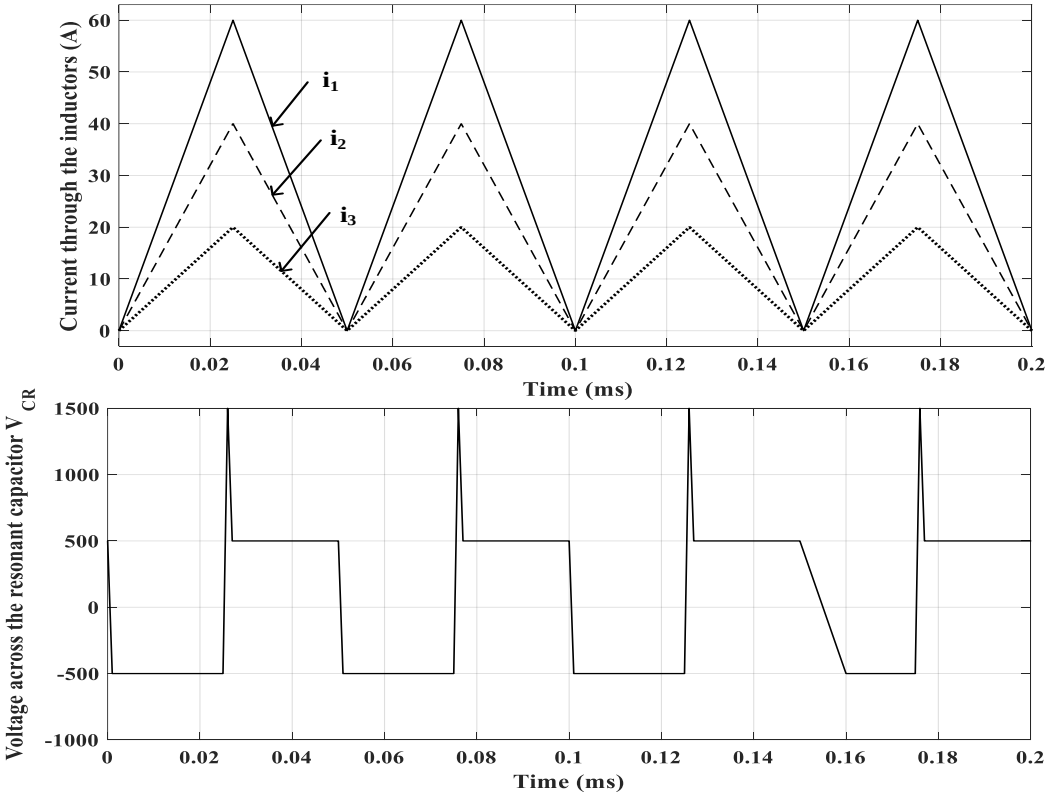

Fig 2.13Current flowing through the inductors ($L_{R1)}$ and voltage across the resonant capacitor $C_{R1.}$

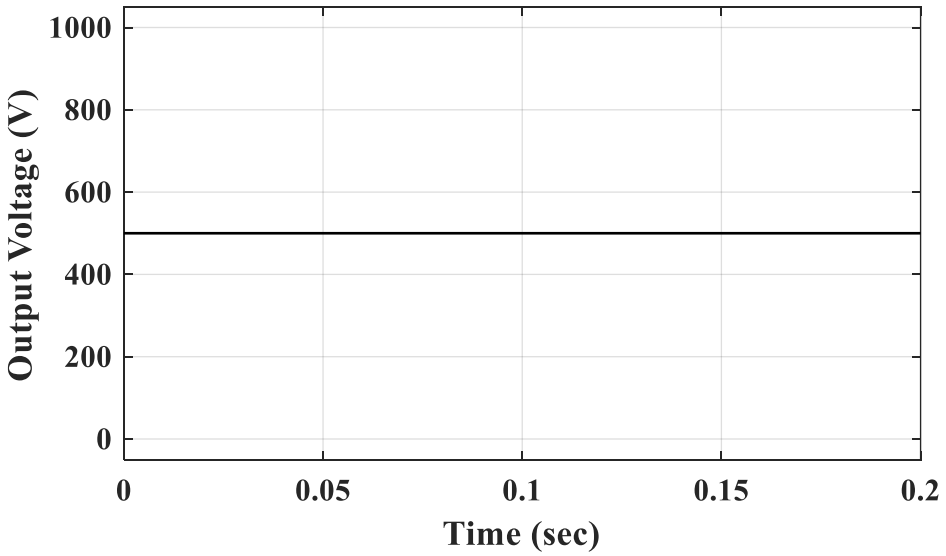

Fig.2.14 Output voltage

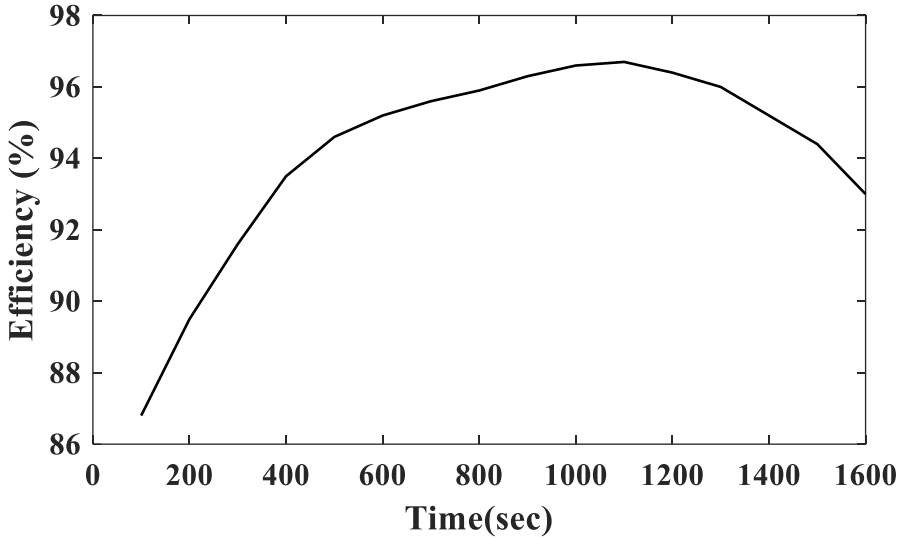

Fig.2.15 Efficiency of the proposed bipolar bidirectional DC-DC converter

2.5. Summary

In this chapter a non-isolated soft switching bi-polar bi-directional DC-DC converter for bi-polar DC micro-grids is proposed to achieve a high voltage gain. Zero current switching is proposed for this modular high gain DC-DC converter to obtain and low voltage stress across the switching devices and zero current transition in both boost mode and buck mode of operation. In the process output voltage control, voltage balance across the capacitors is achieved without any additional controller and control loop. Simulations results highlight the merits achieved from the proposed converter. Maximum efficiency in boost mode of operation and buck mode of operation are 96.2% and 96.6% respectively. This converter topology and control technique may also be suitable for HVDC applications and also electric vehicle charging stations.

Chapter-3

Bipolar Bidirectional DC-DC Converter with an Interleaved Switched Capacitor

3.1 Introduction

To achieve high voltage gain, a non-isolated bi-polar bi-directional DC-DC converter with an interleaved switching capacitor is presented in this chapter for bi-polar DC micro-grids appropriate for both low and high power applications. Interleaved structure on low voltage side is proposed to realize current sharing to reduce current ripple and switched capacitor topology is proposed on high voltage side to achieve high voltage gain. This converter's soft switching, high efficiency, and simple control structure make it suitable for use in a variety of applications such as electric vehicles, DC micro-grids with energy storage systems, and so on. To emphasize the benefits of the proposed converter architecture, detailed analysis, simulation, and hardware results are provided.

3.2 Bi-Polar Bidirectional DC-DC Converter with Interleaved Switched Capacitor

Schematic of the proposed bi-polar bi-directional DC-DC converter with switched capacitor is shown in Fig.3.1. It consists of an interleaved structure at a low voltage side and switched capacitor network at a high voltage side. This converter consists of six power switches (IGBTs) in which switches S_1, S_2 are controlled to operate the converter in boost mode of operation and the duty cycle for both the switches is same with the phase shift of 180^0 and switches S_3, S_4, S_5, S_6 are controlled to operate the converter in buck mode of operation and the duty cycle for the pair of switches (S_3, S_4 and S_5, S_6) is same with the phase shift of 180^0. Where i_{high} and i_{low} represents are the high-voltage side current and low-voltage side current respectively and the voltages V_L, V_{C1}, V_{H1}, V_{H2}, V_{C4} represents the voltages across capacitors C, C_1, C_2, C_3, and C_4 respectively. To achieve high voltage gain in boost mode of operation, the capacitors are charged in parallel and discharged in series and voltage balance is obtained by controlling the switch S_2. In buck mode of operation, the high step-down voltage gain is achieved with the two capacitors charging in series and discharging in parallel. Detailed operation of the proposed converter is discussed in subsequent sections.

3.2.1 Analysis of Bi-Polar Bidirectional DC-DC Converter with Interleaved Switched Capacitor

Steady-state analysis of proposed bi-polar bidirectional DC-DC converter shown in Fig.3.1 is discussed in detail for buck mode and boost mode of operation. For steady-state analysis of the converter, all the switching devices and the energy storage elements are considered as ideal and the current flowing through the inductor is continuous and the voltage across the capacitors is assumed constant.

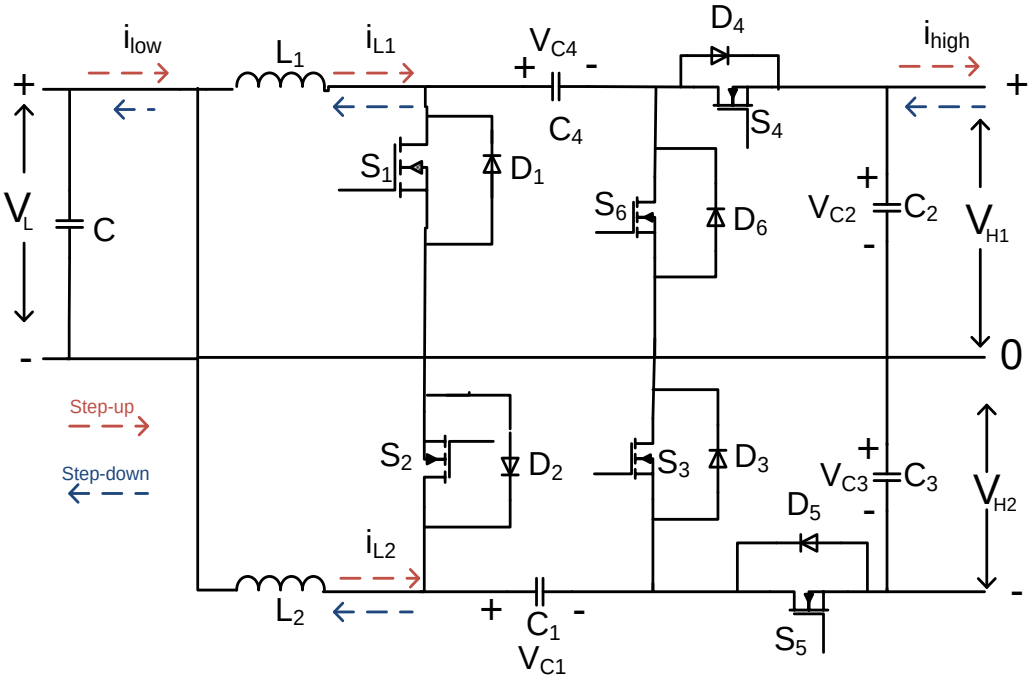

Fig 3.1. Schematic of the proposed converter topology

3.2.2 Boost mode of Operation

In this mode of operation the output voltage of the converter is stepped-up by regulating the switches S_1 and S_2 along with antiparallel diodes across the switches S_3, S_4, $S_5$and S_6 are in operation. To achieve the required voltage gain, duty ratio for S_1 and S_2 are kept same with a phase difference of 180°. The detailed operation of the converter in boost mode of operation is divided into three modes. Fig. 3.2 (a) & (b) represents the waveforms and principle of operation for boost mode respectively.

Mode I: In this mode of operation the switch S_1 is ON, and switch S_2 is OFF. The diodes D_3 and D_6 are ON, and the diodes D_4 and D_5 are OFF. Fig3.2(b) represents the direction of the current flow in inductors i.e i_{L1}, i_{L2}. The inductor L_1 and capacitor C_4 are charged by the DC source voltage V_L, and inductor L_2 and C_2 charges capacitor C_1, and C_3 starts discharging through the load on the high-voltage side.

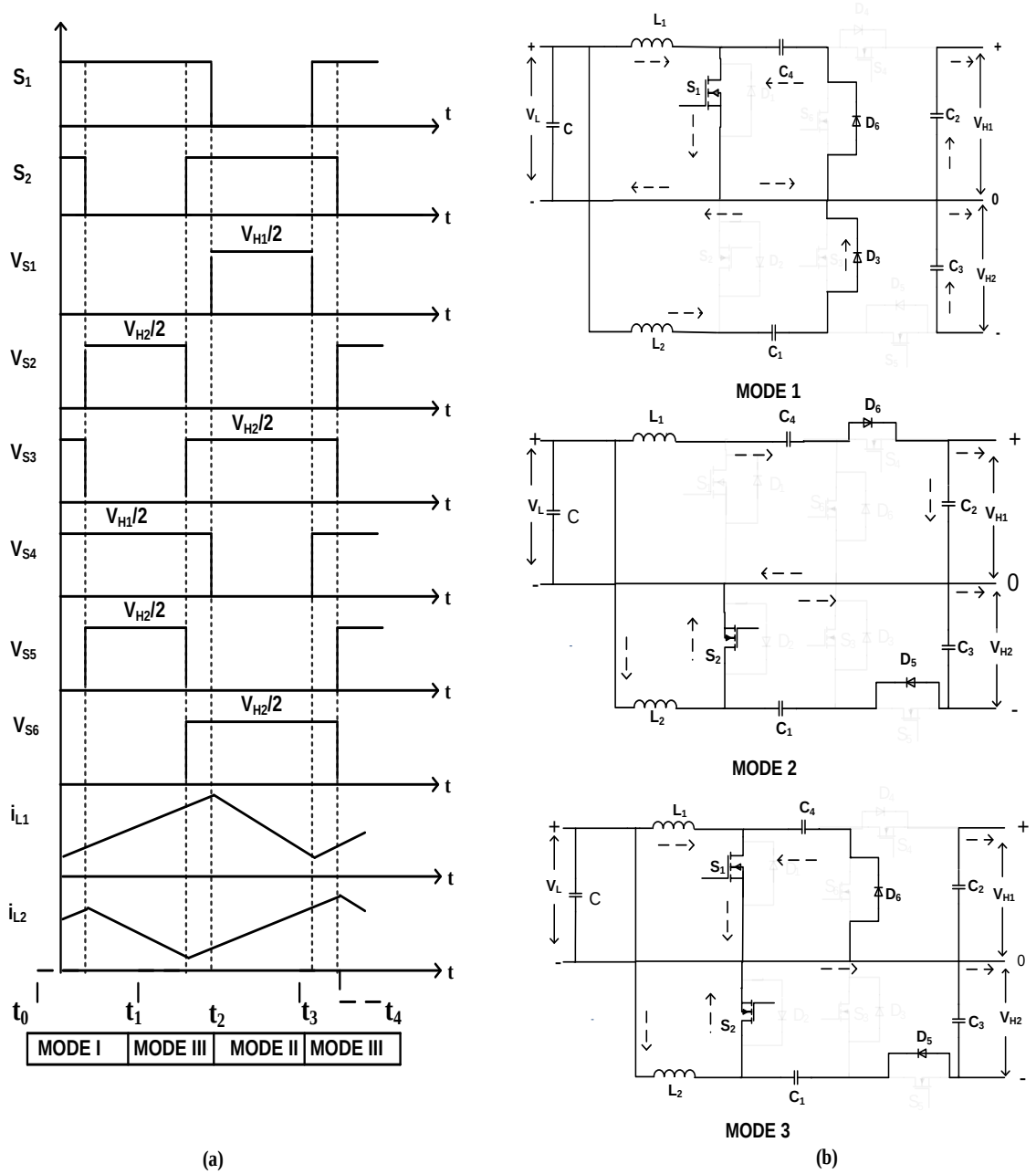

Fig 3.2(a). Waveforms for boost mode of operation in continuous conduction

Fig 3.2(b). Schematic modes of operation for the proposed topology in boost mode.

Mode II: In this mode of operation the switch S_1 is OFF, and switch S_2 is ON. The diodes D_3 and D_6 are OFF; and the diodes D_4 and D_5 are ON. Fig 3.2(b) represents the direction of the current flow in inductors i.e i_{L1}, i_{L2}. Inductor $L_1$and C_4 charges C_1 and C_2 charges the capacitor C_3. The output to the load is supplied by the DC source voltage V_L, and the circuit elements L_1, and C_1.

Mode III: In this mode of operation the switches S_1, S_2 is ON. The diodes D_3, D_4 is OFF, and the diodes D_5 and D_6 are ON. Fig 3.2(b) represents the direction of the current flow in inductors i.e i_{L1}, i_{L2} starts increasing, and capacitor C_1 and C_2 start discharging through the load.

3.2.3 Buck mode of operation

Output voltage of the converter is stepped-down by regulating the switches S_3, S_4, S_5, and S_6 along with antiparallel diodes of the switches S_1 and S_2. Control of the switches S_3 and S_4 are with a phase difference of 180°, and control of the switches S_5 and S_6 are complement to that of switches S_3 and S_4 respectively. The detailed operation of the converter in buck mode is divided into three modes .Fig 3.3 (a) & (b) represents the waveforms and principle of operation for buck mode respectively.

Mode I: In this mode of operation the switches S_3 and S_6 are turned ON and switches S_4 and S_5 are turned OFF. The diodes D_1 and D_2 are in non conducting mode (reverse biased). Fig. 3.3(b) represents the direction of current flow in inductors i.e i_{L1}, i_{L2}. Capacitor C_2 and C_3 are charged with the dc sources V_{H1} and V_{H2} respectively. The inductors L_1, L_2 and capacitors C_1,C_4 gives the output to the loads connected on low voltage side.

Mode II: In this mode of operation the switches S_3, S_4 are OFF, and the switches S_5, S_6 are ON. The diodes D_1 and D_2 are conducting (forward biased). Fig.3.3(b) represents the direction of current flow in inductors i.e i_{L1}, i_{L2} starts decreasing. Capacitor C_1 and C_2 are charged by the DC voltage source V_{H1}. The inductors L_1, L_2 and capacitor C_3 gives the output to the loads connected on low voltage side.

Mode III: In this mode of operation the switches S_3, S_6 are OFF, and the switches S_4, S_5 are ON, D_1 diode is reverse biased, and the D_2 diode is conducting. Fig.3.3(b) represents the direction of the current flow in inductors i.e i_{L1}, i_{L2} . Capacitor C_1 is charged by the dc source V_{H2} and C_3. Simultaneously V_{H2} and capacitor C_2 discharge through the load and supply energy to the inductor L_1.

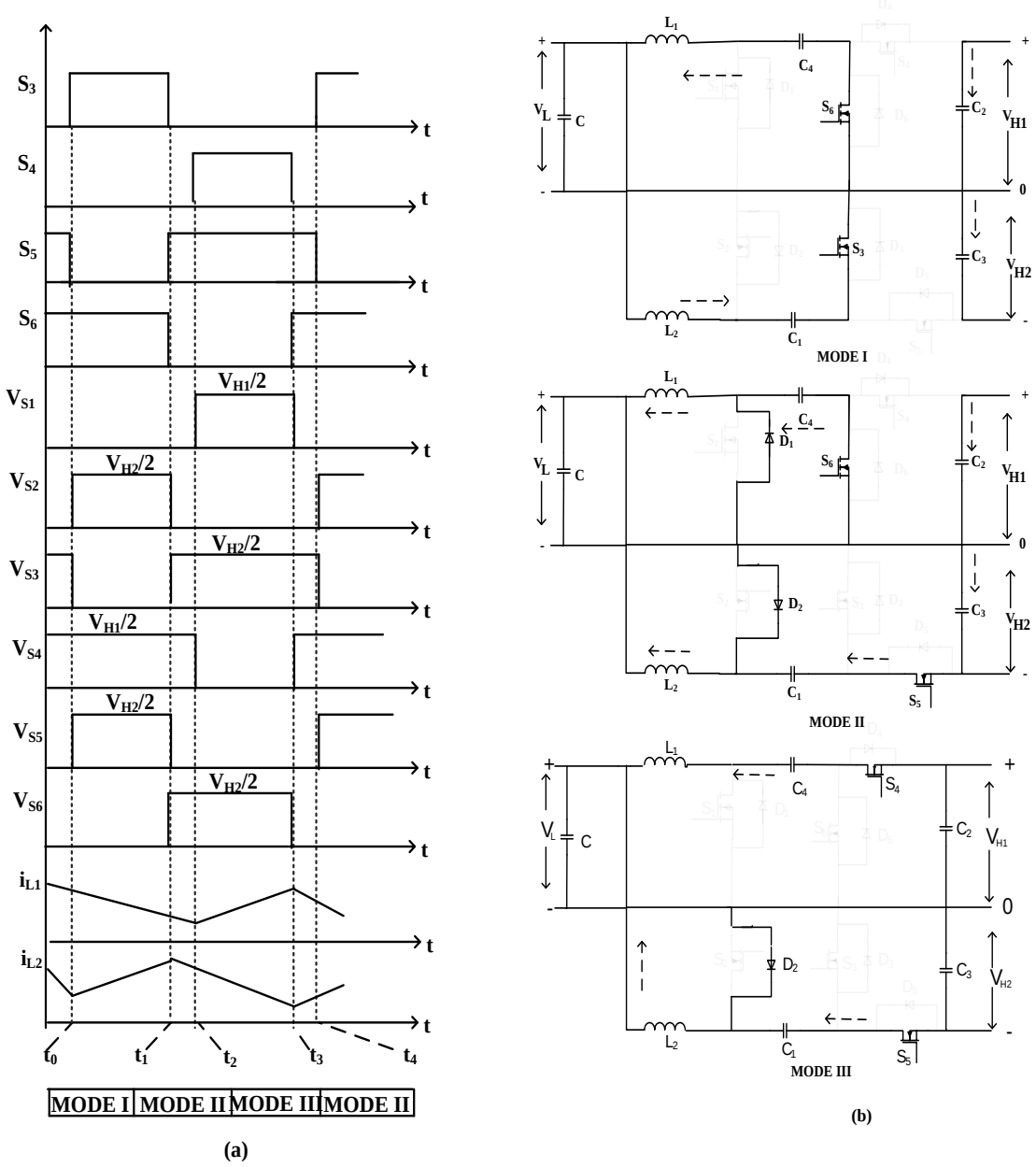

Fig 3.3(a). Waveforms for buck mode in continuous conduction mode

Fig 3.3(b). Schematic Modes of operation for the proposed topology in buck mode.

3.2.4 Control Strategy of the Converter

Fig 3.4 shows the control strategy for bi-directional power flow and also for voltage balance. The voltages V_{H1},$V_{H2,}$ and V_L and the inductor currents i_{L1},i_{L2} are obtained by hall effect voltage and current sensors and fed to digital signal processor TS320F28379D to implement the control strategy. According to the U_{ref} signal, the converter operates either in boost mode or in buck mode. When U_{ref} =1, the converter operates in the boost mode where the boost voltage V_H is controlled with reference voltage V_{ref} and the voltage balance between V_{H1} and V_{H2} is controlled by the PI regulator by setting the voltage error reference to zero. Simultaneously, the feedback inductor currents i_{L1}, i_{L2} is regulated by the current compensator with reference inductor i_{L1}^* and i_{L2}^* in the current-loop. The corresponding duty value obtained is compared with the carrier wave to generate the gate signals for S_1 andS_2 in the boost mode. Similarly, when U_{ref} =0, the converter operates in the buck mode where the buck voltage V_L is regulated by the voltage compensator with the voltage reference, and the current compensator controls the current i_L with the current reference. The resultant signal is compared with repeating sequences to generate the gate signals for S_3 –S_6 in the buck mode.

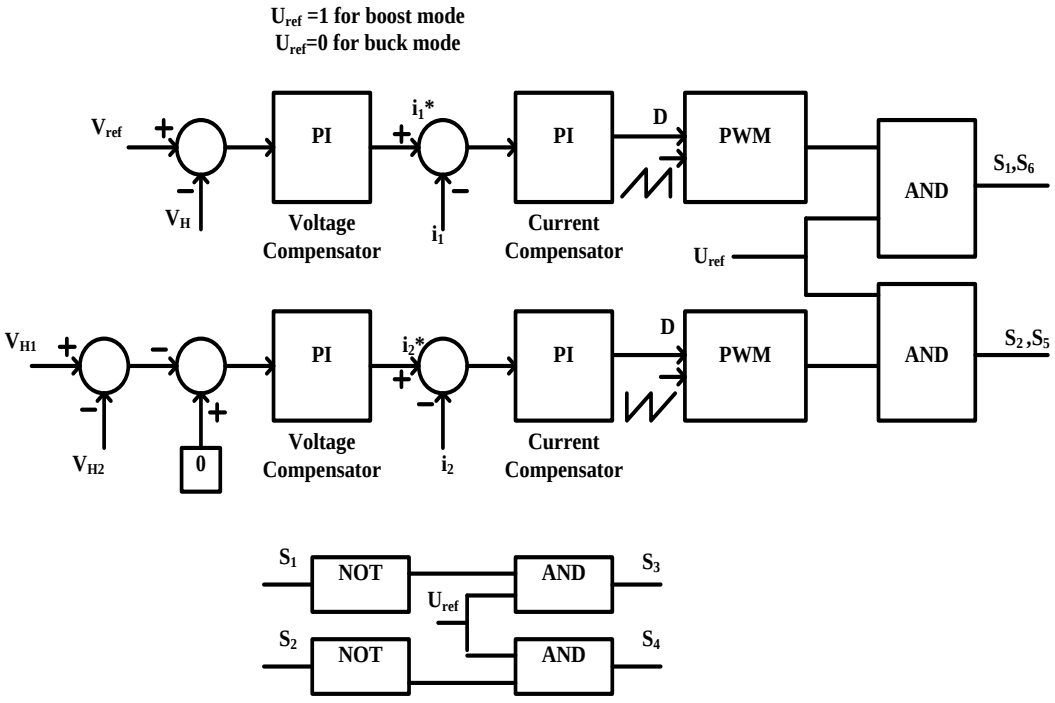

Fig 3.4. Control strategy for voltage balancing and bi-directional power flow.

3.2.5 Voltage Gain of the Converter

Analysis of the proposed converter w. r. t voltage gain, voltage stress across the switches, and current ripple in the converter are explained in detail. To simplify the analysis, all the switching devices and the energy storage elements are considered as ideal and the current flowing through the inductor is continuous and the voltage across the capacitors is assumed constant.

3.2.5.1 Voltage gain in boost mode

From Fig. 3.2(a) & Fig. 3.2.(b), in mode-1 of operation when switch S_1 is ON, the inductor current i_{L1} starts charging from the DC source V_L, and inductor current i_{L2} starts discharging to charge capacitor C_1, the discharge rate are given by

$$L_1 \frac{di_{L1}}{dt} = V_L$$

$$L_2 \frac{di_{L2}}{dt} = V_{C1} - V_L \tag{3.1}$$

From mode-2 operation, the switch S_2 is ON; the i_{L1} inductor current starts discharging to charge the capacitors C_4, C_2, and inductor current i_{L2} starts charging from the dc source V_L, the discharge rate are given by

$$L_1 \frac{di_{L1}}{dt} = V_{C2} - V_{C4} - V_L$$

$$L_2 \frac{di_{L2}}{dt} = V_L \tag{3.2}$$

From mode-3 operation, the switches S_1 and S_2 are turned ON, the inductor current i_{L1} and I_{L2} starts flowing from the dc source V_L, the discharge rates are given by

$$L_1 \frac{di_{L1}}{dt} = V_L$$

$$L_2 \frac{di_{L2}}{dt} = V_L \tag{3.3}$$

Since the capacitors C_1 and C_3, C_2, and C_4, are connected in parallel respectively, to make the voltages equal and the converter is assumed to operate in steady-state, the amount of energy stored in the inductor should be zero in one complete cycle. Therefore,

$$(\Delta i_{L1})_{ON} = (\Delta i_{L1})_{OFF}$$

$$(\Delta i_{L2})_{ON} = (\Delta i_{L2})_{OFF} \tag{3.4}$$

From equations (3.1), (3.2), (3.3)

$$V_{H1} = \frac{1}{1-D} V_L$$
$$V_{H2} = \frac{1}{1-D} V_L \quad (3.5)$$

3.2.5.2 Voltage gain in buck mode

From Fig. 3.3(a) & Fig. 3.3.(b), In mode-1 of operation, when switches S_3 and S_6 are turned ON, the inductor current i_{L1} starts discharging to the load V_L, and inductor current i_{L2} starts charging to charge C_1, the discharge rate is given by

$$L_1 \frac{di_{L1}}{dt} = \frac{V_L}{2}$$
$$L_2 \frac{di_{L2}}{dt} = V_{C1} - V_L \quad (3.6)$$

From mode-2 operation, when S_5 is ON; the inductor current i_{L1} and i_{L2} starts discharging to the load V_L, the discharge rate is given by

$$L_1 \frac{di_{L1}}{dt} = \frac{V_L}{2}$$
$$L_2 \frac{di_{L2}}{dt} = \frac{V_L}{2} \quad (3.7)$$

From mode-3 operation, when S_4 and S_5 are ON, the inductor current i_{L1} starts charging, and i_{L2} starts discharging to the load V_L, the discharge rate is given by

$$L_1 \frac{di_{L1}}{dt} = V_{H1} - V_L$$
$$L_2 \frac{di_{L2}}{dt} = \frac{V_L}{2} \quad (3.8)$$

The capacitors C_1 and C_3, C_2 and C_4, are connected in parallel respectively, to make the voltages equal. Since the converter is assumed to operate in an ideal state, the energy stored in the inductor should be zero in one complete cycle. Therefore,

$$(\Delta i_{L2})_{ON} = (\Delta i_{L2})_{OFF}$$
$$(\Delta i_{L1})_{ON} = (\Delta i_{L1})_{OFF} \quad (3.9)$$

From equations (3.6), (3.7), (3.8)

$$V_{H1} = \frac{V_L}{D}$$
$$V_{H2} = \frac{V_L}{D}$$
$$V_{H1} + V_{H2} = V_H$$

$$V_L = \frac{D}{2} V_H \tag{3.10}$$

3.2.5.3. Voltage stress across the switching device

From the boost mode and buck mode of operation of the converter shown in Fig 3.2(b) & 3.3(b), the switch S_1 is OFF, and S_4 is ON in mode-II; from that, it is observed that switch S_1 and capacitor C_2 are in parallel as a result the voltage across S_1 and C_2 are equal. Similarly, the voltage across S_2 and C_1, S_4 and C_2, S_3 and C_1, S_5 and C_3, S_6 and C_3 are equal. The voltage stress for the switching devices is:

$$V_{C1} = V_{C2} = V_{C3} = \frac{1}{1-D} V_L$$

$$V_H = \frac{2}{1-D} V_L$$

$$V_{S1} = V_{S2} = V_{S3} = V_{S4} = V_{S5} = \frac{V_H}{2} \tag{3.11}$$

3.2.5.4 Current ripple in the inductor

From the boost mode of operation explained in Fig. 3.2(a) & Fig. 3.2.(b), It is assumed that the L_1=L_2=L. From equations (3.1) and (3.2), the current ripple i_{L1}, i_{L2}, i_{low} is given by

$$\Delta i_{L1} = \frac{V_L * D * T_s}{L}$$

Where D=duty cycle

$$\Delta i_{L1} = \Delta i_{L2} = \frac{V_H * D * (1-D) * T_s}{2L} \tag{3.12}$$

From equation (3.1)

$$\Delta i_L = \frac{V_H * (1-D) * (2D-1) * T_s}{2L} \tag{3.13}$$

Similarly from the buck mode of operation explained in Fig. 3.3(a) & Fig. 3.3.(b), It is assumed that L_1=L_2=L. From equations (3.6) and (3.7), the current ripple i_{L1}, i_{L2}, i_{low} is given by

$$\Delta i_{L1} = \Delta i_{L2} = \frac{V_H * D * (1-D) * T_s}{2L} \tag{3.14}$$

From equation (3.6)

$$\Delta i_L = \frac{V_H * D * (1-2D) * T_S}{2L} \quad (3.15)$$

3.3 Simulation Results

To test the feasibility of the proposed bi-polar bi-directional DC-DC converter, simulation studies are carried out from the developed mathematical model of the converter using Matlab/Simulink and results are presented. Table –3.1 represents the specifications and parameters of various components of the converter.

Table-3.1. Converter parameters for the proposed topology-2.

Parameters	**Values**
Rated Power	10 kW
Capacitors values C_1, C_2,C_3,C_4	1000μF
Inductors L_1,L_2	1mH
Switching Frequency	20kHz
Boost voltage V_H	2000 V
Buck voltage V_L	500V

3.3.1 Simulation Results for Boost Mode of Operation

From the simulation results it is observed that for the input voltage of V_L=500V as shown in Fig 3.5(a), the inductor currents obtained with interleaving patterns are shown in Fig 3.5(b). From equation (3.12), the theoretical ripple for inductor currents is 3.125%. The source current i_{low} is shown in Fig 3.5(c). The current ripple from equation (3.13) it is calculated as Δi_{low} is 0.2%. It is noted from the results that the proposed converter behavior w.r.t source current ripple and ripple of the inductor current is close to theoretical values, and source current is continuous with zero ripple. The input power is shown in Fig 3.5(d). The output voltage of positive pole V_{H1}, negative pole V_{H2} are shown in Fig 3.6(a), and boost voltage V_H is shown in Fig 3.6(b). The load currents are shown in Fig 3.6(c) and the output power is shown in Fig 3.6(d). The voltage stress across the switching devices is 200V i.e., half of the boost operation voltage is shown in Fig 3.7(a). The capacitor voltage V_{C1} is 200V i.e., half of the boost operation voltage with a very small ripple as shown in Fig 3.7(b).

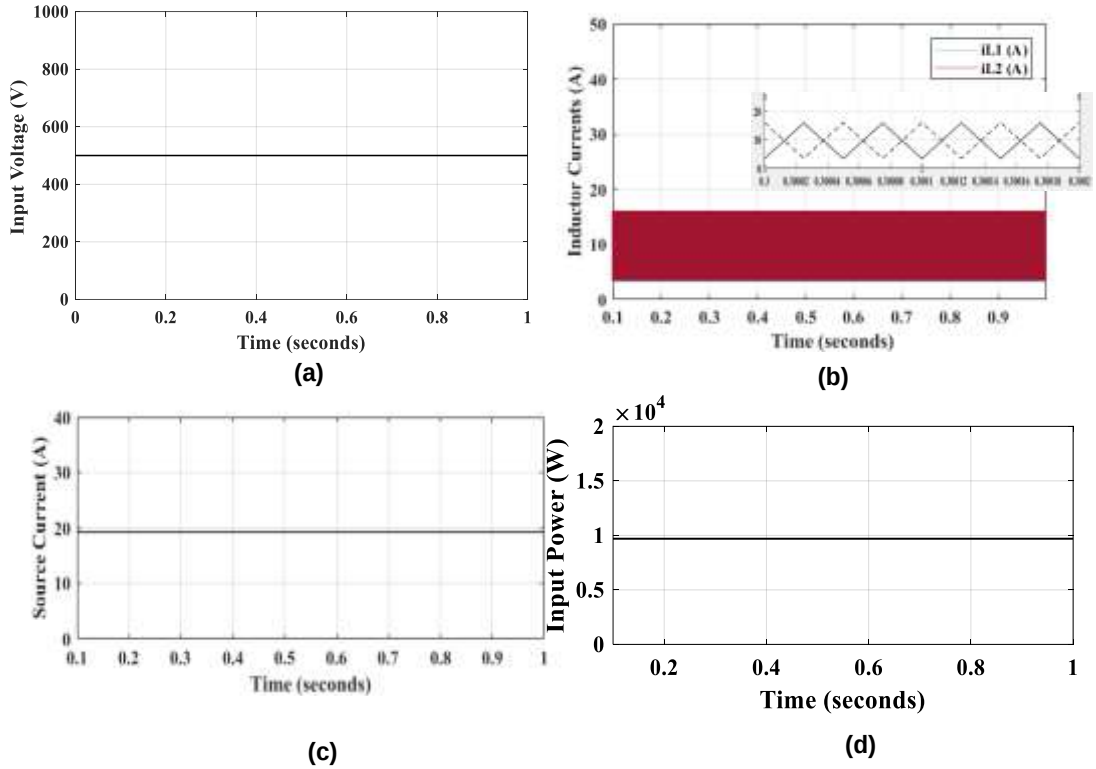

Fig 3.5. Simulation results in boost mode (a) Input voltage (b) Inductor currents with interleaving pattern. (c) Source current i_{low} (d) Input power

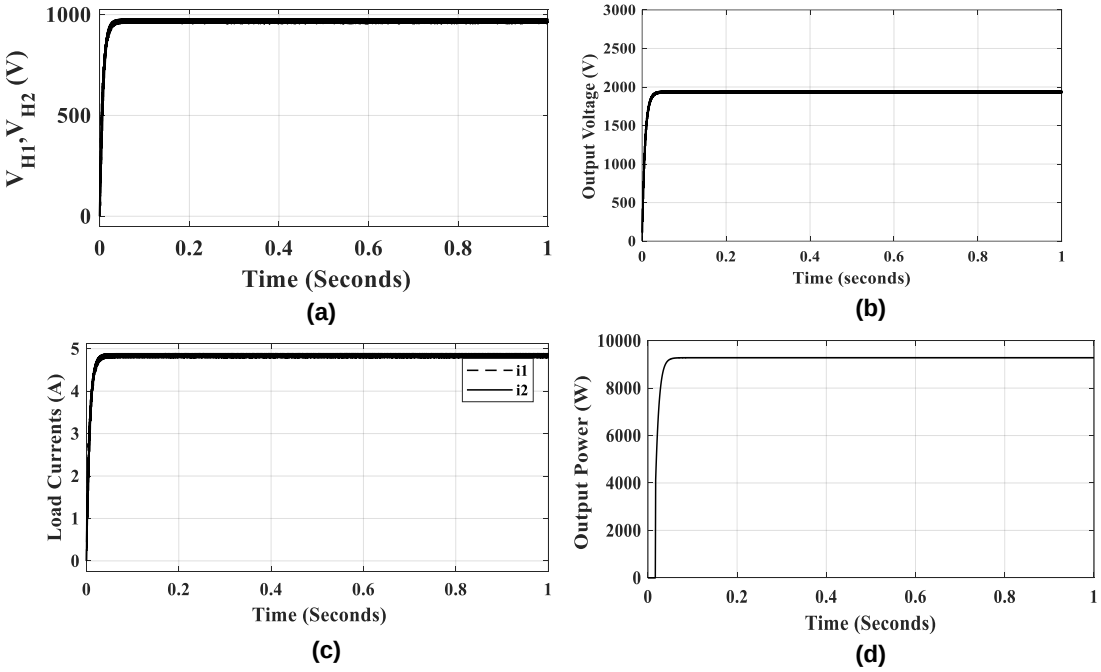

Fig 3.6. Simulation results in boost mode (a) Output voltages V_{H1}, V_{H2}. (b) Total boost voltage (c) Load current i_1, i_2 (d) Output power

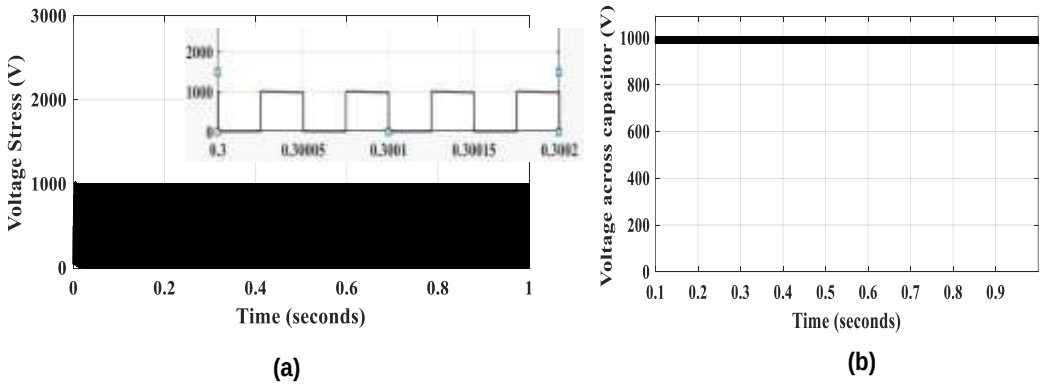

Fig 3.7. Simulation results in boost mode (a)Voltage stress across the switching devices (b) Voltage across capacitor V_{C1}

3.3.2 Simulation Results for Buck Mode of Operation

From the simulation results it is observed that for an input voltage of V_H=2000V as shown in Fig 3.8(a), the input current is shown in Fig 3.8(b) and the input power is shown in Fig 3.8(c).

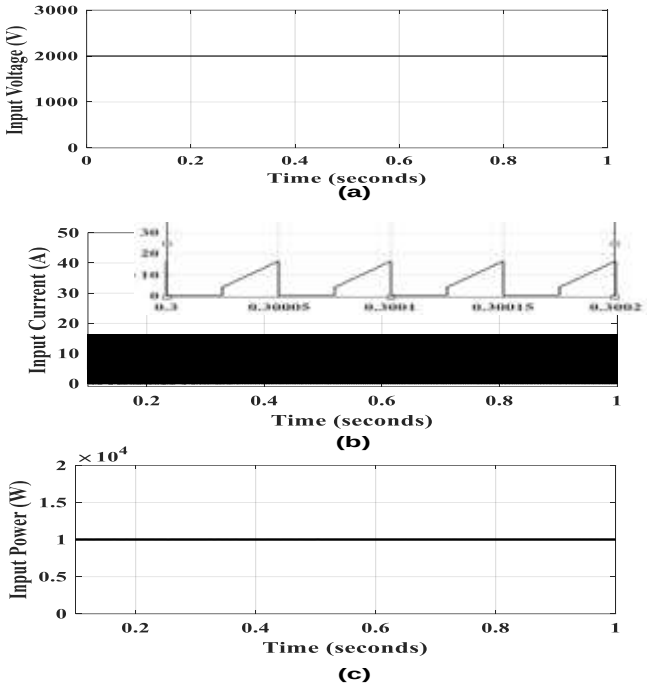

Fig 3.8. Simulation results in buck mode (a) Input voltage (b) Source current i_{low} (c) Input power

The output voltage V_L is shown in Fig 3.9(a), the inductor currents representing interleaving patterns are shown in Fig 3.9(b).Current ripple for i_{L1} and i_{L2} is 3%. From

equation (14), the theoretical value of ripple for inductor currents is 3.125%. The load current i_{low} is shown in Fig 3.9 (c). The load current ripple from the experimental result is Δi_{low} is 2%.

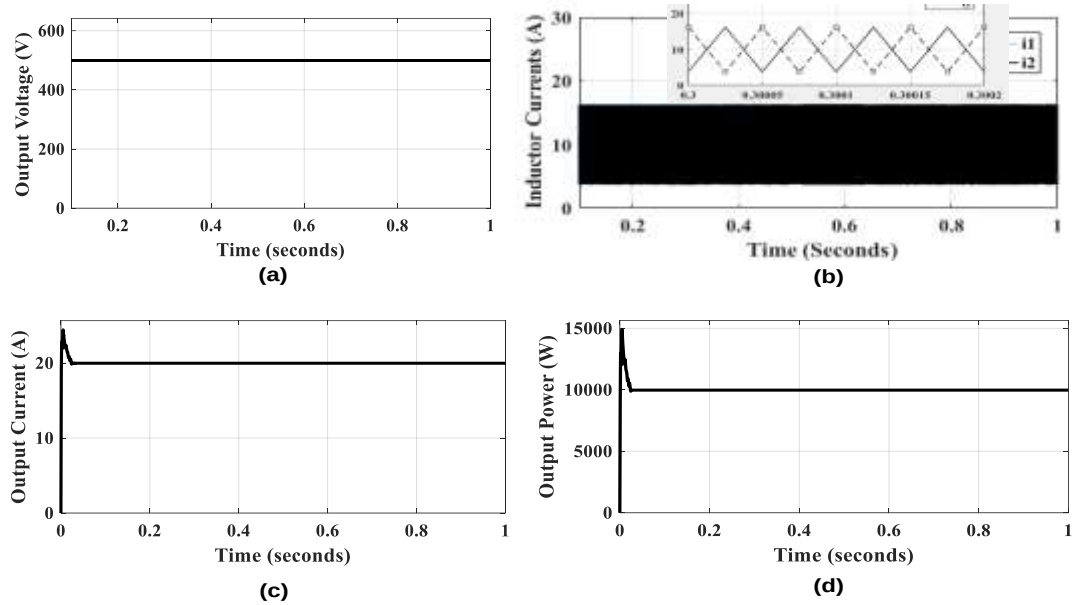

Fig 3.9. Simulation results in buck mode (a) Output voltage. (b) Inductor currents with interleaving pattern.(c) Load current (d) Output power

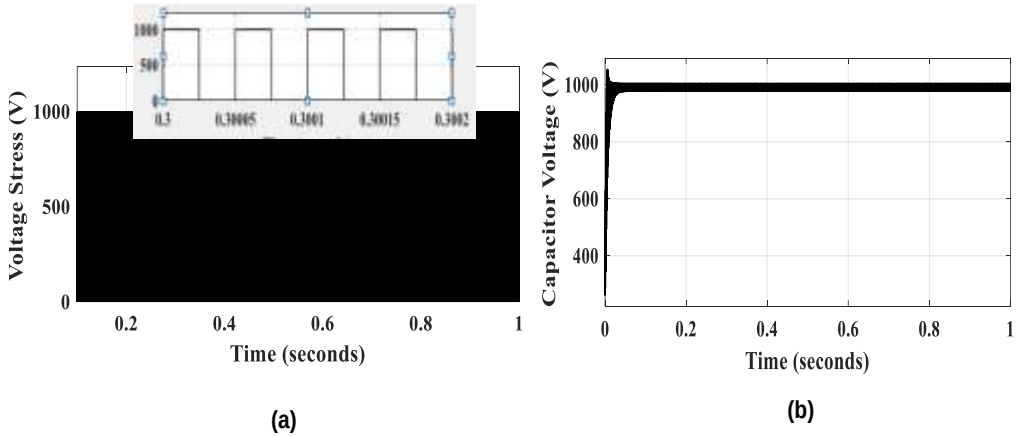

Fig 3.10. Simulation results in buck mode (a) Voltage stress across the switching devices. (b) Voltage across capacitor V_{C1}

From equation (15), the theoretical value of ripple Δi_{low} is 2%. From the results, it is verified that the proposed converter behavior w.r.t to load current ripple and ripple of the inductor current is close to theoretical values and the output power is shown in Fig 3.9(d). Voltage stress across the switching devices is 200V, which is half of the input voltage is shown in Fig 3.10(a) and the voltage across the capacitor V_{C1} is 200V i.e., half of the input voltage with small ripple is shown in Fig 3.10(b).

3.4 Simulation and Experimental Results for Low Power

To validate the proposed bi-polar bi-directional DC-DC converter, a 500 Watt lab scale prototype was designed and fabricated. This low power proposed bi-polar bi-directional DC-DC converter with interleaved converter is simulated with Matlab/Simulink and these simulation results compared with the experimental results of to validity the proposed converter topology.

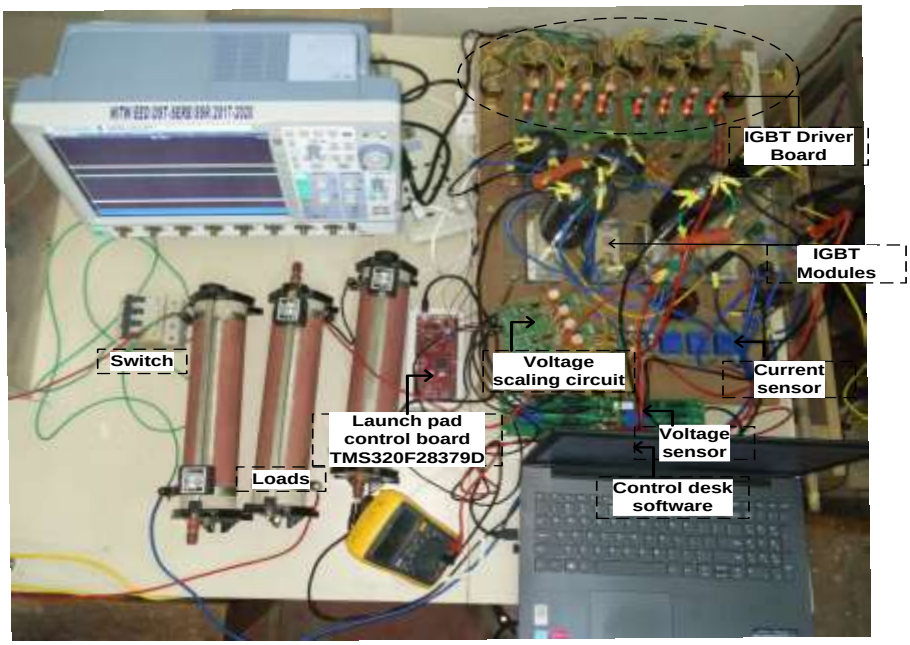

Fig 3.11. Experimental prototype of bi-polar bi-directional DC-DC converter

Fig 3.11 shows the experimental prototype of bi-polar bi-directional DC-DC converter. Table 3.2 represents the specifications and parameters of the lab scale prototype. Simulation and experimental results are presented for boost mode and buck mode of operation.

Table 3.2 Experimental parameters for the proposed topology-2.

Parameters	**Values**
Rated Power	500 W
Switched Capacitors values C_1,C_2,C_3,C_4	1000µF
Filter Inductors L_1,L_2	520µH
Switching Frequency	20kHz
Boost voltage V_H	400 V
Buck voltage V_L	50V

3.4.1 Boost Mode of Operation

For an input voltage of V_L=50V, the inductor currents with interleaving patterns are shown in Fig 3.12(a). From the experimental waveforms various performance parameters are obtained and are compared with the simulated values. Ripple of inductor currents i_{L1} and i_{L2} from the simulation and experimental result is 29.1%. From equation (3.12), the theoretical ripple value for inductor currents is 30.5%. The source current i_{low} is shown in Fig 3.12(b).The current ripple from the simulation and experimental result is Δi_{low} is 18.3%, whereas from equation (3.13) theoretical it is calculated as Δi_{low} is 20%. It is noted from the simulation and experimental results that the proposed converter behavior w.r.t source current ripple and ripple of the inductor current is close to theoretical values, and source current is less than the inductors ripple current. The output voltage of positive pole V_{H1}, negative pole $V_{H2,}$ and boost voltage V_H is shown in Fig 3.12(c) and 3.12(d). The capacitor voltage V_{C1} is 200V i.e., half of the boost voltage with a very small ripple is shown in Fig 3.12(f) and 3.12(i). The voltage stress across the switching devices is 200V i.e., half of the boost voltage is shown in Fig 3.12(e) and 3.12(i). Further, the load variations considered at t=0.5sec, the output power varies from 300W to 400W. The voltage balance between positive pole V_{H1} and negative pole V_{H2} is zero, and the output voltage is constant with the reference voltage of 400V. The output voltage, the load current, is shown in Fig 3.13. When V_H is constant at 400V, and V_L changes continuously between 50V and 120V, the efficiency for boost operation of the proposed converter with different power levels are shown in Fig 3.15(a) and it is observed that the maximum efficiency occurred at 96.6% at a load of 80 Ω.

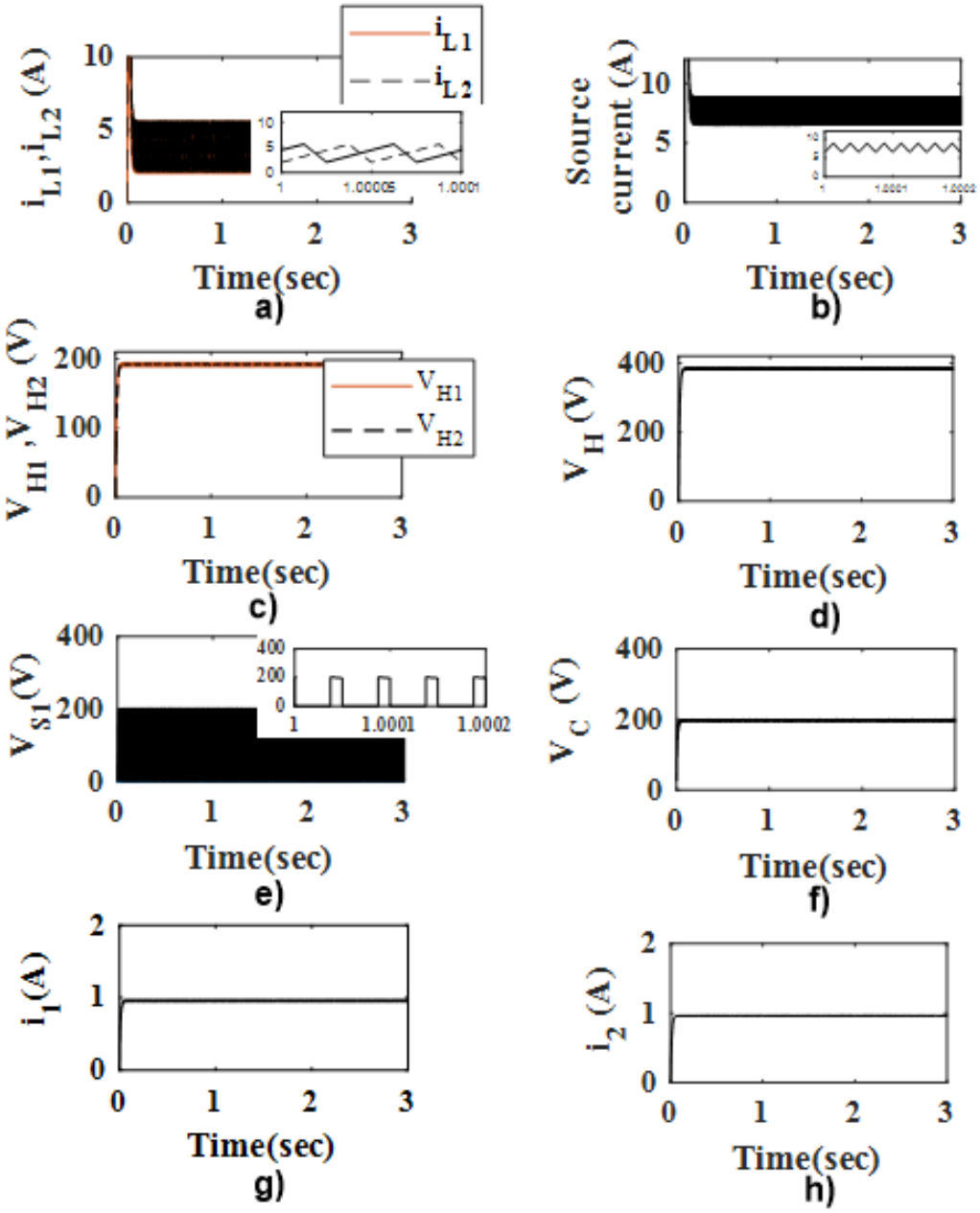
i_{L1}
i_{L2}
i_{L1},i_{L2} (A)
Time(sec)
a)
Source current (A)
Time(sec)
b)
V_{H1}
V_{H2}
V_{H1} ,V_{H2} (V)
Time(sec)
c)
V_H (V)
Time(sec)
d)
V_{S1}(V)
Time(sec)
e)
V_C (V)
Time(sec)
f)
i_1(A)
Time(sec)
g)
i_2 (A)
Time(sec)
h)

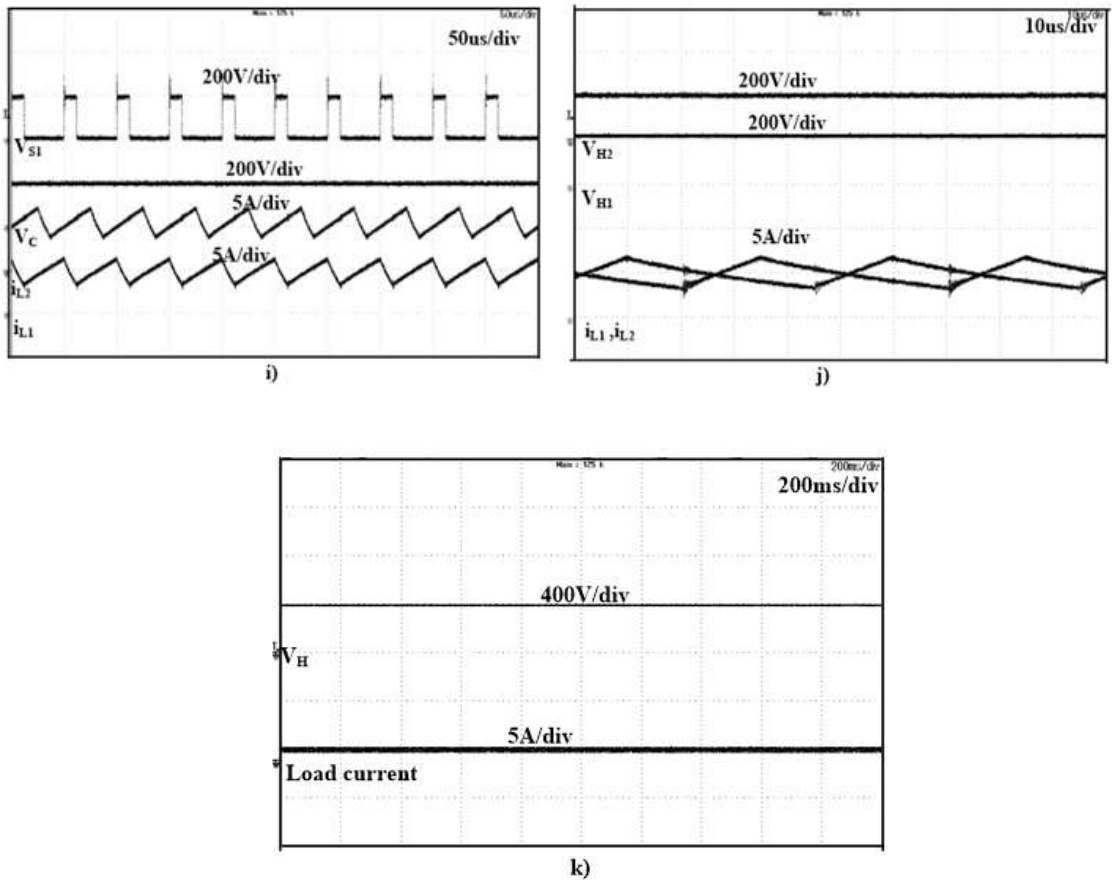

Fig 3.12. Simulation and Experimental results in boost mode

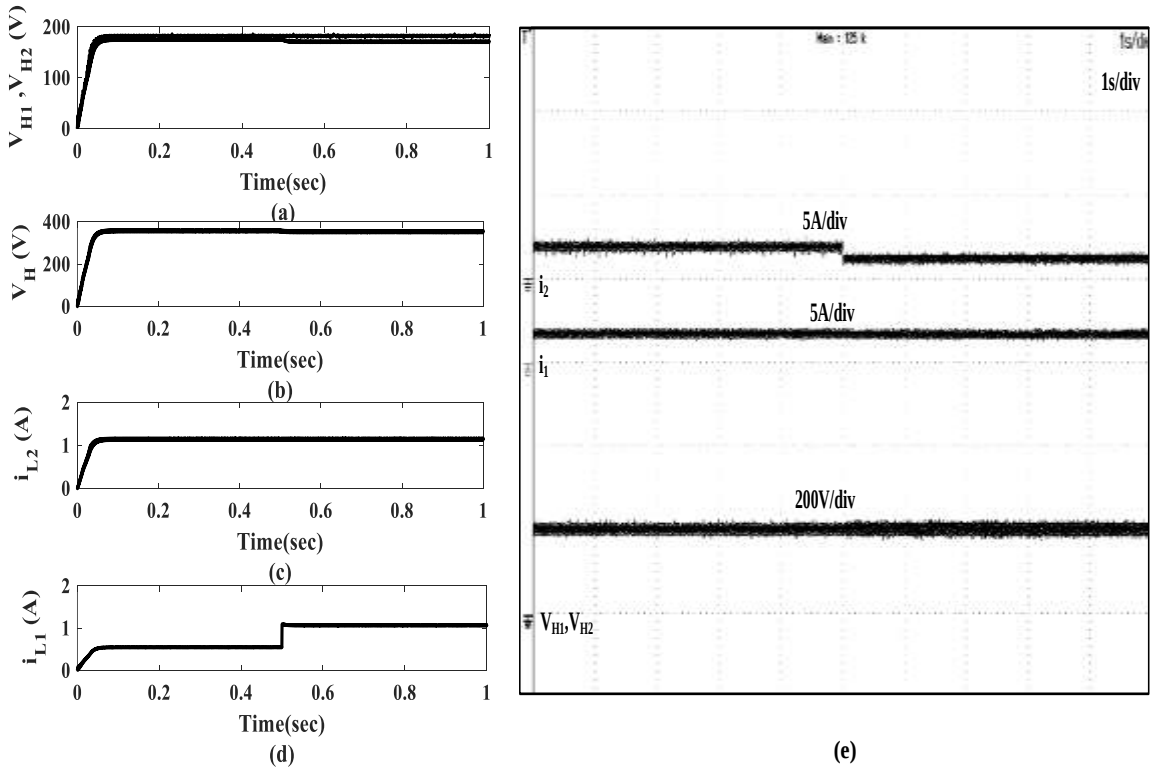

Fig 3.13. Simulation and Experimental results in boost mode with closed-loop controller

3.4.2 Buck Mode of Operation

For an input voltage of V_H=400V, the inductor currents representing interleaving patterns are shown in Fig 3.14(a) and 3.14(f). From the experimental waveforms various performance parameters are obtained and are compared with the simulated values and theoretical values. Current ripple for i_{L1} and i_{L2} is 22.6% from simulation and experimental results. From equation (3.14), the theoretical value of ripple for inductor currents is 24.05%. The load current i_{low} is shown in Fig 3.14(b). The load current ripple from the simulation and experimental result is Δi_{low} is 14.6%. From equation (3.15), the theoretical value of ripple Δi_{low} is 16%. From the simulation and experimental results, it is verified that the proposed converter behavior w.r.t to load current ripple and ripple of the inductor current is close to theoretical values. The output voltage V_L is shown in Fig 3.14(c) and 3.14(f). The voltage across the capacitor V_{C1} is 200V i.e., half of the input voltage with small ripple is shown in Fig 3.14(d) and 3.14(f). The source current is shown in Fig 3.14 (e) and 3.14(g). Voltage stress across the switching devices is 200V, which is half of the input voltage as shown in Fig 3.14(f) and 3.14(g). When V_H is constant at 400V, and V_L changes continuously between 50V and 120V, the efficiency for buck operation of the proposed converter with different power levels are shown in Fig 3.15(b) and it is observed that the maximum efficiency occurred at 96.6% at a load of 2.5 Ω.

3.4.3 Power Loss Calculations

Calculation of power loss using thermal analysis in MATLAB was performed for V_L=50V, V_H=400V, P=1000W are shown in Figure 10. The total losses in boost mode on the converter are 40.48 W. Figure 10 (a) shows 85% of total losses are due to switching of the devices. The condenser losses and copper losses represent 12% of total losses, and the core losses represent 3% of total losses. The converter's total power loss in buck mode is 38.46 W. Figure 10 (b) shows the distribution of the losses.

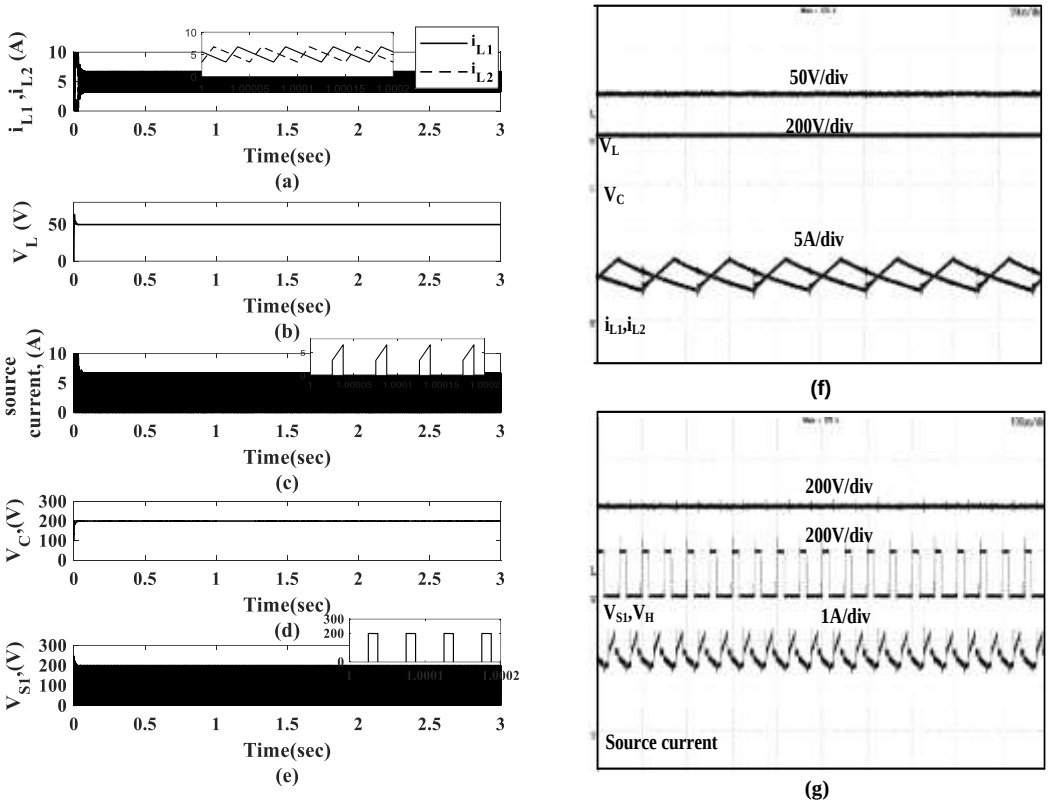

Fig 3.14. Simulation and Experimental results in buck mode.

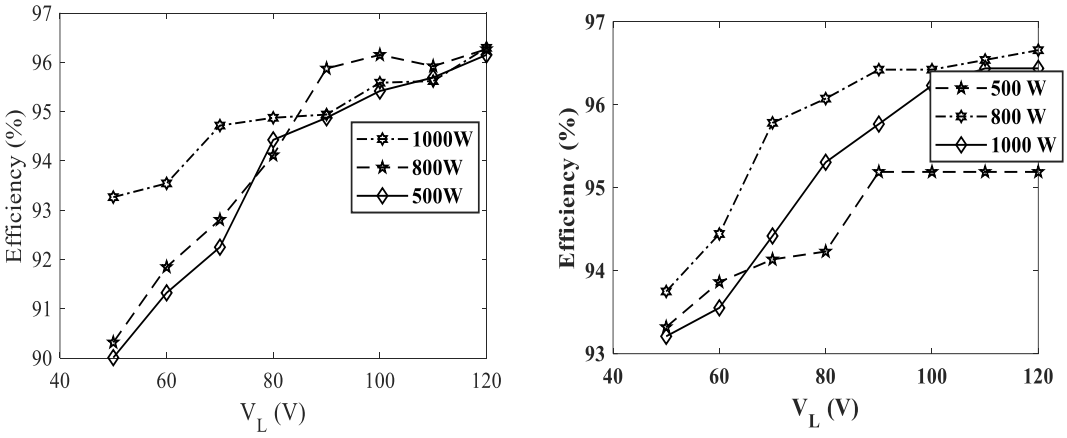

Fig 3.15. Efficiencies of the bipolar BDC converter

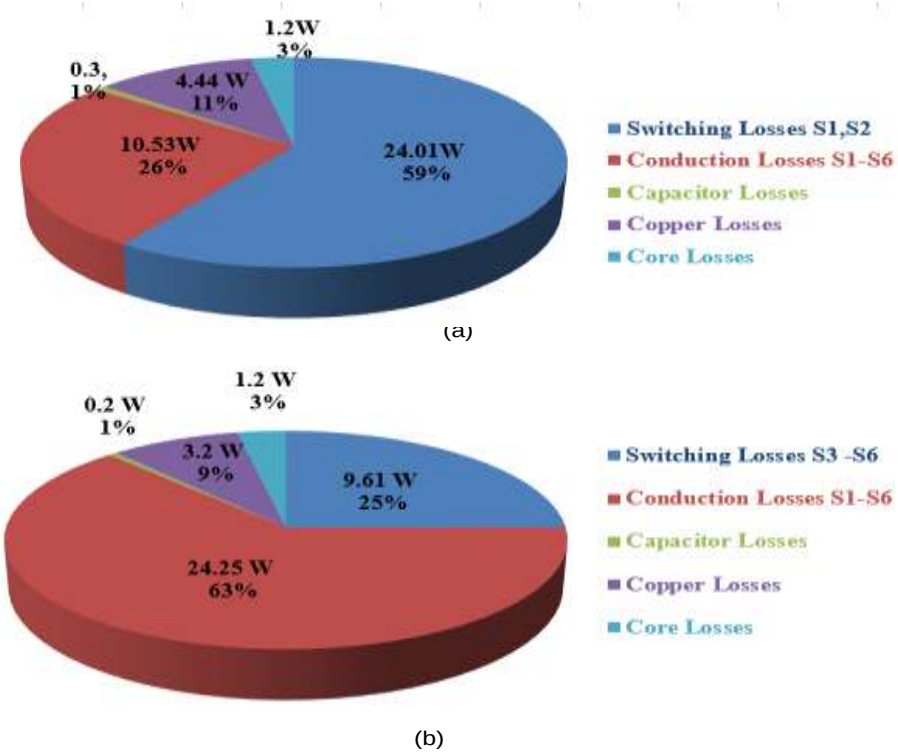

Fig 3.16. Power loss distribution for the proposed bipolar BDC.

The significant power losses are due to the switching of devices is around 88% of total losses. The condenser losses and copper losses represent 10% of total losses, and the core losses represent 3% of total losses.

3.5 Summary

In this chapter a non-isolated bipolar bi-directional DC-DC converter with an interleaved switched capacitor is proposed for bipolar DC micro-grids suitable for both low power and high power applications to achieve high voltage gain. The proposed converter topology is simulated for high power and low power levels in buck mode and boost mode of operation. Further a 500W lab scale prototype is fabricated and verified at a duty cycle of 0.75 to achieve a voltage gain of 8. To accomplish high voltage gain and less switch voltage stress, a zero voltage switching in both boost mode and buck mode of operation is implemented. Further, the proposed control strategy offered a reduced current ripple in the inductors and voltage balance across the output capacitor. The maximum efficiencies in boost and buck mode are 96.2% and 96.6% respectively. The proposed converter can be one of the alternative choices for DC micro-grids with energy storage systems.

Chapter-4

Bipolar Bidirectional DC-DC Converter Topology with Coupled Inductor

4.1. Introduction

For bi-polar DC micro-grids, this chapter proposes a non-isolated bi-polar bidirectional DC-DC converter with linked inductors and switching capacitor. To achieve high voltage gain, this suggested converter operates in both buck and boost mode and is ideal for both low and high power applications. With the combination of the clamping circuit and leakage inductance, all switching devices achieve zero voltage switching. The PI controller is used to connect an energy storage system to the grid in order to accomplish bidirectional power flow, grid voltage balancing, and effective voltage regulation. The soft switching characteristic of the power devices provides excellent efficiency for the converter, and the easy control strategy allows this converter to be used in a variety of applications such as DC micro-grid energy storage systems, electric car charging stations, and so on. To emphasise the benefits of the suggested converter architecture, detailed analysis and simulation results are provided.

4.2. Bipolar Bidirectional DC-DC Converter Topology with Coupled Inductor

The schematic diagram of bi-polar bidirectional DC-DC converter for Solar Photo Voltaic (SPV) based DC micro-grid is shown in Fig.4.1. It consists of a bi-polar bidirectional DC-DC converter, Solar panels, Load and an energy storage system. The bi-polar bidirectional DC-DC converter is connected between battery of nominal voltage 100V and dc micro-grid which allows the power flow in both directions. i.e from grid to battery or battery to grid. The power flow direction is determined by the variations in grid voltage and battery state of charge. The bi-polar bidirectional DC-DC converter consists of four IGBTs S_1-S_4, clamping capacitor C_1, coupled inductors L_1 and L_2 which forms a primary and secondary winding of transformer. Capacitor C_1 along with switch S_2 acts as clamping network which is used for soft switching under ZVS condition to turn-on switch S_1 and also the capacitor C_1 forms the charging path to the capacitor C_2, it contributes to voltage conversion ratio. The power flow direction in boost mode is from battery to grid and the power flow direction in buck mode is from grid to battery. Detailed operation of the proposed converter is discussed in subsequent sections.

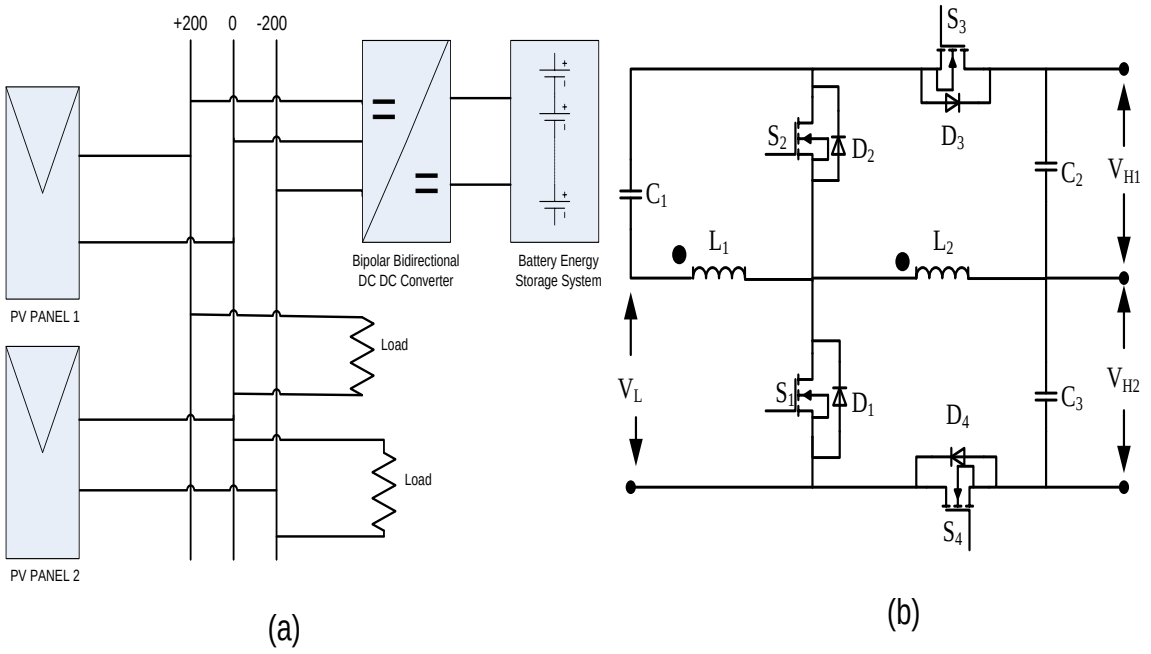

Fig. 4.1(a).Schematic representation of micro-grid with energy storage system.

Fig. 4.1(b).Schematic of proposed bi-polar bidirectional converter in DC micro-grids

4.2.1. Analysis of Proposed Topology-3

Steady-state analysis of proposed bi-polar bidirectional DC-DC converter shown in Fig. 4.1 is discussed in detail for buck mode and boost mode of operation. For steady-state analysis of the proposed converter, all the switching devices and the energy storage elements are considered as ideal, the voltage across the capacitors is assumed constant and coupled inductors are considered as ideal transformer with turns ratio L_2/L_1. Magnetizing and leakage inductance of the inductors are referred to primary side of the ideal transformer.

4.2.1.1 Boost mode of Operation

In this mode of operation the output voltage of the converter is stepped-up controlling the the switch S_1 along with conduction of switches S_2, S_3 and S_4. To achieve the required voltage gain, duty ratio for S_1 and S_3 are considered same and duty ratio for S_2 and S_4 are kept same with a phase difference of 180°. The detailed operation of the converter in boost mode is divided into six modes. Fig. 4.2 (a) & (b) represents the waveforms and principle of operation for boost mode respectively.

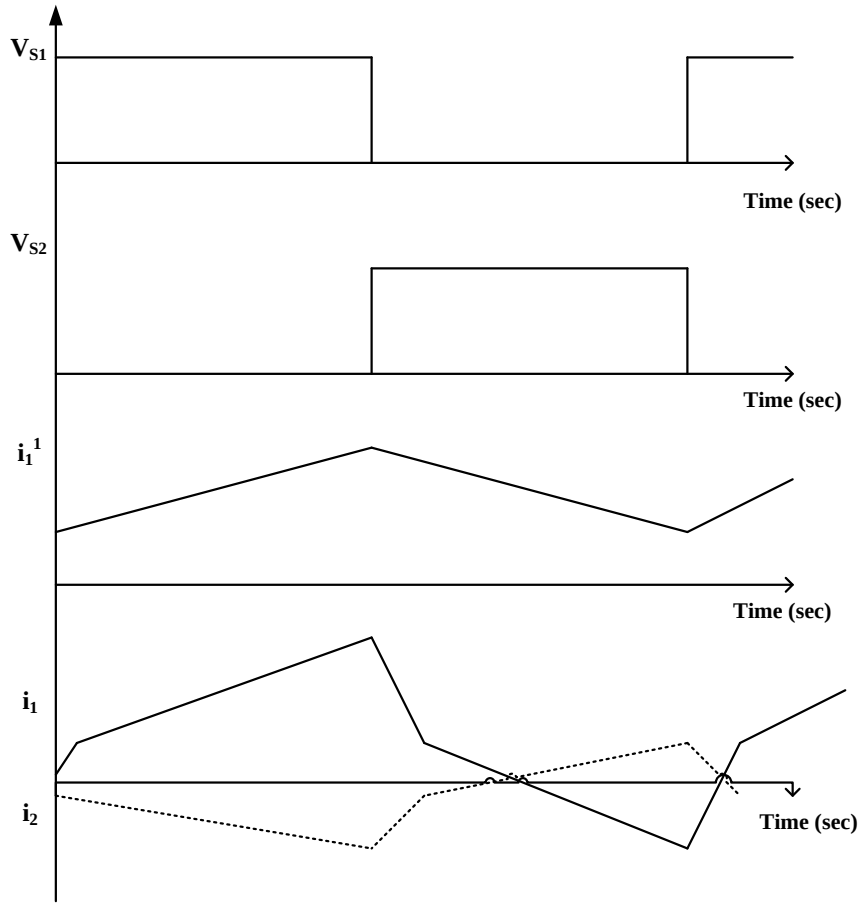

Fig 4.2. Waveforms for continuous conduction mode in boost operation

Mode I: In this mode of operation the switch S_1 is ON and diode D_3 is conducting during zero current switching (ZCS) condition. Fig 4.3 represents the direction of the current flow in the inductors.The inductor L_m is charged by the DC source voltage V_L. The capacitor C_3 is charged by the DC source voltage V_L, C_1 and L_2. Capacitor C_2 is discharged through the load. The mode of operation ends when switch S_1 is OFF and during this interval inductor currents starts increasing.

Mode II: In this mode of operation the switch S_2 is ON and diode D_3 is conducting (forward biased) during zero voltzge switching (ZVS). Fig 4.3 represents the direction of the current flow in inductors. The leakage inductor voltage is reversed and current in the inductor L_2 starts increasing upto certain duration and when inductor current drops to zero, diode D_3 is reverse biased and ZCS condition is achieved.

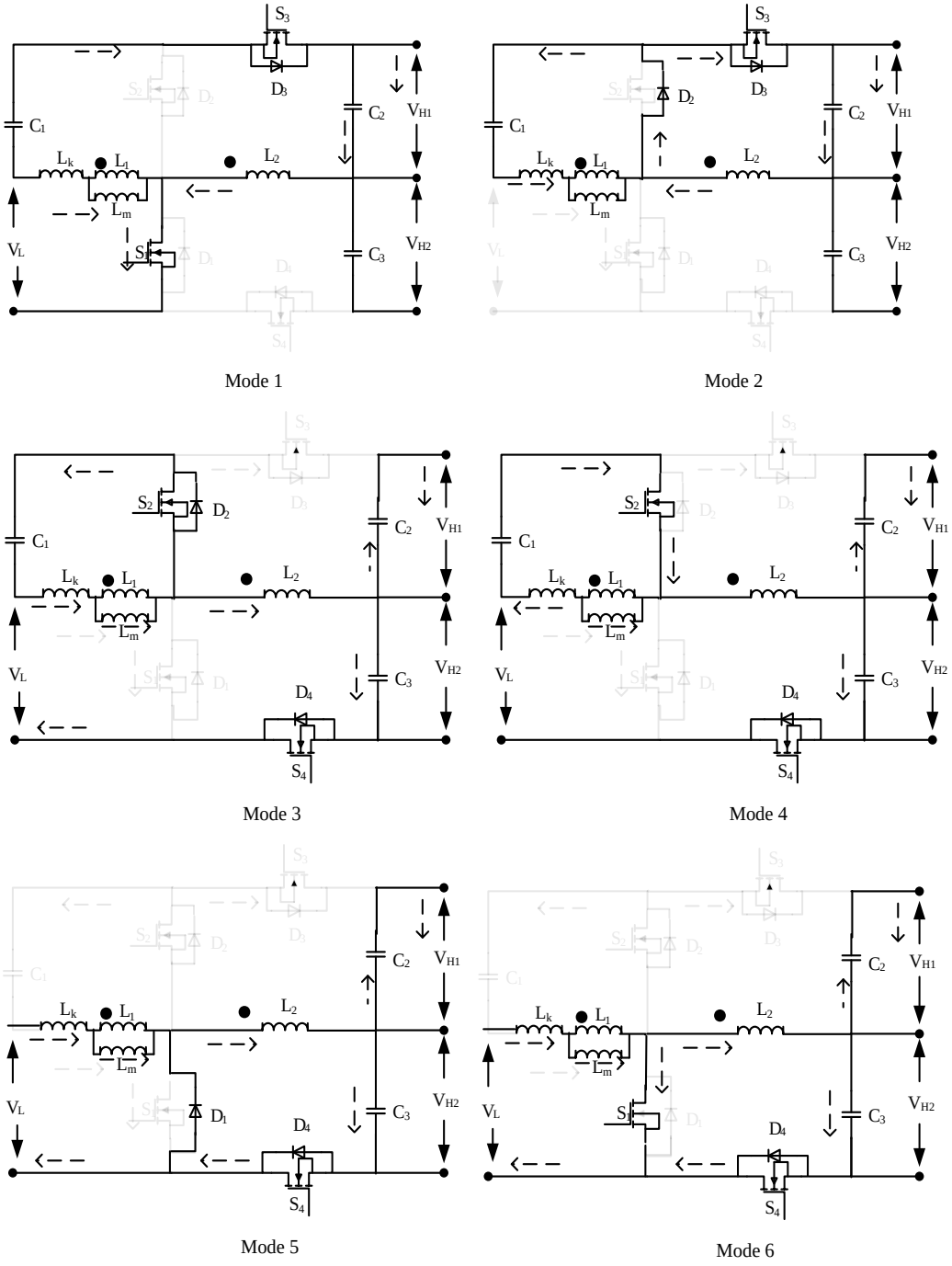

Fig 4.3. Schematic of modes of operation for the proposed topology in boost mode

Mode III: In this mode of operation the switch S_2 is ON and diode D_4 is forward biased during ZCS condition. Fig 4.3 represents the direction of the current flow in inductors. The capacitor C_2 is charged by the DC source voltage V_L, capacitor C_1 and inductor L_1. Capacitor C_3 is discharged through the load. This mode of operation ends whenever the inductor L_2 currents and leakage current are equal and the inductor currents starts decreasing.

Mode IV: In this mode of operation, the switch S_2 is ON and diode D_4 is conducting. Fig 4.3 represents the direction of the current flow in the inductors.The current flowing through the switch S_2 is reversed which will reverse bias the diode D_2 under ZCS condition.The capacitor C_2 is charged by the DC source voltage V_L, capacitor C_1 and inductor L_1. Capacitor C_3 is discharged through the load. This mode of operation ends when switch S_2 is OFF.

Mode V: In this mode of operation the switch S_1 is ON and diode D_4 is forward biased under ZVS condition.Fig 4.3 represents the direction of the current flow in the inductors.The leakage inductor voltage is reversed and inductor current starts increasing.

Mode VI: In this mode of operation the switch S_1 is ON and diode D_4 is forward biased. Fig 4.3 represents the direction of the current flow in inductors. The current flowing through the switch S_1 is reversed as a result the diode D_1 becomes reverse biased under ZCS condition.The inductor L_2 current starts decreasing and when it reaches to zero diode D_4 is reverse biased under ZCS condition.

4.2.1.2 Buck mode of Operation

In this mode of operation the output voltage is stepped-down by controlling the switch S_4 along the conduction of switches S_1,S_2 and S_3.To achieve the required voltage gain, duty ratio for S_2 and S_4 are kept same and duty ratio for S_1 and S_3 are kept same with a phase difference of 180°. The complete operation of the converter in buck mode is divided into six modes. Fig 4.4 & Fig 4.5 represents the waveforms and principle of operation for buck mode respectively.

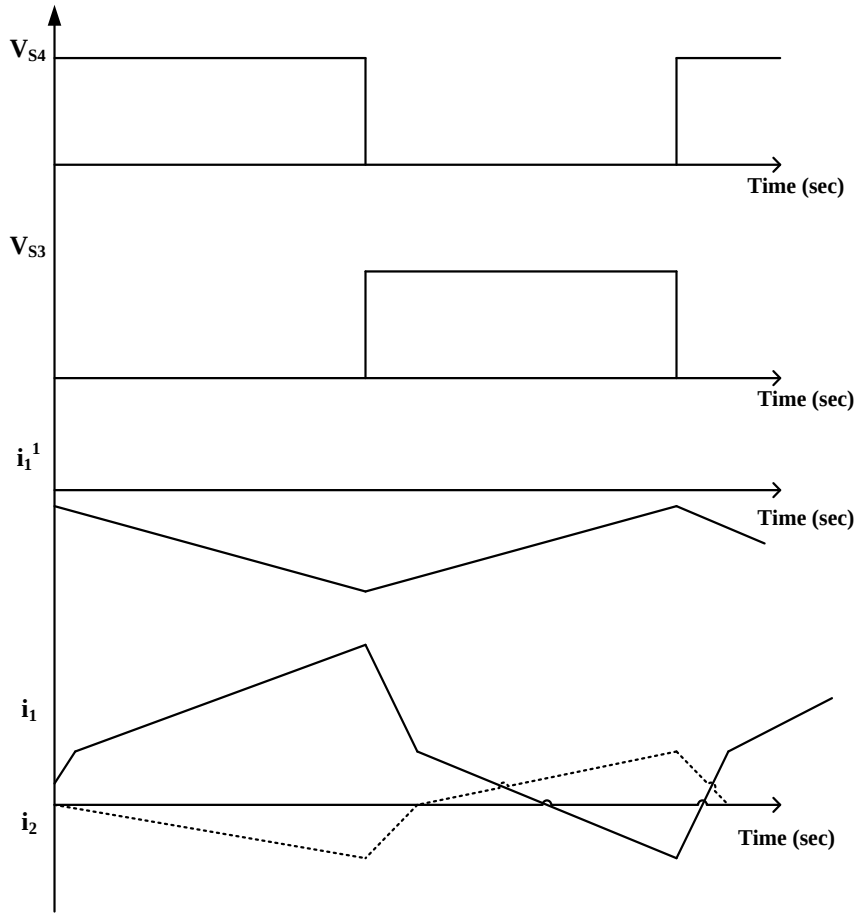

Fig 4.4. Waveforms for buck mode in continuous conduction mode

Mode I: In this mode of operation the switch S_4 is ON and diode D_2 is forward biased. Fig 4.5 represents the direction of the current flow in inductors.The current through inductors L_m, L_k starts increasing and current flows through the diode D_2 during this period switch S_2 is ON due to ZVS condition. The capacitor C_3 is charged through V_H and capacitor C_1 is charged through L_1. This mode of operation ends when the current through the switch S_2 is zero.

Mode II: In this mode of operation the switches S_2 and S_4 are ON. The direction of the current flow in inductors is shown in Fig.4.5. When current flowing through the inductor L_2 is greater than the current flowing through the inductor L_k, the diode D_2 is reverse biased due to ZCS condition. The inductors L_m, L_k is charged by the capacitor C_1.

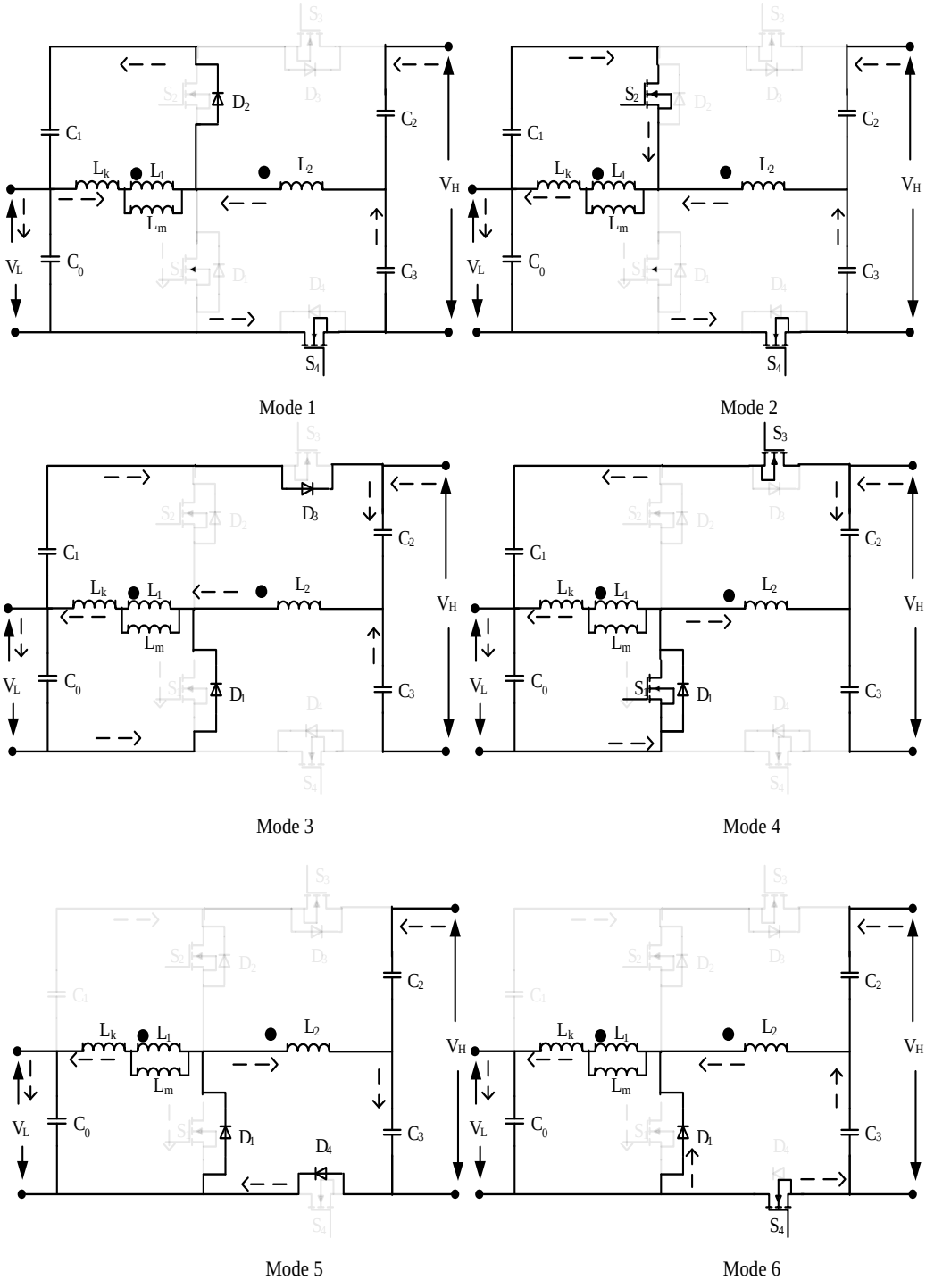

Fig 4.5. Schematic of modes of operation for the proposed topology in buck mode.

Mode III: In this mode of operation the switches S_1 and S_3 ~~is~~ are ON and diodes D_1, D_3 are forward biased under this ZVS condition. The direction of the current flow in inductors can be observed from Fig.4.5. The current flowing through the inductor L_2

starts decreasing and this mode of operation ends when the current through L_2 reaches to zero, and the diode D_3 is reverse biased due to ZCS condition.

Mode IV: In this mode of operation the switches S_1, S_3 is ON. The direction of the current flow in inductors is shown in Fig.4.5. The current flowing through the inductors L_m, L_k starts decreasing and increasing respectively.The capacitor C_1 is charged by the capacitor C_2 and inductors L_1, L_2.

Mode V: In this mode of operation the switch S_4 is ON and diodes D_1, D_4 is conducting under ZVS condition. The direction of the current flow in inductors is shown in Fig 4.5. The current flowing through the inductors L_k, L_2 starts decreasing and mode of operation ends when inductor current L_2 reaches to zero.

Mode VI: In this mode of operation the switch S_4 is ON. The direction of the current flow in inductors is shown in Fig 4.5. The current flowing through the inductor L_2 is reversed and starts flowing through the switch S_4. The capacitor C_2, inductor L_m are charged by the DC source. The current flowing through the inductors L_m, L_k starts increasing and decreasing respectively and at a particular instant of time the magnitude of currents are equal and diode D_1 is reverse biased under ZCS condition.

4.2.1.3 Control Strategy of the Converter

Fig 4.6 shows the control strategy of bi-directional power flow in the converter. According to the voltage reference signal U_{ref}, the converter operates either in boost mode or in buck mode of operation. When U_{ref}=1, the converter operates in the boost mode where the boost voltage V_H is compared with reference voltage V_{ref} and the voltage balance between V_{H1} and V_{H2} is controlled by the PI voltage controller by setting the voltage error reference to zero. The output of the PI voltage controller gives the reference current for the energy storage device. Simultaneously, the inductor currents i_L is regulated by the current compensator with reference battery current in the current-loop. The corresponding duty value obtained is compared with the carrier wave to generate the gate signals for S_1 – S_4 in the boost mode. Similarly, when U_{ref} =0, the converter operates in the buck mode where the buck voltage V_L is regulated by the voltage compensator with the voltage reference, and the current compensator controls the current

i_L with the current reference. The resultant signal is compared with repeating sequences to generate the gate signals for the switches S_1 –S_4 in the buck mode.

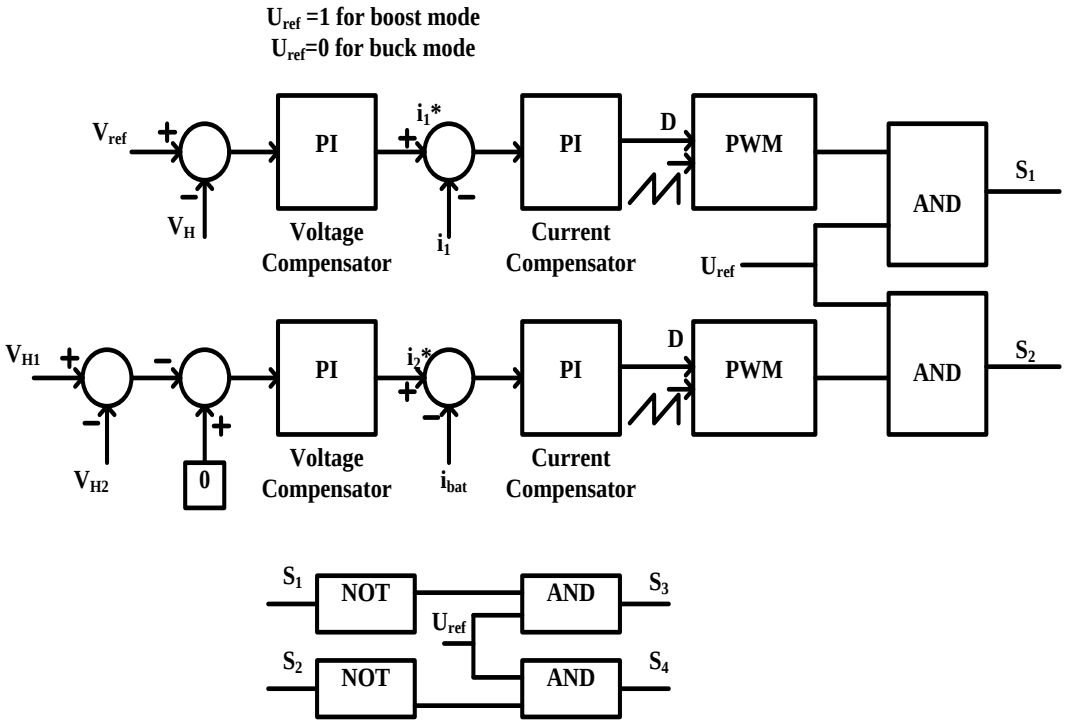

Fig 4.6. Control strategy for voltage balancing and bi-directional power flow.

4.2.2 Analysis of the Converter

Analysis of the proposed converter w.r.t voltage gain, voltage stress across the switches, and current ripple in the converter are explained in detail. To simplify the analysis, all the switching devices and the energy storage elements are considered as ideal and the current flowing through the inductor is continuous and the voltage across the capacitors is assumed constant.

4.2.2.1 Voltage Gain

Mode 1, 3 and 4 play a major role in the operation at steady state, hence these modes are observed to discuss the steady state operation of the converter. According to the ampere-second balance of the HV side capacitors, C_2 and C_3, and taking into account the current waveforms of the body diodes D_3 and D_4, as shown in Fig. 4.2, the voltage across C_2 and C_3 is as follows:

$$V_{C2} = V_{C1}(1+k) + V_L - \frac{2*k^2*f_s*i}{(1-D)^2} * L_k \quad (4.1)\ [73]$$

$$V_{C3} = V_L(1+k) + V_{C1} - \frac{2*k^2*f_s*i}{D^2} * L_k \quad (4.2)\ [73]$$

Where k= L_2/L_1, f_s is the switching current and i is the load current referred to high voltage side.

When the volt-second balance is applied to the magnetizing inductance L_m, the voltage across the capacitor C_1 is given by

$$V_{C1} = \frac{D}{1-D} * V_L + (2 * k * L_k * f_s * i) * \frac{2D-1}{D*(1-D)^2} \quad (4.3)\ [73]$$

Since, V_H is equal to the sum of the voltage across the capacitors C_2 and C_3, the boost gain voltage conversion ratio of the proposed converter is defined as follows:

$$V_{H1} = \frac{(2+k)}{2*(1-D)*(1+n)}$$

$$V_{H2} = \frac{(2+k)}{2*(1-D)*(1+n)} \quad (4.4)\ [73]$$

Where n value depends on coupled inductor leakage inductance.

$$n = \frac{2*k*L_k*f_s}{R} \frac{k(1-D)+2D(1-2D)}{D^2(1-D)^2} \quad (4.5)\ [73]$$

The magnetizing inductance current flows in the opposite direction during the buck operation at the continuous conduction mode, and power is transferred from high voltage to low voltage. The instantaneous modes 5 and 6 are ignored to simplify the steady-state analysis of the proposed converter during buck operation.

From modes 1 and 4, the leakage inductor current are given by,

$$(\Delta i_{Lm})_{ON} = \frac{V_{C1}(1+k) - V_{H1} + V_L}{k*L_k} \quad (4.6)\ [73]$$

$$(\Delta i_{Lm})_{OFF} = \frac{V_{H2} - (1+k)V_L - V_{C1}}{k*L_k} \quad (4.7)\ [73]$$

Since the converter is assumed to operate in steady-state, the amount of energy stored in the inductor should be zero in one complete cycle. Therefore,

$$(\Delta i_{Lm})_{ON} = (\Delta i_{Lm})_{OFF}$$

$$i_{Lm} = [V_{C1}(1+k) - V_{H1} + V_L]D * (2-D) + [\,V_{H2} - (1+k)V_L - V_{C1}](1-D)^2$$

$$=2*k*f_s * L_k * i \qquad (4.8)\ [73]$$

During ON time interval, the clamp capacitor C_1 is charged by the difference of currents between leakage inductor and switch S_4, and is discharged by the switch S_3 current during OFF time interval. According to the ampere-second balance principle, and (4.6), the voltage across C_2 can be expressed as follows:

$$V_{H1} = V_{C1}(1+k) + V_L - \frac{4*k*L_k*f_s*i}{D(k+2)} \qquad (4.9)\ [73]$$

Substituting (4.9) in (4.8) gives

$$V_{H2} = V_L(1+k) + V_{C1} + \frac{2*k*L_k*f_s*i}{(1-D)^2(k+2)}\big(k - 2(1-D)\big) \qquad (4.10)$$

In addition, the clamp capacitor C_1 voltage is determined by applying the volt-second balance to the magnetizing inductance L_m, and

$$V_{C1} = \frac{1-D}{D} * V_L + \frac{2*k*L_k*f_s*i}{D*(1-D)*(k+2)} \qquad (4.11)$$

From (4.9) to (4.11)

$$V_L = \frac{D}{k+2+n} *\ V_H \qquad (4.12)\ [73]$$

4.2.2.2 Voltage stress across the switches

The voltage stress of switching devices may be expressed as a function of the operating modes and the abovementioned analyses.

$$V_{S1} = V_{S2} = \frac{V_H}{2+k} = \frac{V_L}{1-D} \qquad (4.13)$$

$$V_{S3} = V_{S4} = V_{H2} + k * V_{C1} = V_{H1} + k * V_L = \frac{V_L(1+k)}{1-D} \qquad (4.14)\ [73]$$

(4.13) and (4.14) shows that the voltage stress of low voltage side switches is independent of the winding turns ratio. However, with low turn ratios, the voltage stress across the high voltage side switches decreases. As a result, by carefully selecting the winding turns ratio and duty cycle, the voltage stress across the power switches may be optimized.

4.2.2.3 Passive components design

The current flowing through the magnetizing inductance is calculated from power balance equation, $P_{out}=\eta P_{in}$

$$I_{Lm} = \frac{2+k}{(1-D)(1+n)} * \frac{V_H}{R} = \left(\frac{2+k}{(1-D)(1+n)}\right)^2 * \frac{V_L}{R} \quad (4.15)\ [73]$$

Also, the magnetizing inductance current ripple is

$$\Delta I_{Lm} = \frac{D*V_L}{L_m*f_s} \quad (4.16)\ [73]$$

Based on the charge balance equation Q = CΔV, the value of capacitors C_2, C_3 and C_1 can be chosen according to the desired voltage ripple

$$C_2 \geq \frac{V_H*D}{f_s*R*\Delta V_{C2}} \quad (4.17)$$

$$C_3 \geq \frac{V_H*(1-D)}{f_s*R*\Delta V_{C3}} \quad (4.18)$$

$$C_1 \geq \frac{V_H}{f_s*R*\Delta V_{C1}} \quad (4.19)\ [73]$$

4.3 Simulation Results

To test the feasibility of the proposed bipolar bidirectional DC-DC converter, simulation studies are carried out from the developed mathematical model of the converter and results are presented. Table - 4.1 represents the parameters of various components of the converter.

Table 4.1 System Parameters

	Parameters	**Values**
SPV Specifications	open circuit voltage	32.9 V
	Short circuit current	8.214 A
Battery Specifications	Ah capacity	18 Ah
	Voltage	100 V
Converter Parameters	Rated Power	1000 W
	Capacitors values C_1,C_2,C_3	47µF
	Inductors L_m, L_k	150 µH,7 µH
	Turns ratio	4
	Switching Frequency	50kHz
	Boost voltage V_H	400 V
	Buck voltage V_L	50 V

4.3.1 Simulation Results for Boost mode of operation.

From the simulation results it is observed that for the input voltage of V_L=50V, the output voltage of positive pole V_{H1}, negative pole $V_{H2,}$ and boost voltage V_H are shown in Fig.4.7(a). Further, the load variation is considered at time t=1sec, as a result the output power varies from 500W to 700W. The voltage balance between positive pole V_{H1} and negative pole V_{H2} is zero, and the output voltage is constant with the reference voltage 400V.

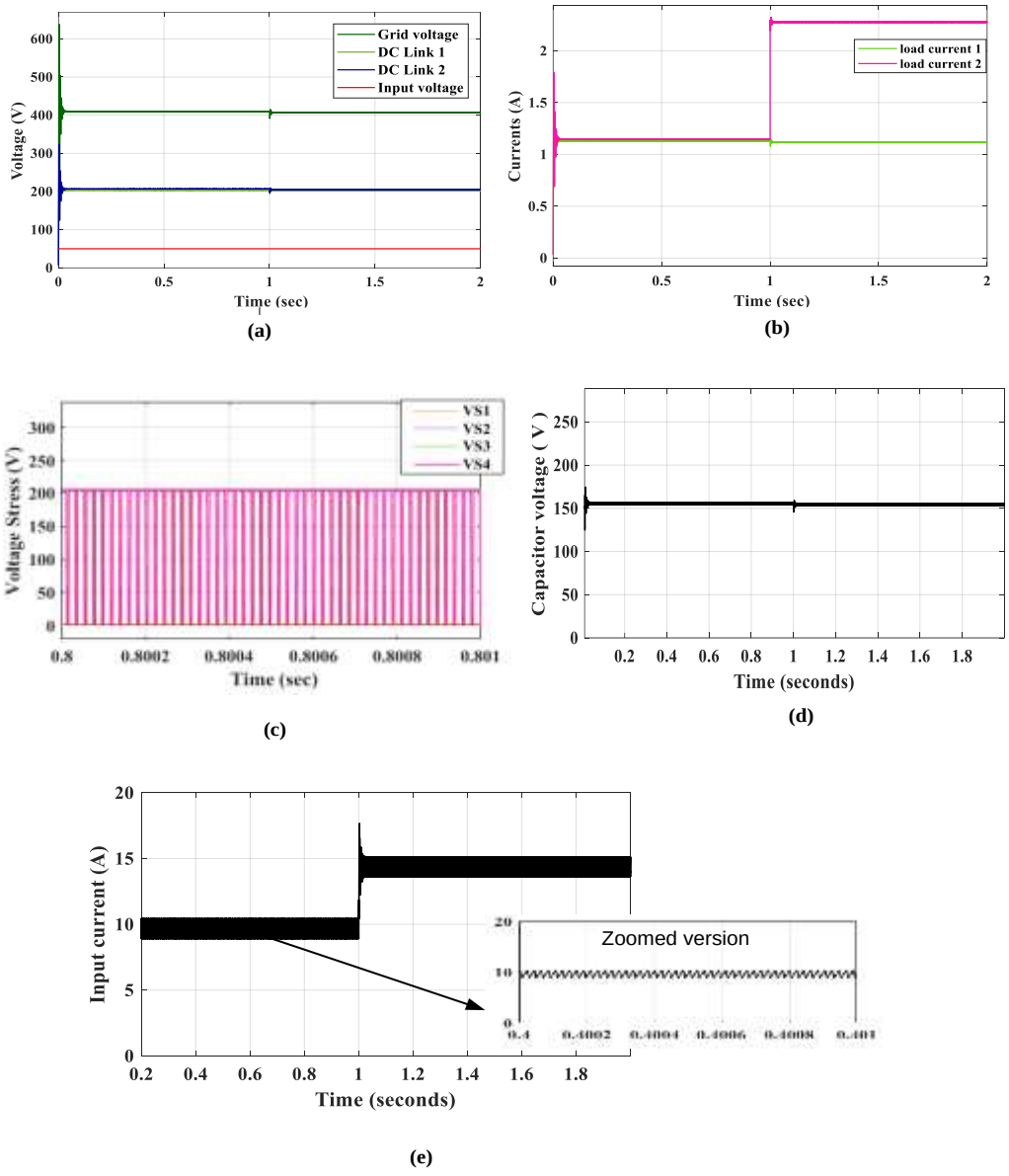

Fig.4.7. Simulation results in boost mode with open loop

Fig. 4.7(b), shows the load currents i_1, i_2, as the load increases the load current starts increases at t=1 sec. The voltage stress across the switching devices is 200V i.e., half of the boost voltage as shown in Fig.4.7(c). From Fig.4.7 (d) it can be observed that the voltage across the capacitor V_{C1} is 200V i.e., half of the boost voltage and also it has a very small ripple. Fig. 4.7(e) shows the source current $i_{low.}$ From this it can be observed that the current ripple is less and within the permitted limits. When V_H is constant at 400V, the efficiency in the boost mode of operation of the proposed converter with different power levels are shown in Fig 4.10(a). From this it is observed that the maximum efficiency occurred at 96.4% at a load of 180Ω.

4.3.2. Simulation Results for Buck mode of operation.

For the input voltage of V_H=400V, the output voltage V_L is shown in Fig 4.8(a). Voltage stress across the switching devices is 200V, which is half of the input voltage as shown in Fig. 4.8(b).The voltage across the capacitor V_{C1} is 200V i.e., half of the input voltage with small ripple is shown in Fig. 4.8(c).The inductor current are shown in Fig. 4.8 (d), the current ripple is 6.8%.

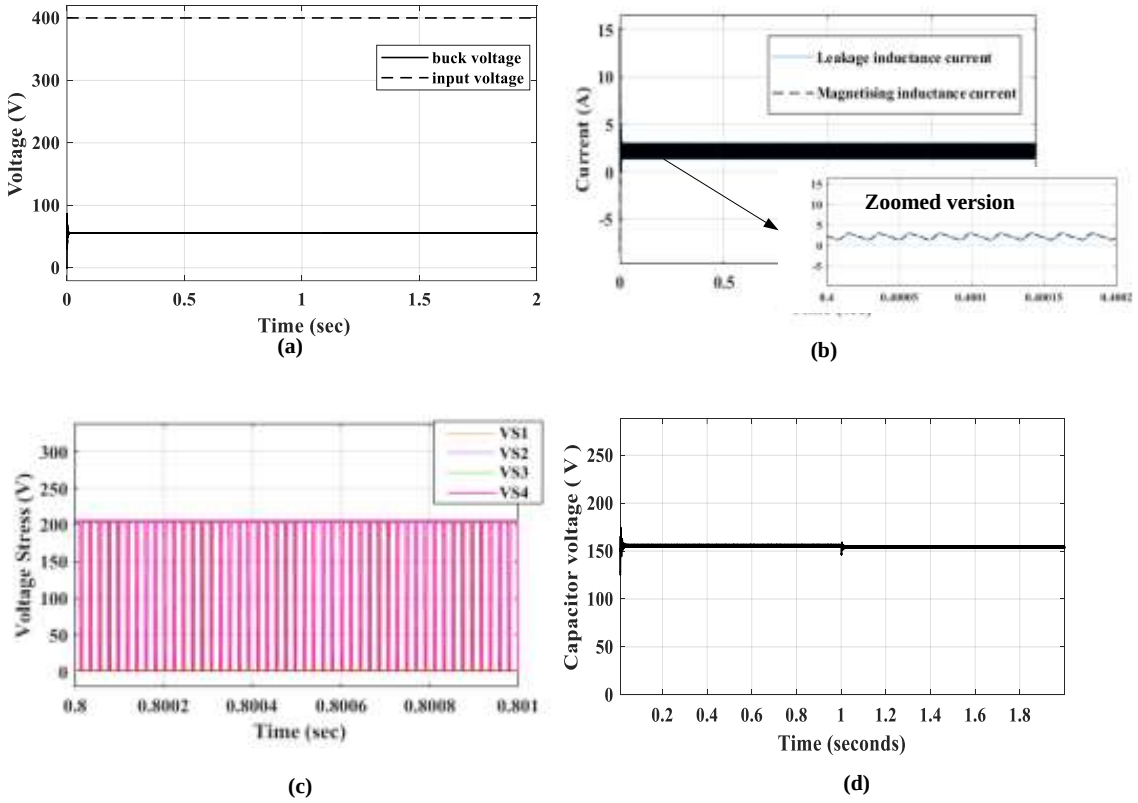

Fig.4.8. Simulation results in buck mode.

When V_H is constant at 400V, and power level changes continuously between 400W and 2000W, the efficiency curve for buck operation of the proposed converter is shown in Fig 4.10(b) and it is observed that the maximum efficiency occurred at 97% at a load of 2.5 Ω.

4.3.3. Integration of Energy Storage System to the Grid

For the considered solar photovoltaic (SPV) panel 1, i_{pv1} is changed at t=2sec, 4sec and 5sec, the boost voltage remains constant by varying the duty cycle of the converter and the power level tracks to the given limits which is shown from Fig. 4.9(a).

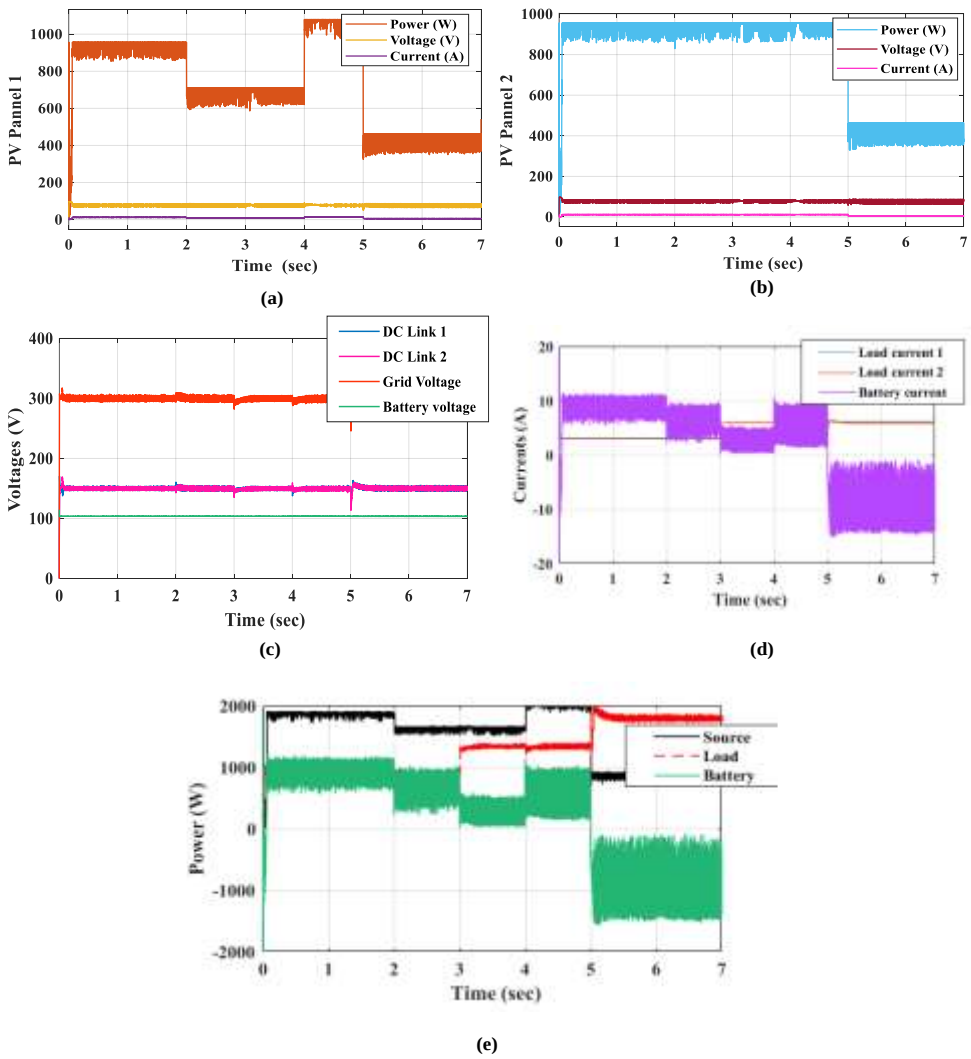

Fig. 4.9. Simulation results for change in load and SPV generation with closed-loop controller .

For SPV panel 2, i_{pv2} is changed at t= 5sec, the boost voltage remains constant by varying duty cycle of the converter and the power level tracks to the given limits is shown in from Fig. 4.9(b). At t=3sec and t=5 sec the load is varied by changing Resistance R value from 50Ω to 25Ω in each positive pole and negative pole respectively. From Fig. 4.9(c) it is observed that the voltage difference between the capacitors is zero and the boost voltage is regulated to the grid voltage of 300 V and also the battery voltage remains constant. The change in load current and battery current is shown in Fig. 4.9(d). The changes in powers are shown in Fig. 4.9(e).

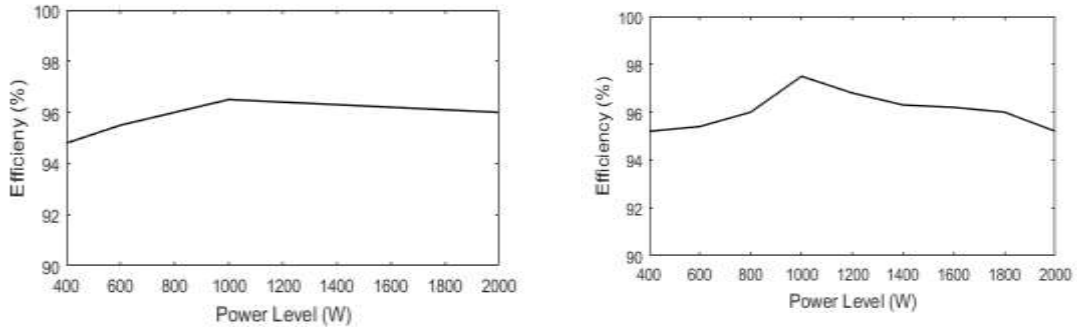

(a) (b)

Fig 4.10. Efficiency of the bipolar bidirectional DC-DC converter
(a) Boost Mode (b) Buck Mode

4.4 Summary

In this chapter a non-isolated bipolar bi-directional DC-DC converter with coupled inductors is proposed for bipolar DC micro-grids suitable for both low power and high power applications to achieve high voltage gain with low voltage stress across the switches.To obtain these features a zero voltage switching in both boost mode and buck mode of operation is implemented. Inherent voltage balance across the capacitors is achieved without any additional control technique. The maximum efficiency occurred in boost and buck mode of operation are 96.4% and 97% respectively.

Chapter-5

Bipolar Bidirectional DC-DC Converter with High Voltage Gain

5.1 Introduction

In this chapter, a non-isolated bipolar bidirectional DC-DC converter for renewable energy system is presented to achieve a high voltage-gain with lower values of duty cycle for the converter. Further control strategies are proposed to reduce the ripple in the inductor current and also to achieve voltage balance across the series connected capacitors in the proposed converter topology. Detailed analysis, simulation and experimental results are presented to highlight the merits of the proposed converter topology.

5.2 High Gain Bipolar Bidirectional DC-DC Converter

The proposed converter consists of a low voltage half bridge converter and a high voltage L-C half bridge resonant network. This configuration consists of four IGBTs S_1, S_2, S_3, and S_4 which are controlled to obtain both boost mode and buck mode of operation for the converter. The L-C resonant circuit is formed by the inductor L_a and capacitor C_a. Capacitors C_1, C_2 and C_3 are connected at the input and output terminals of the converter. Voltage across C_1, C_2, and C_3 are V_L, V_{H1} and V_{H2} respectively. Whereas i_{high} and il_{ow} represent the high-voltage and low-voltage side currents. Detailed operation of the proposed converter is discussed in subsequent sections.

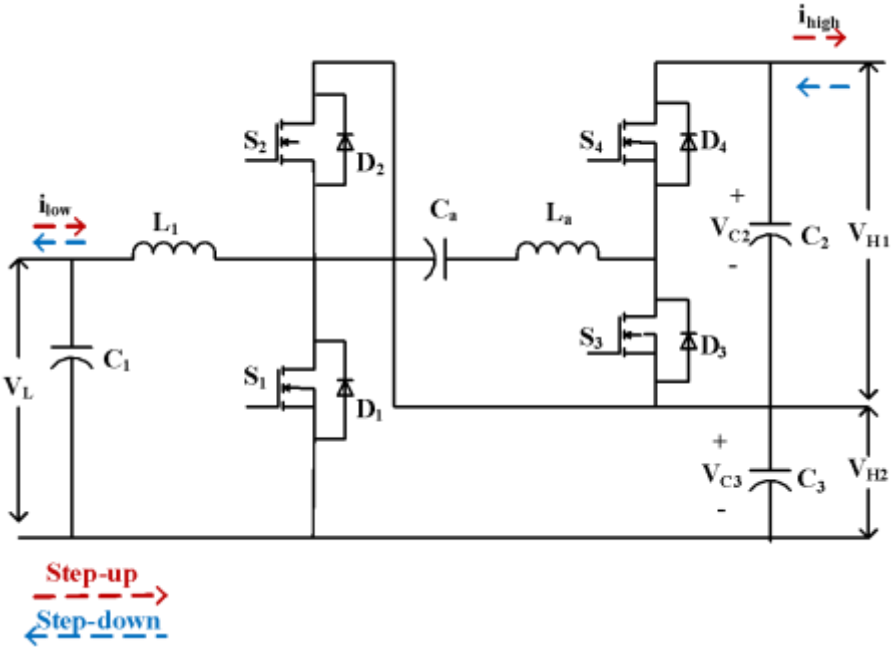

Fig 5.1. Proposed bipolar bidirectional DC-DC converter topology

5.2.1 Analysis of the Proposed Topology-4

For steady-state analysis of the proposed bi-directional DC-DC converter, all the switching devices and the energy storage elements are considered as ideal and the current in inductor is continuous**;** the voltage across the capacitors is assumed constant.

5.2.1.1 Boost mode of Operation

In this mode of operation the output voltage of the converter is stepped-up by controlling the switches S_1, S_2, S_3 and S_4. To achieve the required voltage gain, duty ratio for S_1 and S_2 are kept same with 180° phase difference and duty ratio for S_4 and S_3 are kept same with a phase difference of 180°. The complete operation of the converter in boost mode is divided into five modes. Fig 5.2 & Fig 5.3 represents the waveforms and operation in boost mode respectively.

Mode I: In this mode of operation the switch S_1 is ON under ZVS condition, and switchesS_2, S_3 and S_4 are OFF. The diodes D_1 and D_4 are forward biased, and the diodes D_2 and D_3 are reverse biased. Fig. 5.3 shows the direction of current i_{La}, i_{L1} in the inductors L_a and L_1. The inductor $L_1$is charged by the DC voltage source V_L, and inductor L_a discharges, whereas inductor La charges the capacitor C_2, C_3 and C_a.

Mode II: During this mode of operation when current flowing through the inductor i_{L1} is larger than the current flowing through the inductor i_{La}, the polarity of the current through the switch S_1 changes which makes the switch S_1 to ON. When the discharging current i_{La} reduces to zero, the switch S_4 is OFF under ZCS condition and diode D_3 is forward biased.

Mode III: In this mode of operation the switch S_3 is ON under ZVS condition. Fig 5.3 shows in which direction current is flowing in the inductor i.e i_{L1}, i_{La}. The inductor L_a is charged by the capacitor C_a. The current flowing in the switch S_1 is sum of the currents flowing through the inductors i_{L1} and i_{La}.

Mode IV: In this mode of operation the switches S_1, $S_3$is OFF. The diodes D_2, D_3 is forward biased. Fig 5.3 shows in which direction current is flowing in the inductor i.e i_{L1},

i_{La} which starts decreasing. The switch S_2 is ON under ZVS condition. When the decreasing current i_{La} of the inductor $_{La}$ reaches zero, the S_3 is OFF under ZCS condition and whenever the polarity of i_{La} is reversed, the diode D_4 is forward biased.

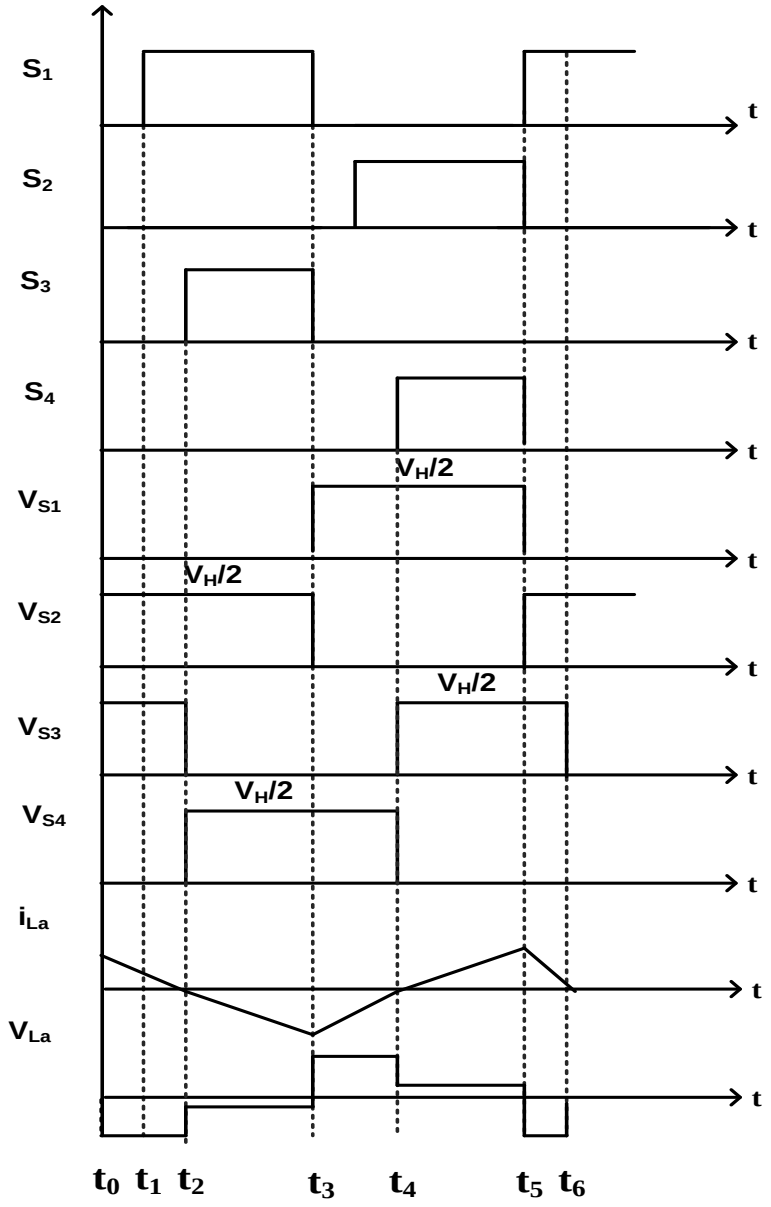

Fig 5.2. Waveforms for boost operation in continuous conduction mode

Mode V: In this mode of operation the switch S_4 is ON under ZVS condition. The direction of currents flowing in the inductor L_1 and L_a are shown in Fig. 5.3. Current in the inductor L_1,(i_{L1}) starts decreasing, whereas current flowing in the inductor La (i_{La}) starts increasing. The capacitors C_2 and C_3 starts discharging through the load.

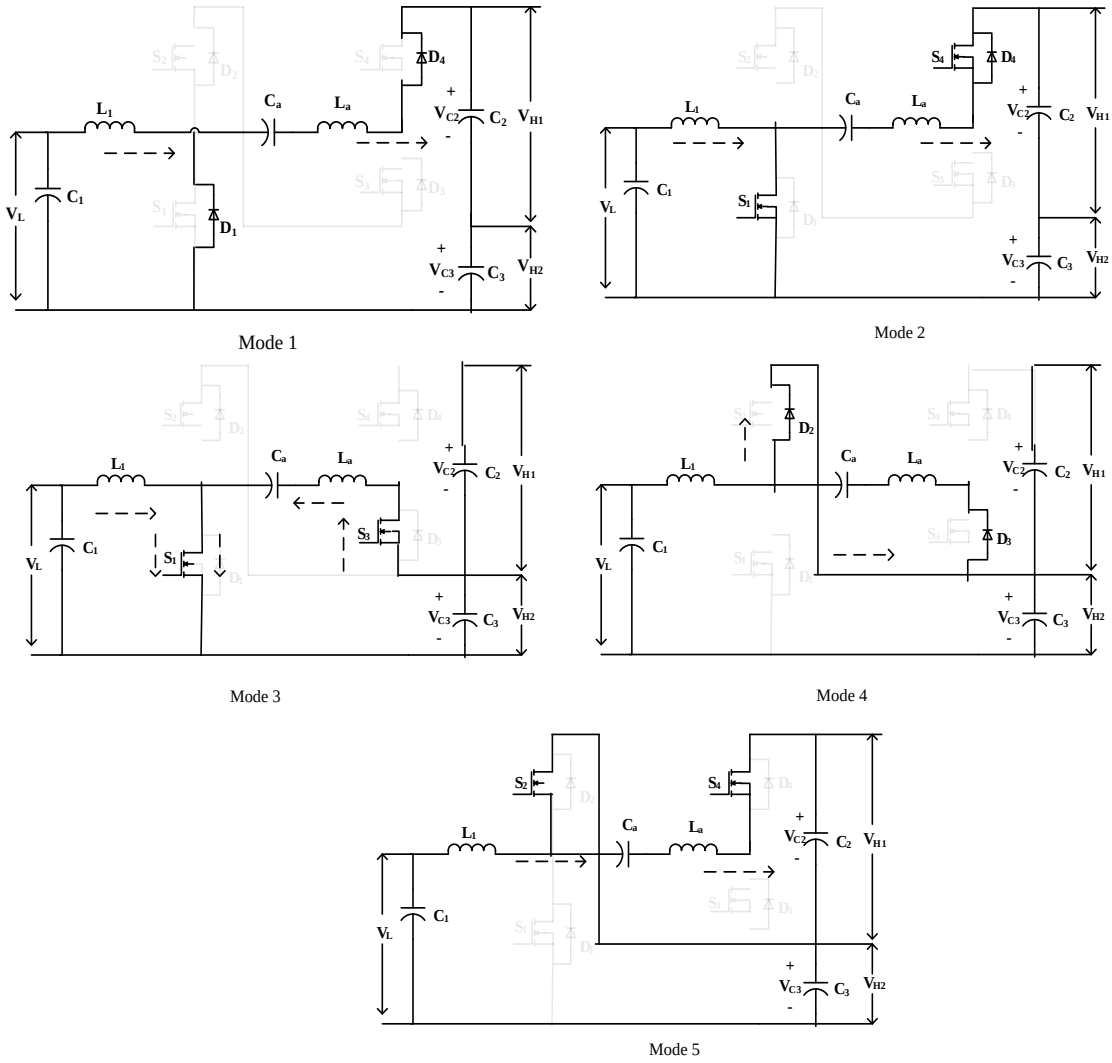

Fig 5.3. Modes of operation for the converter in boost mode

5.2.1.2 Buck mode of Operation

In this mode of operation voltage is stepped-down by regulating the switches S_1, S_2, S_3, and S_4. To achieve the required voltage gain, duty ratio for S_3 and S_4 are kept same with a phase difference of 180° and duty ratio for S_1 and S_2 are kept same with a phase difference of 180°.The detailed operation of the converter in buck mode is fragmented to five modes. Fig 5.4 & Fig 5.5 shows the waveforms and principle of operation for buck mode respectively.

Mode I: In this mode of operation the switches S_2 and S_4 are OFF. The diodes D_1 and D_3 are forward biased. Fig 5.5 shows the direction of current in the inductors. The inductor currents i_{L1}, i_{La} starts increasing and decreasing respectively. Capacitor C_2 and C_3

are charged by the DC sources V_{H1} and V_{H2} respectively. The inductors L_1, L_a gives the output to the load connected on low voltage side.

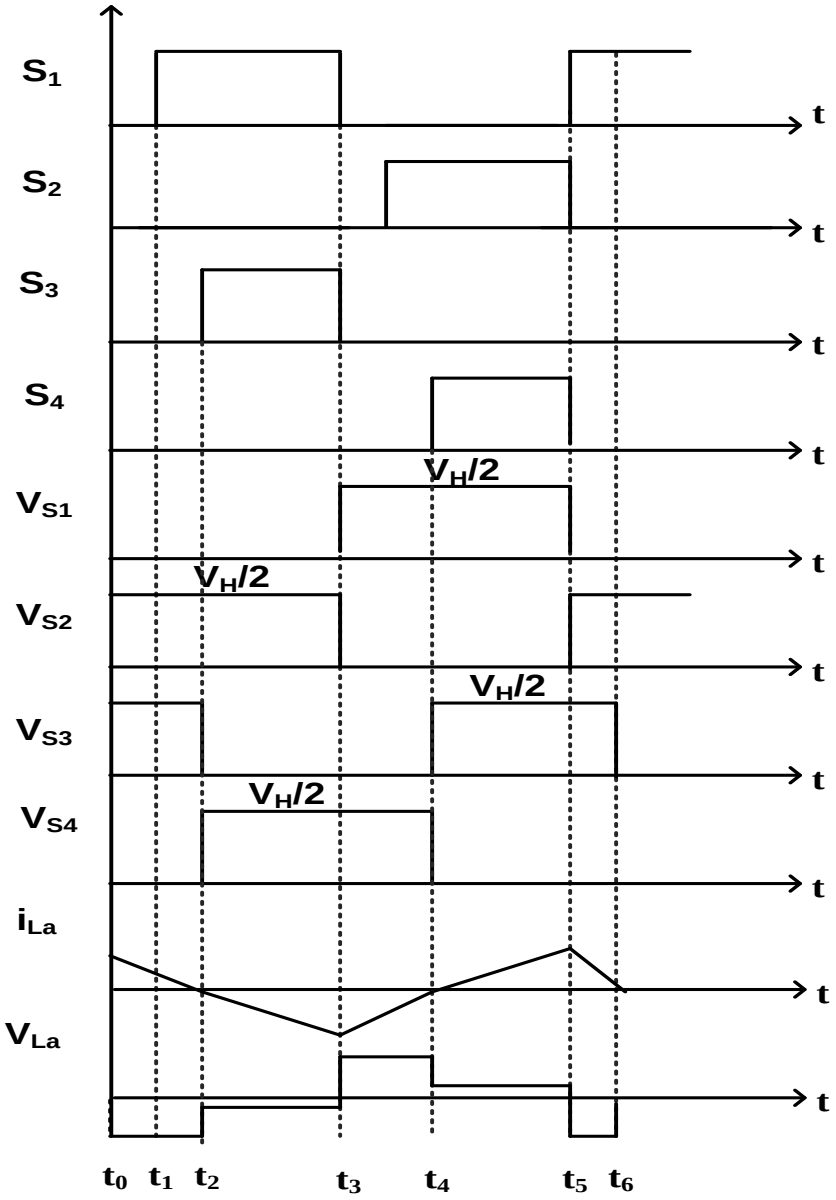

Fig 5.4. Waveforms for buck mode in continuous conduction mode

Mode II: In this mode of operation the switch S_3 is ON under ZVS condition and with dead time the switch S_1 is ON. Fig 5.5 shows the direction of current flowing in the inductors L_1 and L_a. Currents i_{L1}, i_{La} starts increasing and decreasing respectively. Current flowing through i_{La} reaches to zero at the end of this mode.

Mode III: In this mode of operation the switch S_3 is ON and with dead time the switch S_1 is ON. Fig 5.5 shows in which direction current is flowing in the inductor i.e i_{L1}, i_{La}. The polarity of i_{La} changes and current flowing through the inductor L_a (i_{La}) starts increasing.

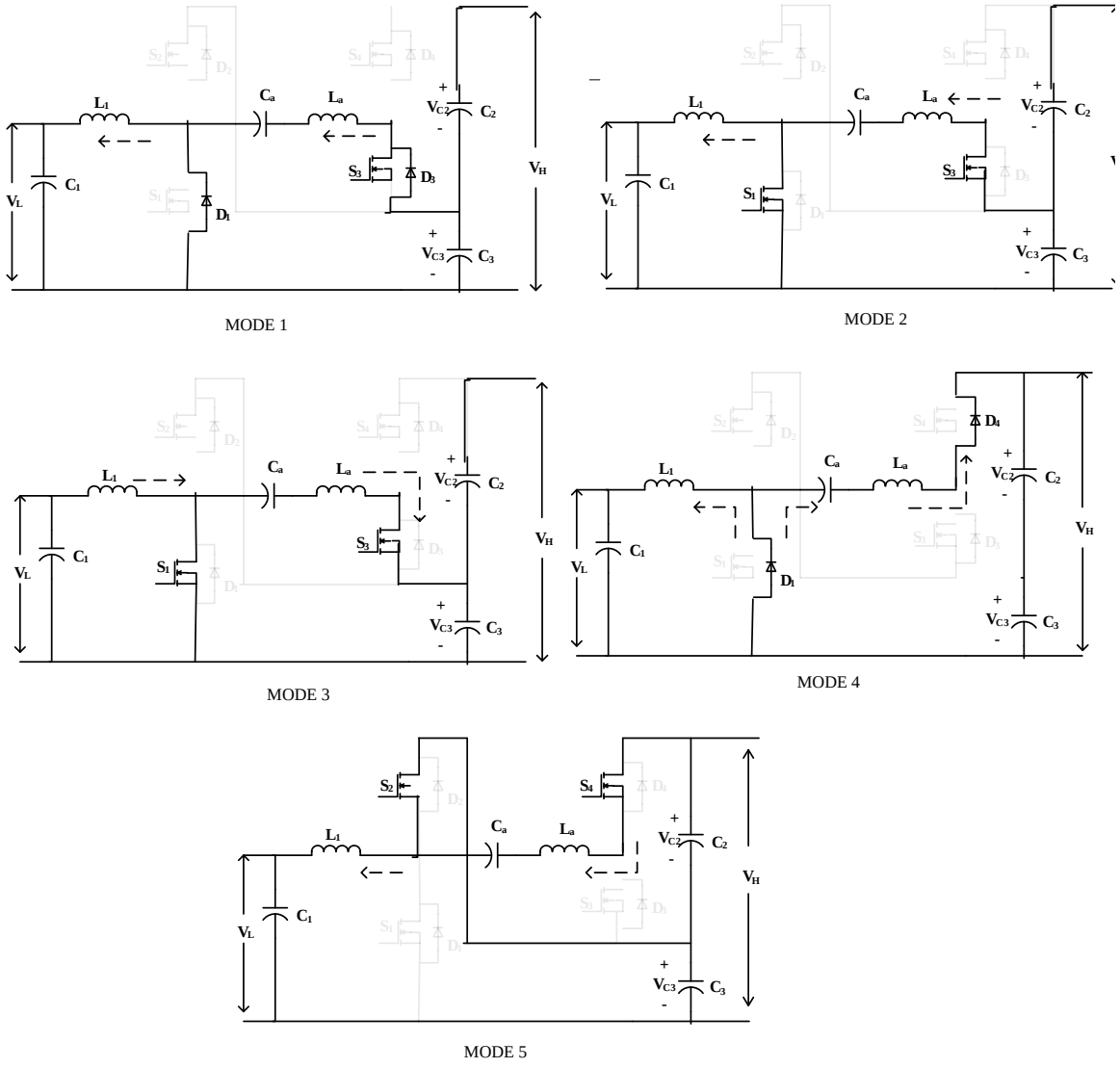

Fig 5.5. Types of operation in buck mode.

Mode IV: In this mode the switch S_4 is ON under ZVS condition and switches S_1 and S_3 are OFF. The diodes D_1 and D_4 are forward biased .Fig 5.5 shows the direction of current ~~is~~ flowing in the inductors L_1 and L_a (i.e i_{L1}, i_{La}). The current through the inductor L_a starts decreasing and at the end of this the mode the current reaches to zero.

Mode V: In this mode when current flowing through the inductor L_a is greater than the-current flowing in the inductor L_1, the diode D_1 is reverse biased under ZCS condition. The diode D_2 is forward biased. Fig 5.5 shows the direction of current ~~is~~ flowing in the

inductors L_1 and L_a (i.e i_{L1}, i_{La}) starts increasing and decreasing respectively. The switch S_2 is ON under ZVS condition.

5.2.1.3 Control Strategy of the Converter

Fig 5.6 shows the control strategy of bi-directional power flow in the proposed converter. This control strategy also offer voltage balance. The voltages V_{H1}, $V_{H2,}$ and V_L and the inductor current i_{L1} are measured by using hall effect voltage and current sensors and fed to digital signal processor TMS320F28379D to implement the control strategy. The converter works in either boost or buck mode depending on the U_{ref} signal. When U_{ref}=1, the converter works in boost mode, where boost voltage V_H is compared to the reference voltage V_{ref} and the PI regulator controls it by setting the voltage error reference to zero. Simultaneously, the inductor current i_{L1} is regulated by the current compensator with reference inductor i_{L1}^* in the current-loop. The corresponding duty value obtained is correlated with the carrier wave to produce the gate signals for S_1–S_4 in boost mode. Similarly, when Uref =0, the converter operates in the buck mode where the buck voltage V_L is regulated by the voltage compensator with the voltage reference, and the current compensator controls the current i_L with the current reference. The resultant signal is compared with repeating sequences to produce gate signals for S_1 –S_4 in the buck mode.

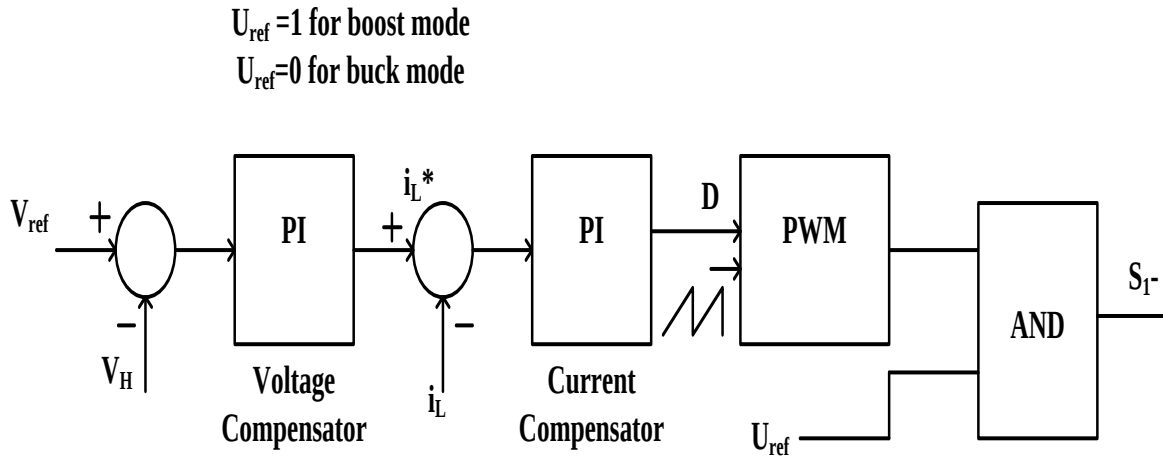

Fig 5.6. Control strategy for bi-directional power flow.

5.2.1.4 Voltage Gain of the Converter

To simplify the analysis, all the switching devices and the energy storage elements are considered as ideal and the current flowing through the inductor is continuous and the

voltage across the capacitors is assumed constant. Analysis of the proposed converter w.r.t voltage gain and voltage stress over the switches, and current wave in the converter are explained in detail below:

Voltage gain in boost mode

From the mode-1 operation of boost converter shown in Fig.5.3, switch S_1 is ON current in inductor i_{L1} starts charging from the dc source V_L, and the inductor current i_{La} starts discharging to charge C_a, the discharge rate are given by

$$L_1 \frac{di_{L1}}{dt} = V_L$$

$$L_a \frac{di_{La}}{dt} = V_{Ca} - V_{C1} - V_{C2} \tag{5.1}$$

In mode-3, switch S_3 is ON, current in inductor i_{La} starts increasing linearly, the discharge rate is given by

$$L_a \frac{di_{La}}{dt} = V_{Ca} - V_{C1} \tag{5.2}$$

In mode-4, switch S_2 is ON, the current flowing through the inductors i.e i_{L1}, i_{La} starts decreasing, the discharge rate is given by

$$L_1 \frac{di_{L1}}{dt} = V_L - V_{C1}$$

$$L_a \frac{di_{La}}{dt} = V_{Ca} \tag{5.3}$$

In mode-5, switch S_4 is ON, current in inductor i_{La} starts increasing linearly, the discharge rate is given by

$$L_a \frac{di_{La}}{dt} = V_{Ca} - V_{C2} \tag{5.4}$$

Since the converter is assumed to work in steady state, the amount of energy stored in the inductor should be zero in one complete cycle. Therefore,

$$(\Delta i_{L1})_{ON} = (\Delta i_{L1})_{OFF}$$

$$(\Delta i_{La})_{ON} = (\Delta i_{La})_{OFF} \tag{5.5}$$

From equations (5.1), (5.2), (5.3), (5.4)

$$V_{H1} = \frac{1}{1-D} V_L$$

$$V_{H2} = \frac{1}{1-D} V_L \tag{5.6}$$

Voltage gain in buck mode

From the mode-1 operation of buck converter shown in Fig.5.4 & Fig.5.5, diodes D_1 and D_3 are forward biased, the current flowing the inductor i_{L1} starts decreasing linearly, the discharge rate is given by

$$L_1 \frac{di_{L1}}{dt} = V_L \tag{5.7}$$

In mode-3, switches S_1 and S_3 are ON, current flowing the inductor i_{La} starts increasing linearly, the discharge rate is given by

$$L_a \frac{di_{La}}{dt} = V_{Ca} - V_{C1} \tag{5.8}$$

In mode-4, switch S_4 is ON, current flowing the inductor i_{La} starts decreasing linearly, the discharge rate is given by

$$L_a \frac{di_{La}}{dt} = V_{Ca} - V_{C1} - V_{C2} \tag{5.9}$$

In mode-5, diode D_2 is ON, current flowing the inductors i_{La} and i_{L1} starts decreasing and increasing linearly respectively, the discharge rate is given by

$$L_1 \frac{di_{L1}}{dt} = V_L - V_{C1}$$

$$L_a \frac{di_{La}}{dt} = V_{Ca} - V_{C2} \tag{5.10}$$

Assuming the converter to work in an ideal state, the energy stored in the inductor should be zero in one complete cycle. Therefore,

$$(\Delta i_{La})_{ON} = (\Delta i_{La})_{OFF}$$

$$(\Delta i_{L1})_{ON} = (\Delta i_{L1})_{OFF} \tag{5.11}$$

From equations (5.7), (5.8), (5.9), (5.10)

$$V_{C1} = \frac{V_L}{D}$$

$$V_{C2} = \frac{V_L}{D}$$

$$V_{C1} + V_{C2} = V_H$$

$$V_L = \frac{D}{2} V_H \tag{5.12}$$

5.2.1.5 Voltage stress across the switching devices

From buck mode of operation and the boost mode of operation shown in Fig 5.5 & Fig 5.3, respectively, when switch S_3 is ON, and S_4 is OFF in mode-III; it is clear that S_3 and C_3 are in parallel. So, voltage across S_3 and C_3 are equal. Similarly, the switch S_3 is OFF, and S_4 is ON in mode-V; it is observed thatS_4 and C_2 are in parallel. So, voltage across S_4 and $C_2$are equal. The voltage stress for the switching devices is:

$$V_{C2} = V_{C3} = \frac{1}{1-D} V_L$$

$$V_H = \frac{2}{1-D} V_L$$

$$V_{S1} = V_{S2} = V_{S3} = V_{S4} = \frac{V_H}{2} \tag{5.13}$$

5.2.1.6 Current ripple in the inductors

In Boost mode of operation,

From equations (5.1), the current ripple i_{L1} is given by

$$\Delta i_{L1} = \frac{V_L * D * T_s}{L_1}$$

Where D=duty cycle

$$\Delta i_{L1} = \frac{V_H * D * (1-D) * T_s}{2L_1} \tag{5.14}$$

From equation (5.3), the current ripple $i_{La}$is given by

$$\Delta i_{La} = \frac{V_{Ca} * (1-D) * T_s}{L_a}$$

$$\Delta i_{La} = \frac{V_H * (1-D) * T_s}{2L_a} \tag{5.15}$$

In Buck mode of operation,

From equations (5.7), the current ripple i_{L1} is given by

$$\Delta i_{L1} = \frac{V_H * D * (1-D) * T_s}{2L_1} \tag{5.16}$$

From equation (5.8), the the current ripple i_{La} is

$$\Delta i_{La} = \frac{V_H * D * (1-2D) * T_s}{2L_a} \tag{5.17}$$

5.3. Simulation and Experimental Results

Simulations are carried out on the developed mathematical model using Matlab/Simulink. To validate the simulation results, experiments are carried out on a 500 Watt Lab scale prototype bi-polar bi-directional DC-DC converter. Fig 5.7 represents the photograph of experimental set up of bi-polar bi-directional DC-DC converter. Table 5.1 shows the parameters of different components of the converter.

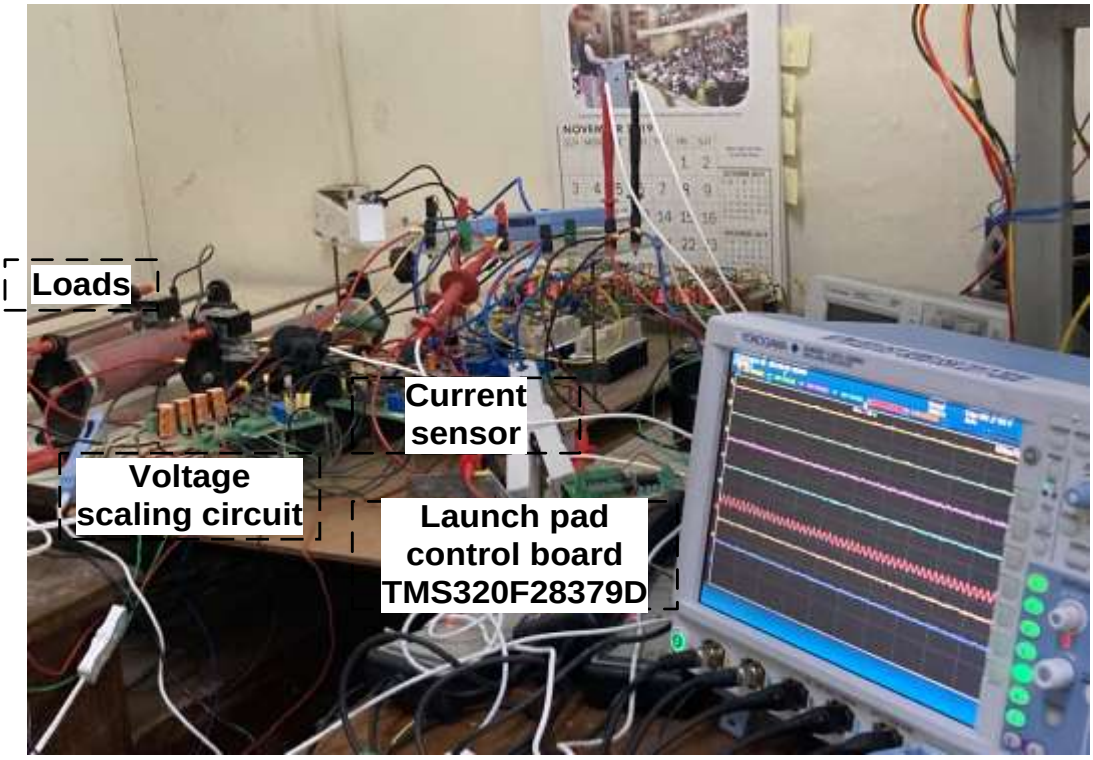

Fig 5.7.Experimental prototype of bi-polar bi-directional DC-DC converter

Table 5.1 Converter Parameters.

Parameters	**Values**
Rated Power	500 W
Switched Capacitors values C_1,C_2,C_3	1000µF
Inductor L_1	600µH
Resonant Parameters	L_a=2µH,C_a=20 µF
Switching Frequency	10kHz
Boost voltage V_H	400 V
Buck voltage V_L	100V

5.3.1 Simulation and Experimental Results in Boost Mode

From the simulation and experimental results it is observed that for the input voltage of V_L=100V, the inductor current is shown in Fig 5.8 and Fig 5.9. From the experimental results it is observed that ripple in the inductor current i_{L1} is 18.3%. From equation (5.14), the theoretical **v**alue and also from simulation results, it is observed that ripple in the inductor current is 20%. Therefore it is observed that the ripple in the inductor current in both cases is close. The voltage stress across the switching devices is 200V i.e., half of the boost voltage is represented in Fig 5.8 and Fig.5.9, and the current through the switch is shown in Fig 5.8 and Fig.5.9. From the result it is proven that the switch is turned ON under ZVS condition and ZCS turn OFF condition.

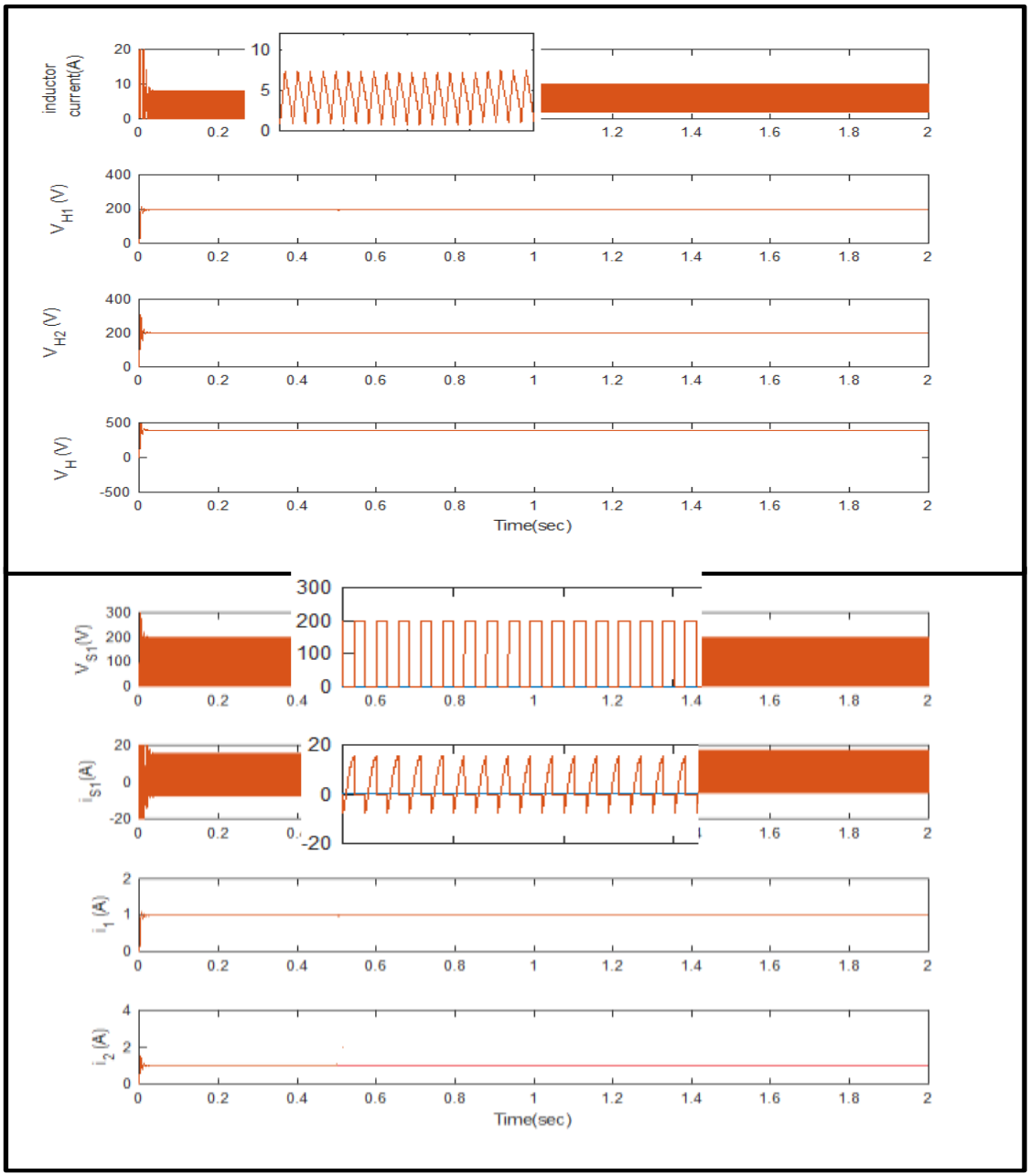

Fig 5.8. Simulation results in boost mode open loop (a) Inductor current, output voltages V_{H1}, V_{H2}, Total boost voltage, V_H. (b) Voltage stress across the switching device, current through the switching device, load current i_1, i_2.

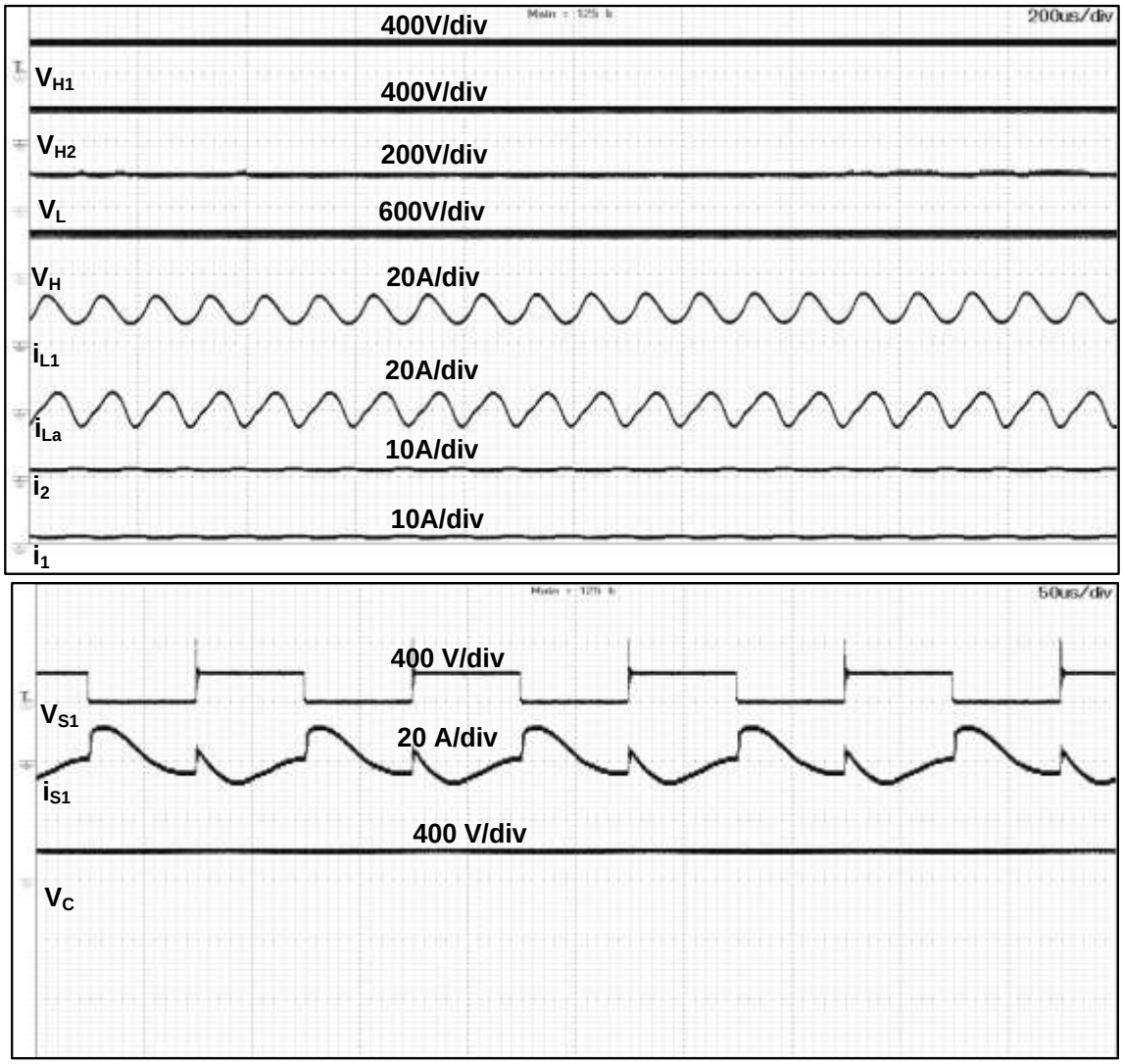

Fig 5.9.Experimental results in boost mode (a) Output voltages V_{H1}, V_{H2}, input voltage, total boost voltage V_H, inductor currents i_{L1} and i_{La}, load current i_1, i_2. (b) Voltage stress across power device, current through the switching device, voltage across capacitor V_{Ca}.

Further, the load variations considered at t=0.5sec, the output power varies from 400W to 300W. The voltage balance between positive pole V_{H1} and negative pole V_{H2} is zero, and the output voltage is constant with the reference voltage 400V. The inductor current, output voltages, the load currents are shown in Fig 5.10 and Fig.5.11. Along with load variations, the reference voltage is also controlled with the closed loop controller, at t=0.5 sec, the load variations shows the variation in power from 400W to 300W and at t=1sec, the reference voltage variation is shown from V_H=400V to V_H=300V. The inductor current, output voltages, the load currents are shown in Fig 5.12.

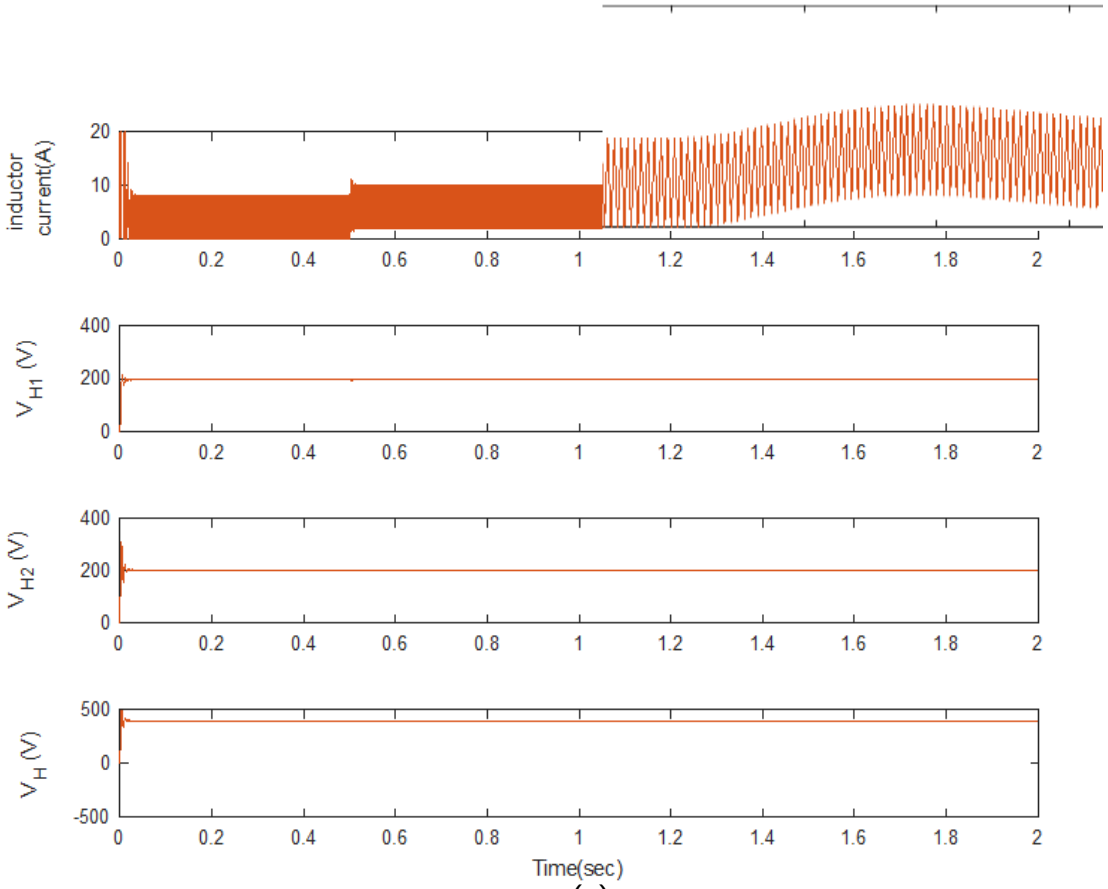

(a)

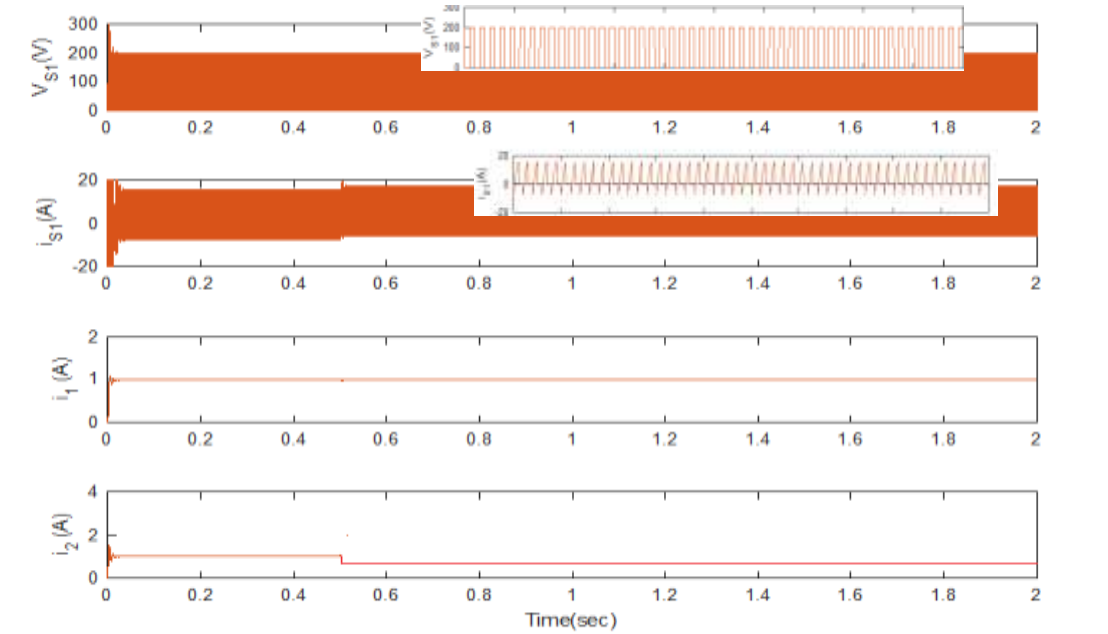

(b)

Fig 5.10. Simulation results in boost mode with load variations (a) output voltages V_{H1}, V_{H2}, Total boost voltage, V_H. (b) Voltage stress across the switching device, current through the switching device, load current i_1, i_2.

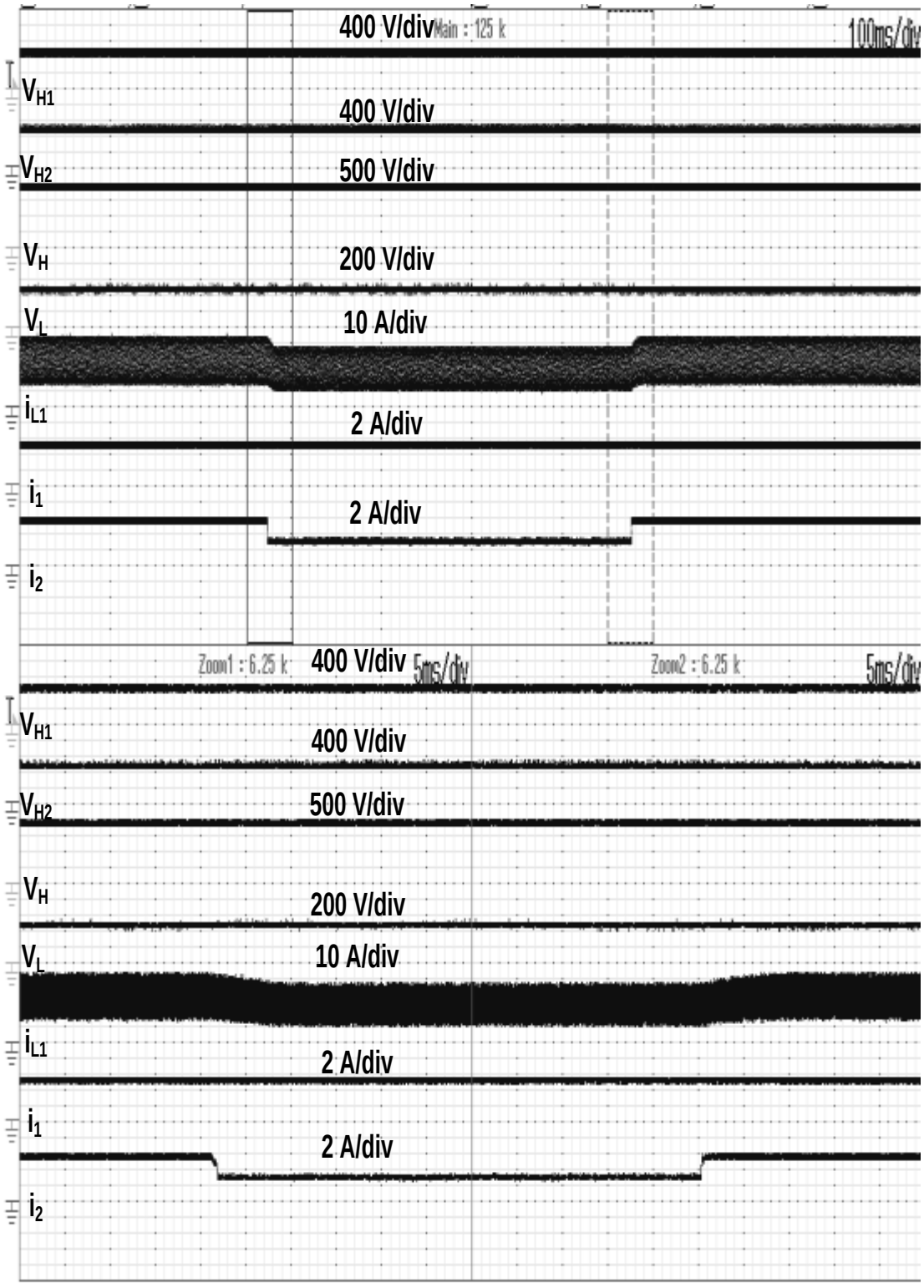

Fig.5.11. Experimental results in boost mode: output voltages V_{H1}, V_{H2}, total boost voltage, V_H, Input voltage V_L, inductor current i_{L1}, load current i_1, and i_2.

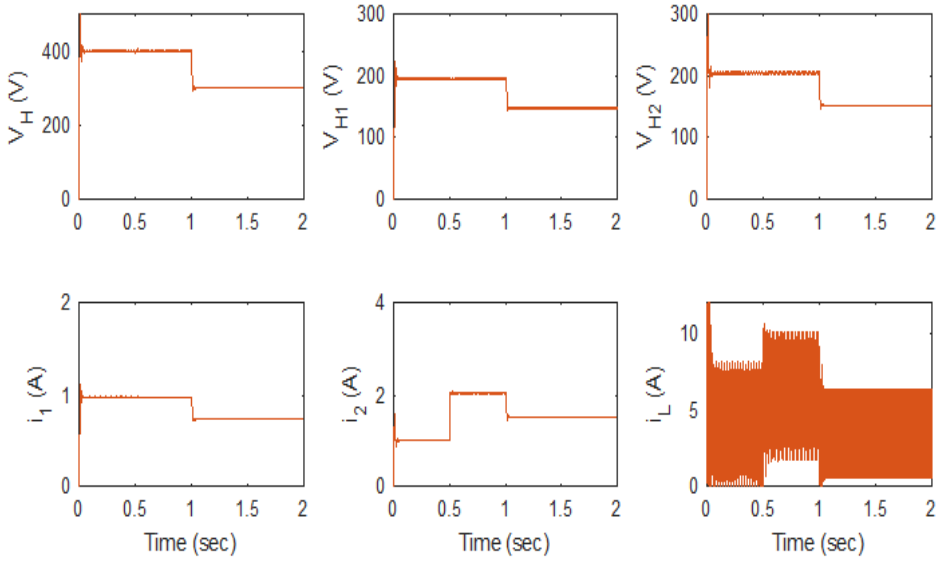

(a)

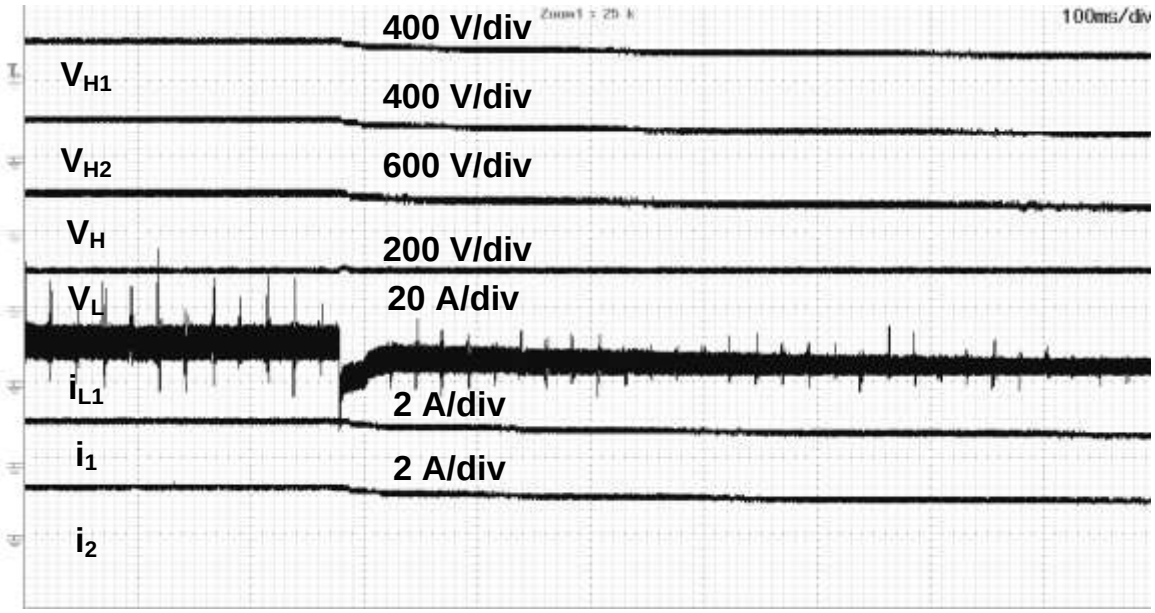

(b)

Fig 5.12(a). Simulation results in boost mode with closed-loop controller: Output voltages V_{H1}, V_{H2}, Total boost voltage, V_H, Inductor current i_{L1}, Load current i_1, and i_2.

(b). Experimental results in boost mode with closed-loop controller: Output voltages V_{H1}, V_{H2}, Total boost voltage, V_H, Input voltage V_L, Inductor current i_{L1}, Load current i_1, and i_2.

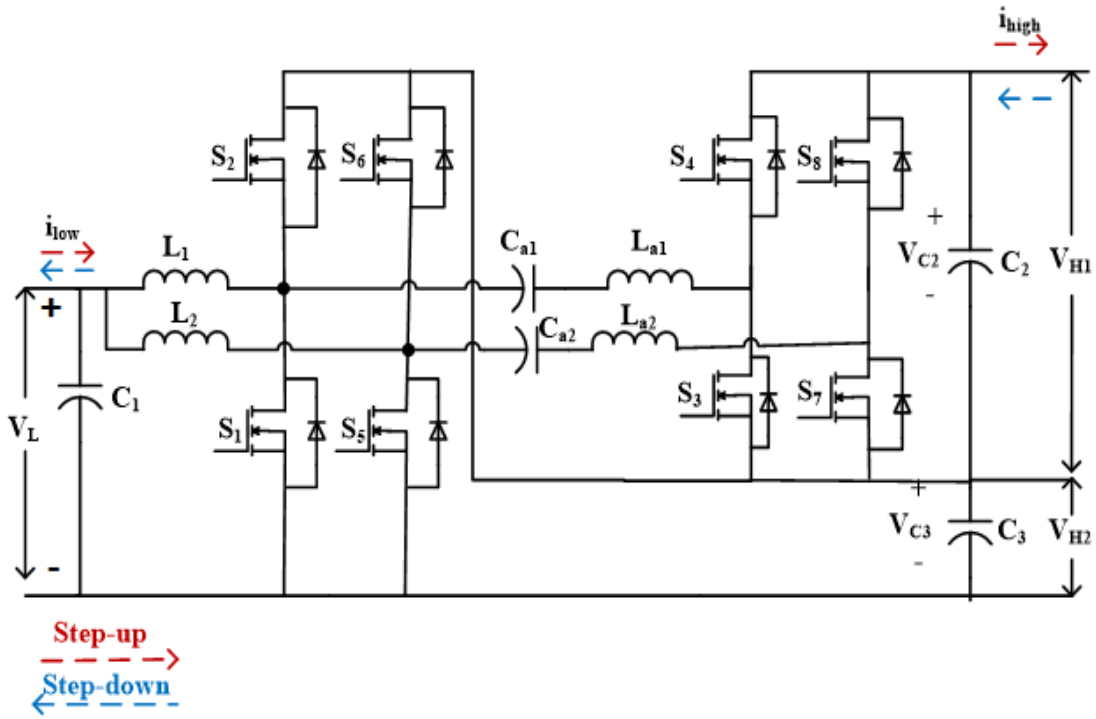

Fig 5.13. Interleaved bi-polar bi-directional DC-DC converter

Interleaved pattern for the proposed half bridge resonant based bi-polar bidirectional DC-DC converter is implemented and shown in Fig 5.13. To decrease output current ripple, a redesigned interleaved half bridge resonant circuit is used. Because the capacitors, C_2 and C_3, are employed for voltage division and subsequently discharge to and charge from the low-voltage side, a high bidirectional voltage conversion ratio may be accomplished with a suitable duty ratio. From Fig. 5.14, it can be seen that the voltage stresses across the switches is 200V. Fig. 5.14 illustrates the currents of I_{L1}, I_{L2} and (I_{L1}+I_{L2}). It can be seen from Fig. 5.14, the current ripples for I_{L1} and I_{L2} are both about 2% and the current ripple for (I_{L1}+I_{L2}) is reduced to 0.8% due to interleaved configuration structure. From Fig 5.14 it is observed that the source current is continuous and also ripple is small. The output voltage of positive pole V_{H1}, negative pole V_{H2}, and boost voltage V_H are shown in Fig 5.14. The capacitor voltage V_{C1} is 200V i.e., half of the boost voltage with a small ripple is shown in Fig 5.14.

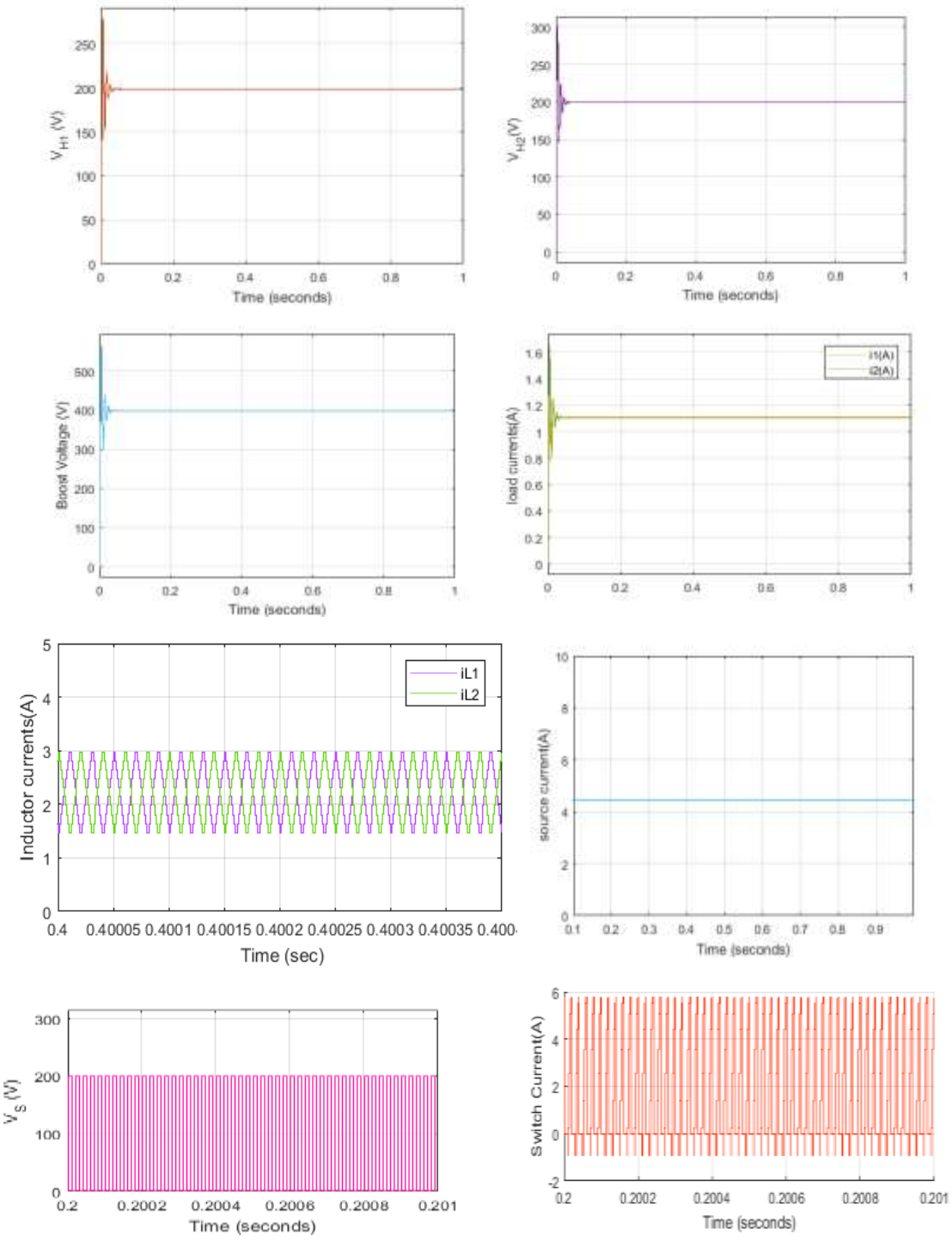

Fig 5.14. Simulation results in boost mode with interleaved pattern: Output voltages V_{H1}, V_{H2}, Total boost voltage, V_H, Load current i_1, and i_2, Source current, Inductor currents i_{L1}, i_{L2}, Voltage stress across the switching device, Current through the switching device.

When V_H is constant at 400V, and V_L changes incessantly between 50V and 100V, the efficiency curves (boost operation of the proposed converter with different power levels) are shown in Fig 5.17 (a) and it is observed that the maximum efficiency occurred at 97.8% at a load of 80 Ω.

5.3.2 Simulation and Experimental Results in Buck Mode

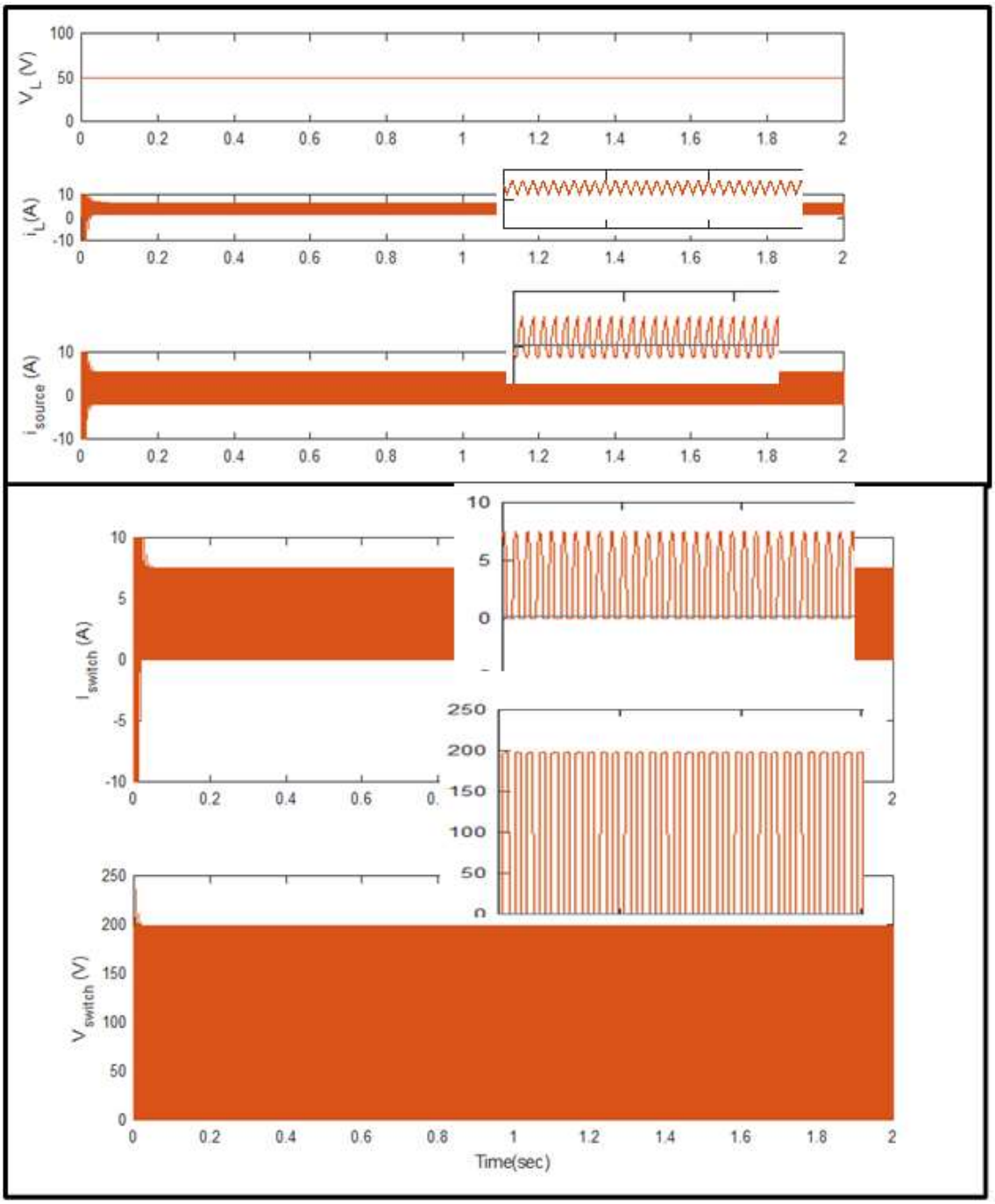

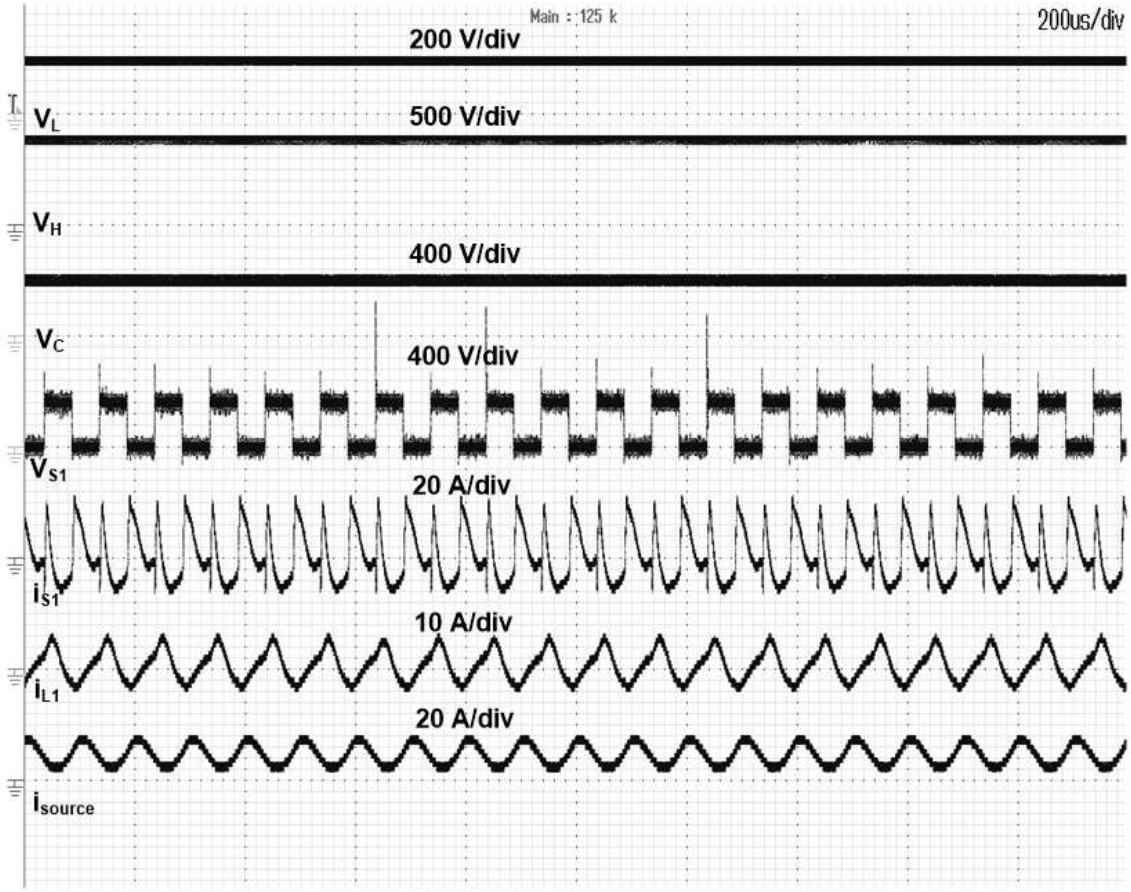

Fig 5.15. Simulation results in buck mode: inductor current, buck Voltage V_{low}, Source current, voltage stress in switch $V_{S1,}$ current through the switch $S_{1.}$

Experimental results in buck mode: Inductor current, buck Voltage V_{low}, voltage across capacitor, source current, and voltage stress in switch $V_{S1,}$ current through the switch $S_{1.}$

For the input voltage of V_H=400V, the inductor current is shown in Fig 5.15. The load current ripple from the experimental result is Δi_{low} is 14.6%. From equation (5.16), the theoretical value of ripple Δi_{low} is 16%. From the simulation and experimental results, it is verified that the proposed converter behaviour w.r.t to load current ripple is close to theoretical value. From Fig 5.15 it is clear that the ripple of the load current is very small and it is almost continuous current. The output buck voltage V_L is shown in Fig 5.15.The voltage across the capacitor V_{C1} is 200V i.e., half of the input voltage with small ripple is shown in Fig 5.15. The source current is shown in Fig 5.15. The voltage stress across the switching devices is 200V i.e., half of the boost voltage is shown in Fig 5.15and the current through the switch is shown in Fig 5.15. From the result it is proven that the switch is turned ON under ZVS condition and switched OFF under ZCS condition. When V_H is constant at

400V, and V_L changes incessantly between 50V and 100V, the efficiency in buck mode of operation of the proposed converter with different power levels are shown in Fig 5.17(b) and it is observed that the maximum efficiency occurred at 97.6% at a load of 2.5 Ω.

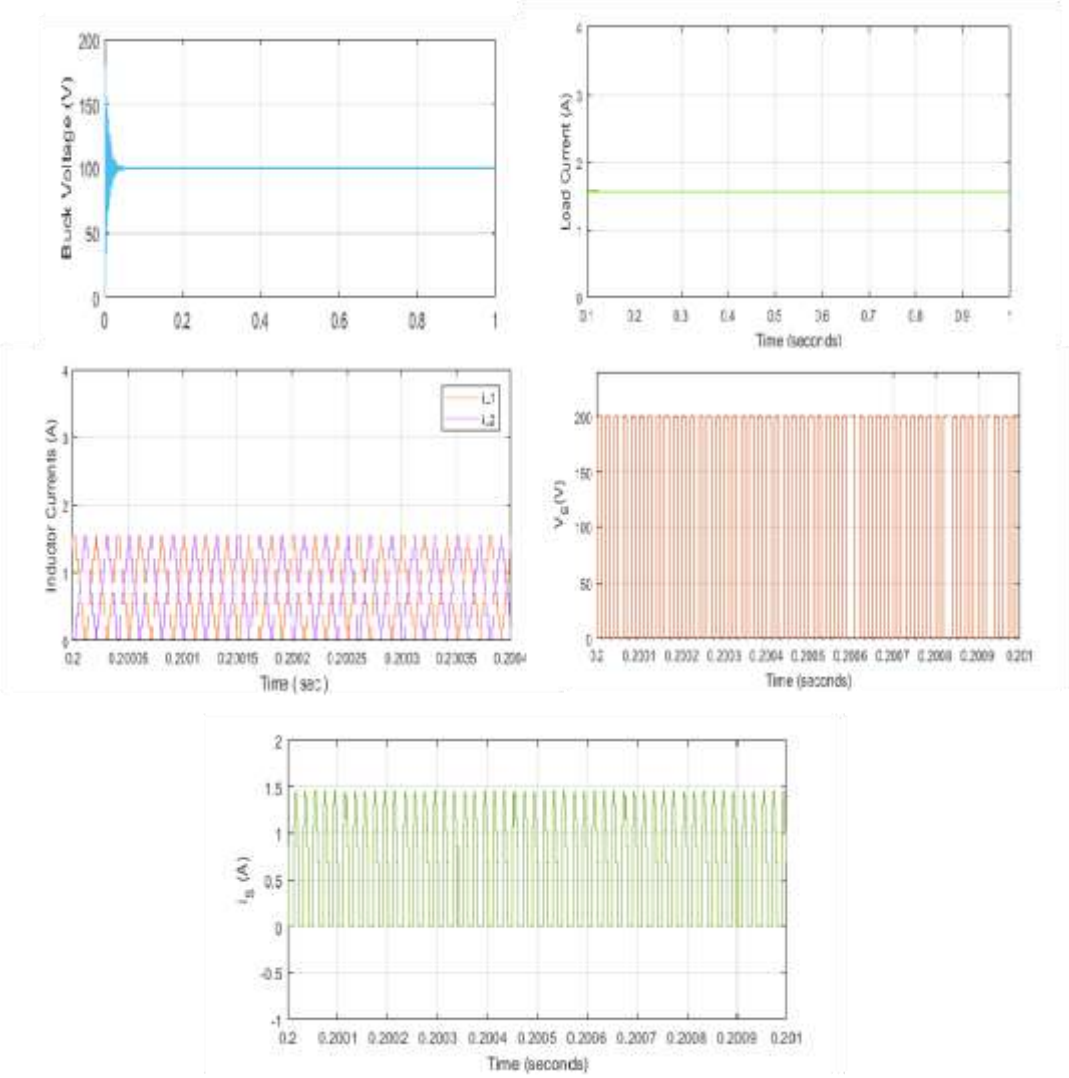

Fig 5.16. Simulation results in buck mode: Buck Voltage V_{low}, Load current, Inductor currents i_{L1}, i_{L2}, Voltage stress in switch $V_{S1,}$ Current through the switch S_1.

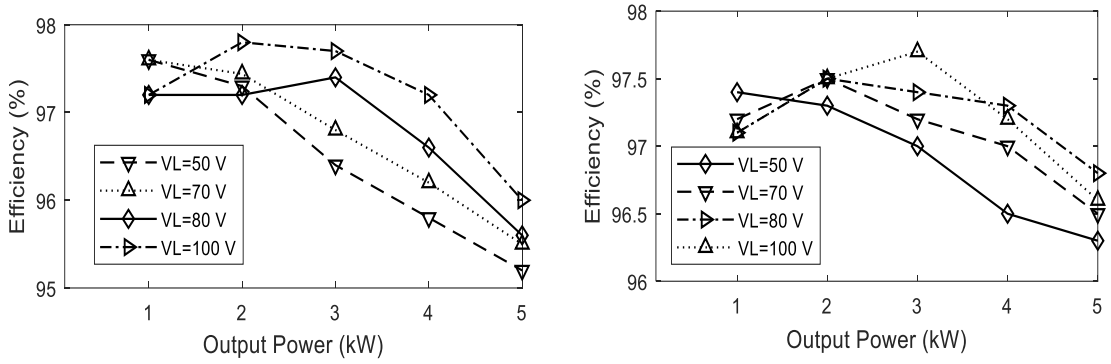

(a) In boost mode

(b) In buck mode

Fig 5.17. Efficiencies of the bipolar bidirectional DC-DC converter

5.4 Summary

In this chapter a non-isolated soft switching bi-polar bi-directional DC-DC converter for bi-polar DC micro-grids with energy storage systems is proposed to achieve high voltage gain of 4 to meet high power requirements. A 500W prototype bi-polar bi-directional DC-DC converter is fabricated and verified at a duty cycle of 0.5 with a switching frequency of 10 kHz is used to achieve a voltage gain of 4. To accomplish high voltage gain and less switch voltage stress, a zero voltage switching during turn-on and zero current switching during turn-off in both boost mode and buck mode of operation is implemented and results are presented in Table-5.2 w.r.t the number of components used, voltage gain, voltage stress and current stress. Further, the proposed control strategy offered a reference grid voltage and voltage balance across the output capacitor. The maximum efficiencies achieved in boost and buck modes are 97.8% and 97.6% respectively. The proposed converter can be used as one of the alternative choices for bipolar bi-directional DC micro-grids with energy storage systems for urban/suburban areas and may also be preferred for electric vehicle charging stations.

Table-5.2 Comparison of proposed converters with conventional bipolar bidirectional DC-DC converters

Converter	Switches	L	C	Gain (boost mode)	Gain (buck mode)	Voltage stress	Current stress	Current ripple	Efficiency In Boost Mode	Efficiency In Buck Mode	Soft Switching
Conventional Bipolar BDC	6	1	2	$\frac{1}{(1-d_1)}$	d_2	0.5*V_{high}	High	Low	91.02%	92.2%	No
Flying Capacitor Based Bipolar BDC	4	1	2	$\frac{1}{(1-d_1)}$	d_2	0.5*V_{high}	High	Low	94.9%	94.5%	No
Switched Capacitor Based Bipolar BDC	6	5	4	$\frac{2}{(1-d_1)}$	$d_2/2$	0.5*V_{high}	High	High	92.08%	92.9%	No
Neutral Point Clamped Based Bipolar BDC	12	1	3	$\frac{1}{(1-(d_3+d_4)}$	$(d_1+d_2)-1$	0.5*V_{high}	High	High	95.6%	95.4%	Zero current turn-on
Proposed Bipolar BDC for medium and high voltage DC micro-grids (N =PU module)	4*N	2*N	2*N	N+1	$\frac{1}{N+1}$	$\frac{2 * \text{Vhigh}}{(N+1)}$	High	High	96.8%	96.7%	Zero current turn-on and turn-off for all switches
Proposed Interleaved Switched-Capacitor Based Bipolar BDC	6	2	4	$\frac{2}{(1-d_1)}$	$d_2/2$	0.5*V_{high}	Low	Low	96.6%	96.6%	Zero current turn-on
Proposed Bipolar BDC with Coupled Inductors	4	1	1	$\frac{2+n}{(1-d_1)}$	$\frac{d_2}{n+2}$	$V_{S1} = \frac{V_H}{2+n}$	Low	Low	96.4%	97%	zero-voltage-switching for all switches
Proposed Bipolar BDC with High Voltage Gain	4	2	1	$\frac{2}{(1-d_1)}$	$d_2/2$	0.5*V_{high}	Low	Low	97.8%	97.6%	zero-current-switching turn off of some switches

Chapter-6

Conclusions and Future Scope

6.1. Conclusions

In this research work an attempt was made to propose various non-isolated bipolar bidirectional DC-DC converter topologies for bipolar DC micro grids with energy storage systems. The proposed converter offer high voltage gain with reduced switching losses due to resonant switching (ZVS/ZCS) also offered an inherent voltage balance across the output capacitors there by achieving good voltage regulation at the both the poles of the Bipolar DC bus. The conclusions derived out of this research work are listed below.

The following conclusions have been derived from this research work.

1. The proposed converter topology-1 achieves high voltage gain and low voltage stress across the switching devices. Zero voltage switching and zero current transition are achieved in both boost mode and buck mode. In the process of control, voltage balance across the capacitors is achieved without any additional controller and control loop. Simulations results show the merits achieved out of it and maximum efficiency in boost and buck mode of operation is 96.2% and 96.6% respectively. This converter topology and control technique is suitable for HVDC transmission and also electric vehicle charging stations.

2. In proposed converter topology-2, a 500W prototype bi-polar bi-directional DC-DC converter is fabricated and verified at a duty cycle of 0.75 is used to achieve a voltage gain of 8. To accomplish high voltage gain and less voltage stress across the switches, a zero voltage switching in both boost mode and buck mode of operation is implemented. Further, the proposed control strategy offered a reduced current ripple and voltage balance across the output capacitor. The maximum efficiencies obtained in boost and buck mode is 96.2% and 96.6% respectively. The proposed converter can be one of the alternative choices for DC micro-grids with energy storage systems and electric vehicle charging stations.

3. In proposed converter topology-3, a non-isolated soft switching bipolar bidirectional DC-DC converter for bipolar DC micro-grid is simulated to facilitate the energy storage at low voltage. This converter simulation results are presented for a grid voltage of 400 V and battery voltage of 50 V for boost mode and buck mode of operation.

The topology provides bidirectional power flow from grid to battery and inherent voltage balance across the capacitors is achieved without any control technique. The maximum efficiencies achieved in boost and buck modes are 96.4% and 97% respectively.

4. In proposed converter topology-4, a 500W prototype bi-polar bi-directional DC-DC converter is fabricated and verified at a duty cycle of 0.5 at switching frequency of 10 kHz to achieve a voltage gain of 4. To accomplish high voltage gain and less switch voltage stress, a zero voltage switching during turn-on and zero current switching during turn-off in both boost mode and buck mode of operation is implemented. Further, the proposed control strategy offered a reference grid voltage and voltage balance across the output capacitor. The maximum efficiencies achieved in boost and buck modes are 97.8% and 97.6% respectively. The proposed converter can be used as one of the alternative choices for bipolar bi-directional DC micro-grids with energy storage systems for urban/suburban areas and also for electric vehicle charging stations.

6.2. Future scope

- Experimental verification of the proposed converters in the battery energy storage system would help to further analyze and investigate the behavior of the power electronic interface and the energy storage system dynamics under transient operation in real-time.
- Further research could be done by examining the performance of the grid with an active combination of two or more energy storage devices (such as batteries and ultra-capacitors) interfaced via bidirectional DC-DC converters on the low voltage, high current side. Interaction of battery energy storage and ultra-capacitor energy storage with the grid under various power demands can be studied. Such an active combination could possibly lead to an efficient energy storage system with reduced size.
- Research on the power management strategy can be done to incorporate the transition between the energy storage systems and to the grid smoothly.

Appendix-A

Appendix A: Simulation and Experimental Parameters for all the Proposed Converter Topologies.

A1: Simulation Parameters

Start time	0.0 sec
Stop time	1.0 sec
Solver type	Fixed step
Solver	Ode 1 (Euler)
Tasking mode	Single tasking

A2: Experimental Parameters

Start time	0.0 sec
Stop time	Infinite
Solver type	Fixed step
Solver	Ode 1 (Euler)
Tasking mode	Single tasking

References

References

[1] Jacobson, M.Z., Delucchi, M.A., Bazouin, G., Bauer, Z.A., Heavey, C.C., Fisher, E., Morris, S.B., Piekutowski, D.J., Vencill, T.A., & Yeskoo, T,"100% clean and renewable wind, water, and sunlight (WWS) all-sector energy roadmaps for the 50 United States," *Energy and Environmental Science,* Vol.8,pp. 2093-2117, 2015.

[2] IRENA (2020), "Renewable capacity statistics 2020 International Renewable Energy Agency (IRENA) ," Abu Dhabi

[3] National Renewable Energy Laboratory: Solar Has The Most Potential of Any Renewable Energy Source Archived 22 January 2015.

[4] IEA (2020), "Renewables 2020," *IEA*, Paris https://www.iea.org/reports/renewables-2020

[5] Y. Zhou and X. Li, "Vehicle to grid technology: A review," *2015 34th Chinese Control Conference* (CCC), 2015, pp. 9031-9036, doi: 10.1109/ChiCC.2015.7261068.

[6] M. Hirakawa, Y. Watanabe, M. Nagano, K. Andoh, S. Nakatomi, S. Hashino, Honda R&D Co., Ltd, "High power dc/dc converter using extreme close-coupled inductors aimed for electric vehicles", *IPEC* 2010

[7] Kansuke Fuji, Peter Koellensperger, Rik W. De Doncker, "Characterization and comparison of high blocking voltage IGBTs and IEGTs under hard and soft-switching conditions", *Power Electronics Specialists Conference*, 2006. PESC '06. 37th IEEE.

[8] Akira Nabae, Isao Takahashi, Hirofumi Akagi, "A new neutral-point-clamped PWM inverter", *IEEE Transactions on Industry Applications*, 1981.

[9] J. R. Pinheiro and I. Barbi, "The three-level ZVS PWM converter-a new concept in high voltage dc-to-dc conversion," *Proceedings of the 1992 International Conference on Industrial Electronics, Control, Instrumentation, and Automation*, Vol.1, pp. 173-178, 1992.

[10] K. Jin, M. Yang and X. Ruan, "Three-level bi-directional converter — A novel dc-dc converter suitable for fuel cell power system," *2006 37th IEEE Power Electronics Specialists Conference*, pp. 1-6, 2006.

[11] M. T. Zhang, Yimin Jiang, F. C. Lee and M. M. Jovanovic, "Single-phase three-level boost power factor correction converter," *Proceedings of 1995 IEEE Applied Power Electronics Conference and Exposition - APEC'95*, Vol.1, pp. 434-439, 1995.

[12] P. J. Grbović, P. Delarue, P. Le Moigne and P. Bartholomeus, "A bidirectional three-level dc–dc converter for the ultra-capacitor applications," *IEEE Transactions on Industrial Electronics*, Vol. 57, No. 10, pp. 3415-3430, Oct. 2010.

[13] Fang Zheng Peng, "A generalized multilevel inverter topology with self-voltage balancing," *IEEE Transactions on Industry Applications*, Vol. 37, No. 2, pp. 611-618, March-April 2001.

[14] Xinbo Ruan, Bin Li and Qianhong Chen, "Three-level converters-a new approach for high voltage and high power dc-to-dc conversion," *2002 IEEE 33rd Annual IEEE Power Electronics Specialists Conference. Proceedings (Cat. No.02CH37289)*, Vol.2, pp. 663-668, 2002.

[15] Bi, H.; Wang, P.; Wang, Z., "Common grounded h-type bidirectional dc-dc converter with a wide voltage conversion ratio for a hybrid energy storage system," *Energies*, Vol. 11, 349, 2018.

[16] Zhi, N.; Zhang, H.; Xiao, X. “Switching system stability analysis of DC micro-grids with DBS control”, *Proceedings of the 2016 IEEE Applied Power Electronics Conference and Exposition (APEC)*, Long Beach, CA, USA, 20–24 March 2016; pp. 3338–3345.

[17] Guo, X.; Yang, Y.; Wang, B.; Blaabjerg, F. “Leakage current reduction of three-phase Z-source three-level four-leg inverter for transformer less PV system, ” *IEEE Transactions on Power Electronics*, Vol.34, pp. 6299–6308, 2019.

[18] Guo, X.; Zhou, J.; He, R.; Jia, X.; Rojas, C.A., “Leakage current attenuation of a three-phase cascaded inverter for transformer less grid-connected PV systems,” *IEEE Transactions on Industrial Electronics*, Vol. 65, pp. 676–686, 2018.

[19] Jiang, T.; Zhang, J.; Wu, X.; Sheng, K.; Wang, Y, “A bidirectional three-level LLC resonant converter with PWAM control, ” *IEEE Transactions on Power Electronics*, Vol.31, pp. 2213–2225,2016.

[20] Sha, D.; Lin, Q.; You, F.; Wang, X.; Xu, G.; Chen, H, “ A ZVS bidirectional three-level dc–dc converter with direct current slew rate control of leakage inductance current, ” *IEEE Transactions on Industry Applications*, Vol.52, pp.2368–2377,2016.

[21] Jin, L.; Liu, B.; Duan, S, “ ZVS operation range analysis of three-level dual active bridge dc-dc converter with phase-shift control, ” *IEEE Transactions on Industry Applications*, Vol.55, pp.362–366,2019.

[22] Filba-Martinez, A.; Busquets-Monge, S.; Nicolas-Apruzzese, J.; Bordonau, J, “Operating principle and performance optimization of a three-level NPC dual-active-bridge dc-dc converter,” *IEEE Transactions on Industrial Electronics*, Vol.63, pp. 678–690, 2016.

[23] Uno. M, “High step-down converter integrating switched capacitor converter and PWM synchronous buck converter,” *Proceedings of the Intelec 2013; 35th International Telecommunications Energy Conference, Smart Power and Efficiency*, Hamburg, Germany, 13–17 October 2013.

[24] Li, X.; Zhang, W.; Li, H.; Xie, R.; Xu, D, “ Design and control of bi-directional dc/dc converter for 30kW fuel cell power system,” *Proceedings of the 8th International Conference on Power Electronics - ECCE Asia*, Jeju, South Korea, 30 May–3 June 2011; pp. 1024–1030.

[25] Jin, K.; Yang, M.; Ruan, X.; Xu, M, “Three-level bidirectional converter for fuel-cell/battery hybrid power system,” *IEEE Transactions on Industrial Electronics*, Vol.57, pp.1976–1986, 2010.

[26] Chen, W.; Ruan, X.; Yan, H.; Tse, C.K, “DC/DC conversion systems consisting of multiple converter modules: stability, control, and experimental verifications,” *IEEE Transactions on Power Electronics*, Vol.24, pp. 1463–1474, 2009.

[27] Vazquez, A.; Rodriguez, A.; Lamar, D.G.; Hernando, M.M, “Advanced control techniques to improve the efficiency of IPOP modular QSW-ZVS converters,” *IEEE Transactions on Power Electronics*, Vol.33, pp. 73–86, 2018.

[28] Oliveira, T.R.; Silva, W.W.A.G.; Donoso-Garcia, P.F, “Distributed secondary level control for energy storage management in DC micro-grids,” *IEEE Transactions on Smart Grid*, Vol.8, pp.2597–2607, 2017.

[29] Obaid, Z.A.; Cipcigan, L.M.; Abrahim, L.; Muhssin, M.T, “Frequency control of future power systems: reviewing and evaluating challenges and new control methods,” *J. Mod. Power Systems on Clean Energy*, Vol.7, pp. 9–25, 2018.

[30] Wang, Y.; Tan, K.T.; Peng, X.Y.; So, P.L, "Coordinated control of distributed energy-storage systems for voltage regulation in distribution networks," *IEEE Transactions on. Power Delivery*, Vol.31, pp. 1132–1141, 2016.

[31] Yang, H.; Li, S.; Li, Q.; Chen, W, "Hierarchical distributed control for decentralized battery energy storage system based on consensus algorithm with pinning node*," Proceedings on. Control Modern Power Systems*, Vol.3, pp.6, 2018.

[32] J. Zhang, J.-S. Lai and W. Yu, "High-power density design of a soft switching high-power bidirectional dc–dc converter," *IEEE Transactions on Power Electronics*, Vol. 22, No. 4, pp. 1145-1153, July 2007.

[33] Williamson, S. S., Rathore, A. K., Musavi, F.: "Industrial electronics for electric transportation: current state-of-the-art and future challenges," *IEEE Transactions on Industrial Electronics*, Vol.62, No.5, pp. 3021–3032, 2015.

[34] Lai, J. S., Nelson, D. J.: "Energy management power converters in hybrid electric and fuel cell vehicles," *Proceedings in IEEE*, Vol.95, No.4, pp. 766–777, 2007.

[35] Meghdad, T., Jafar, M., Bijan, A.: "High step-up current-fed ZVS dual half bridge dc–dc converter for high-voltage applications," *IET Power Electronics*, Vol.8, No.2, pp. 309–318, 2015.

[36] Peng, F. Z., Li, H., Su, G.-J., et al.: "A new ZVS bidirectional dc–dc converter for fuel cell and battery application," *IEEE Transactions on Power Electronics*, Vol.19, No.1, pp. 54–65, 2004.

[37] Mazumder, S. K., Burra, R. K., Acharya, K.: "A ripple-mitigating and energy efficient fuel cell power-conditioning system," *IEEE Transactions on Power Electronics*, Vol.22, No.4, pp. 1437–1452,2007.

[38] Sullivan, C. R., Awerbuch, J. J., Latham, A. M.: "Decrease in photovoltaic power output from ripple: simple general calculation and the effect of partial shading," *IEEE Transactions on Power Electronics*, Vol.28, No.2, pp. 740–747, 2013.

[39] Abeywardana, D. B. W., Hredzak, B., Agelidis, V. G.: "Single-phase grid connected LiFePO4 battery–super capacitor hybrid energy storage system with interleaved boost inverter," *IEEE Transactions on Power Electronics*, Vol.30, No.10, pp. 5591–5604, 2015.

[40] Song, W., Lehman, B.: "Current-fed dual-bridge dc–dc converter," *IEEE Transactions on Power Electronics*, Vol.22, No.2, pp. 461–469, 2007.

[41] Sun, X., Wu, X., Shen, Y., et al.: "A current-fed isolated bidirectional dc–dc converter," *IEEE Transactions on Power Electronics*, Vol.32, No.9, pp. 6882–6895, 2017.

[42] Wang, Z., Li, H.: "A soft switching three-phase current-fed bidirectional dc– dc converter with high efficiency over a wide input voltage range," *IEEE Transactions on Power Electronics*, Vol.27, pp.2, pp. 669–684, 2012.

[43] Xuewei, P., Rathore, A. K.: "Comparison of bi-directional voltage-fed and current-fed dual active bridge isolated dc/dc converters low voltage high current applications, "*Proceedings on ISIE'2014*, Istanbul, pp. 2566–2571, 2014.

.[44] Chakraborty, S., Chattopadhyay, S, "Analysis and comparison of voltage source and current-source asymmetric dual-active half-bridge converters,"*2014 IEEE Energy Conversion Congress and Exposition (ECCE),* Pittsburgh, PA, pp. 2072–2079, 2014.

[45] Yu, S., Nguyen, M. Q., Choi, W,"A novel soft-switching battery charge/ discharge converter with the zero voltage discharge function," *IEEE Transactions on Power Electronics*, Vol.31, No.7, pp. 5067–5078, 2016.

[46] Sree, K. R., Rathore, A. K, "Analysis and design of impulse-commutated zero-current-switching single-inductor current-Fed three-phase push–pull ," *IEEE Transactions on Industry Applications*, Vol.53, No.2, pp. 1517–1526, 2017.

[47] Watson, R., Lee, F. C, "A soft-switched, full-bridge boost converter employing an active-clamp circuit," *PESC Record. 27th Annual IEEE Power Electronics Specialists Conf., Baveno*, vol. 2, pp. 1948–1954, 1996.

[48] Yakushev, V., Meleshin, V., Fraidlin, S, "Full-bridge isolated current fed converter with active clamp," *Fourteenth Annual Applied Power Electronics Conf. Exposition, APEC '99, Dallas*, TX, vol. 1, pp. 560–566, 1999.

[49] Ahmed, O. A., Bleijs, J. A. M, "High-efficiency dc–dc converter for fuel cell applications: performance and dynamic modeling,"*2009 IEEE Energy Conversion Congress and Exposition, San Jose*, CA, pp. 67–74, 2009.

[50] Wang, K., Lin, C. Y., Zhu, L., et al, "Bi-directional dc to dc converters for fuel cell systems," *Power Electronics in Transportation (Cat. No.98TH8349)*, Dearborn, MI, pp. 47–51, 1998.

[51] Jang, S.-J., Lee, T.-W., Lee, W.-C., et al, "Bi-directional dc–dc converter for fuel cell generation system,"*2004 IEEE 35th Annual Power Electronics Specialists Conf. (IEEE Cat. No.04CH37551)*, Aachen, Germany, Vol. 6, pp. 4722–4728, 2004.

[52] Mao, H., Abu-Qahouq, J., Luo, S., et al, "Zero-voltage-switching half-bridge dc–dc converter with modified PWM control method," *IEEE Transactions on Power Electronics*, Vol.19, No.4, pp. 947–958, 2004.

[53] Ahmed, O. A., Bleijs, J, "Optimized active-clamp circuit design for an isolated full-bridge current-fed dc–dc converter,"*2011 4th Int. Conf. on Power Electronics Systems and Applications*, Hong Kong, pp, 2011.

[54] Wu, T. F., Chen, Y. C., Yang, J. G., et al, "Isolated bidirectional full-bridge dc–dc converter with a fly back snubber," *IEEE Transactions on Power Electronics*, Vol.25, No.7, pp. 1915–1922, 2010.

[55] Zakis, J., Vinnikov, D., Kolosov, V., et al, "New active clamp circuit for current-fed galvanically isolated DC/DC converters,"*2013 Int. Conf.- Workshop Compatibility and Power Electronics*, Ljubljana, pp. 353– 358, 2013.

[56] Rathore, K., Mazumder, S. K, "Novel zero-current switching current-fed half bridge isolated dc/dc converter for fuel cell based applications,"*2010 IEEE Energy Conversion Congress and Exposition*, Atlanta, GA, pp. 3523– 3529, 2010.

[57] Rathore, K., Prasanna, P. U, "Analysis, design, and experimental results of novel snubber-less bidirectional naturally clamped ZCS/ZVS current-fed half bridge dc/dc converter for fuel cell vehicles," *IEEE Transactions on Industrial Electronics*, Vol.60, No.10, pp. 4482–4491, 2013.

[58] Xuewei, P., Rathore, A. K, "Novel bidirectional snubber-less naturally commutated soft-switching current-fed full-bridge isolated dc/dc converter for fuel cell vehicles," *IEEE Transactions on Industrial Electronics*, Vol. 61, No.5, pp. 2307– 2315, 2014.

[59] Xuewei, P., Rathore, A. K, “Novel bidirectional snubberless naturally clamped ZCS current-fed full-bridge voltage doubler: analysis, design, and experimental results,”*2013 IEEE Energy Conversion Congress and Exposition, Denver*, CO, pp. 5518–5525, 2013.

[60] Chakraborty, D., Rathore, A. K., Breaz, E., et al, “Parasitics assisted softswitching and naturally commutated current-fed bidirectional push-pull voltage doubler,”*2015 IEEE Industry Applications Society Annual Meeting, Addison*, TX, pp. 1–8, 2015.

[61] Bal, S., Rathore, A. K., Srinivasan, D, “Naturally commutated current-fed three-phase bidirectional soft-switching dc–dc converter with 120° modulation technique,”*IEEE Transactions on Industrial Applications*, Vol.52, No.5, pp. 4354–4364, 2016.

[62] T. Kang, C. Kim, Y. Suh and H. Park, "A design and control of bidirectional non-isolated dc-dc converter for rapid electric vehicle charging system," *in Proc. of 27th Annual IEEE Applied Power Electronics Conference and Exposition (APEC 2012)*, Orlando, pp.5-9, Feb. 2012.

[63] F. Caricchi, F. Crescimbini, G. Noia and D. Pirolo, "Experimental study of a bidirectional dc-dc converter for the dc link voltage control and the regenerative braking in PM motor drives devoted to electrical vehicles," *in Proc. of 9th Annual Applied Power Electronics Conference and Exposition (APEC 1994)*, Orlando,pp. 13-17, Feb. 1994.

[64] S. B. Tank, K. Manavar and N. Adroja, "Non-isolated bi-directional dc-dc converters for plug-in hybrid electric vehicle charge station application," *in Proc. of Emerging Trends in Computer & Electrical Engineering (ETCEE 2015)*, April 2015.

[65] S. Waffler and J. W. Kolar, "A novel low-loss modulation strategy for high-power bidirectional buck boost converters," *IEEE Transactions on Power Electronics*, Vol. 24, No. 6, pp. 1589-1599, June 2009.

[66] N. B. Dawood, "Review of different dc to dc converters based for renewable energy applications," *International Research Journal of Engineering and Technology*, Vol. 3, No. 3, pp. 46-50, May 2016.

[67] M. R. Mohammadi and H. Farzanehfard, "A new bidirectional ZVSPWM Cuk converter with active clamp," *in Proc. of 19th Iranian Conference on Electrical Engineering*, Tehran, pp.17-19, May 2011.

[68] Y.-S. Lee and M.-W. Cheng, "Intelligent control battery equalization for series connected lithium-ion battery strings," *IEEE Transactions on Industrial Electronics*, Vol. 52, No. 5, pp. 1297-1307, Oct. 2005.

[69] E. Adib and H. Farzanehfard, "Soft switching bidirectional dc–dc converter for ultracapacitor–batteries interface," *Energy Conversion and Management*, Vol. 50, No. 12, pp. 2879-2884, Dec. 2009.

[70] D. C. Denny and M. Shahin, "Analysis of bidirectional SEPIC/Zeta converter with coupled inductor," *in Proc. of International Conference on Advancements in Power and Energy (TAP Energy 2015)*, Kollam, pp.24- 26, June 2015.

[71] M.-S. Song, Y.-D. Son and K.-H. Lee, "Non-isolated bidirectional softswitching sepic/zeta converter with reduced ripple currents," *Journal of Power Electronics*, Vol. 14, No. 4, pp. 649-660, July 2014.

[72] S. R. Gurrala and K. V. Lakshmi, "A novel bidirectional dc-dc converter with battery protection," *International Journal of Modern Engineering Research*, Vol. 2, No. 6, pp. 4261-4265, Dec. 2012.

[73] L.-S. Yang and T.-J. Liang, "Analysis and implementation of a novel bidirectional dc–dc converter," *IEEE Transactions on Industrial Electronics*, Vol. 59, No. 1, pp. 422-434, Apr. 2011.

[74] M. N. Gitau, F. M. Mwaniki and I. W. Hofsajer, "Analysis and design of a single-phase tapped-coupled-inductor boost dc-dc converter," *Journal of Power Electronics*, Vol. 13, No. 4, pp. 636-646, July 2013.

[75] H. S. Chung, A. Ioinovici and W.-L. Cheung, "Generalized structure of bi-directional switched-capacitor DC/DC converters," *IEEE Transactions on Circuits and Systems*, Vol. 50, No. 6, pp. 743-753, June 2003.

[76] I.-H. Lee, J.-G. Kim and Y.-C. Jung, "A new bidirectional dc-dc converter with ZVT switching," *in Proc. of IEEE Vehicle Power and Propulsion Conference*, Seoul, 9-12 Oct. 2012.

[77] J.-W. Yang and H.-L. Do, "Soft-switching bidirectional dc-dc converter using a lossless active snubber," *IEEE Transactions on Circuits and Systems*, Vol. 61, No. 5, pp. 1588-1596, Jan. 2014.

[78] Saman Dadjo Tavakoli, Mohammad Mahdavy fakhra, Mohsen Hamzeha, Keyhan Sheshyekanib, and Ebrahim Afjei, "A unified control strategy for power sharing and voltage balancing in bipolar DC micro-grids", *Sustainable Energy, Grids and Networks*,Vol.11, ISSN 2352-4677,pp.58-68,2017.

[79] Y. Gu, Y. Chi, Y. Li, W. Sun, W. Li and X. He, "DC symmetrical component method for analysis and control of bipolar LVDC grid," *2015 IEEE Applied Power Electronics Conference and Exposition (APEC)*, 2015, pp. 2802-2807, doi: 10.1109/APEC.2015. 7104747.

[80] S. Rivera, R. Lizana F., S. Kouro, T. Dragičević and B. Wu, "Bipolar DC power conversion: state-of-the-art and emerging technologies," in *IEEE Journal of Emerging and Selected Topics in Power Electronics*, Vol. 9, No. 2, pp. 1192-1204, April 2021.

[81] Banne. Swapna, "Space vector controlled bipolar LVDC micro grid analysis with DC symmetrical component technique," *IJRECE*, Vol. 6, No. 4, 2018.

[82] Victor Khasiev, "Bipolar, bidirectional DC-to-DC supply sources and sinks current from 5 V to 24 V input", *Electronics*, 2020.

[83] Saman Dadjo Tavakoli, "Interlinking converters in application of bipolar DC microgrids", *8th Power Electronics, Drive Systems & Technologies Conference (PEDSTC 2017) 14-16 Feb. 2017*, Ferdowsi University of Mashhad, Mashhad, Iran.

[84] Jackson Lago, JoabelMoia, and Marcelo L. Heldwein "Evaluation of power converters to implement bipolar dc active distribution networks dc-dc converters," *in Energy Conversion Congress and Exposition (ECCE)*, pp. 985–990, 2011.

[85] Pérez Litrán, S. P., Durán Aranda, E., Semião, J. & Barroso Rodríguez, R. S. "Single-switch bipolar output dc-dc converter for photovoltaic application". *Electronics*, Vol.9, No.7, 1171, 2020.

[86] P. Prabhakaran and V. Agarwal, "Novel four-port dc–dc converter for interfacing solar PV–fuel cell hybrid sources with low-voltage bipolar dc micro-grids," in *IEEE Journal of Emerging and Selected Topics in Power Electronics*, Vol. 8, No. 2, pp. 1330-1340, June 2020.

[87] Taha Ahmadi, Esmaeel Rokrok , and Mohsen Hamzeh, “Mitigation of voltage unbalances in bipolar dc micro-grids using three-port multidirectional dc-dc converters,” *Journal of Power Electronics*, Vol. 18, No. 4, pp. 1223-1234, July 2018.

[88] Hiroaki Kakigano, Yushi Miura, and ToshifumiIse, “Low-voltage bipolar-type dc micro-grid for super high quality distribution,” *IEEE Transactions on Power Electronics*, Vol. 25, No. 12, pp. 3066-3075, Dec 2010.

[89] JoabelMoia, Jackson Lago, Arnaldo J. Perin, and Marcelo L. Heldwein, “Comparison of three-phase PWM rectifiers to interface AC grids and bipolar DC active distribution networks,”*3rd IEEE International Symposium on Power Electronics for Distributed Generation Systems (PEDG) 2012*.

[90] Mohsen Kamalirad, Hossein Iman-Eini, Member, IEEE, and BabakFarhangi, “A bidirectional buck-boost bipolar dc/dc converter with inductive DC link”, *9th Annual Power Electronics, Drives Systems and Technologies Conference (PEDSTC), 2018*.

[91] Y. Li, A. Junyent-Ferré and J. Rodriguez-Bernuz, "A three-phase active rectifier topology for bipolar DC distribution," in *IEEE Transactions on Power Electronics*, Vol. 33, No. 2, pp. 1063-1074, Feb. 2018.

[92] Binbin Li, Shukai Mao, and Xiaodong Zhao, “DC/DC converter for bipolar LVDC system with integrated voltage balance capability,” *IEEE Transactions on Power Electronics*, Vol. 36, No. 5, pp. 5415-5424, May 2021.

[93] Tack-Hyun Jung,Gi-HyeonGwon, Chul-Hwan Kim,Joon Han, and Yun-Sik “Voltage regulation method for voltage drop compensation and unbalance reduction in bipolar low-voltage dc distribution system,” *IEEE Transactions on Power Delivery*, Vol. 33,No. 1, pp. 141-149, Feb. 2018.

[94] Zhe Zhang, Donghan Shi, Chi Jin, and Leong Hai Koh, “Droop control of a bipolar DC micro-grid for load sharing and voltage balancing,”*2017 IEEE 3rd International Future Energy Electronics Conference and ECCE Asia (IFEEC 2017 - ECCE Asia)*, 2017, pp. 795-799, doi: 10.1109/IFEEC.2017.7992141.

[95] M. B. Ferrera, S. P. Litrán, E. Durán and J. M. Andújar, "A SEPIC-Cuk converter combination for bipolar DC micro-grid applications," *2015 IEEE International Conference on Industrial Technology (ICIT), 2015*, pp. 884-889, doi: 10.1109/ICIT. 2015.7125209.

[96] J. Ma, M. Zhu, Q. Li and X. Cai, "From “voltage balancer” to “interlinking converter” —A shift of operation concept for distributed bipolar DC system," *IECON 2017 - 43rd Annual Conference of the IEEE Industrial Electronics Society*, 2017, pp. 1166-1171, doi: 10.1109/IECON.2017.8216199.

[97] Sanchit Mishra,Visweshwar Chandrasekaran, Sreekanth T., and Ned Mohan, “Design of bipolar interface converter for purely DC micro-grid with minimally processed maximum power point operation of photovoltaics,”*2019 IEEE Energy Conversion Congress and Exposition (ECCE)*, 2019, pp. 2650-2657, doi: 10.1109/ECCE.2019. 8912231.

[98] Zhi, N.; Zhang, H.; Xiao, X, “Switching system stability analysis of DC micro-grids with DBS control,” *Proceedings of the 2016 IEEE Applied Power Electronics Conference and Exposition (APEC)*, Long Beach, CA, USA, 20–24 March 2016; pp. 3338–3345.

[99] Guo, X.; Yang, Y.; Wang, B.; Blaabjerg, F, " Leakage current reduction of three-phase Z-source three-level four-leg inverter for transformer-less PV system," *IEEE Transaction on. Power Electronics*, Vol.34, pp.6299–6308, 2019.

[100] Guo, X.; Zhou, J.; He, R.; Jia, X.; Rojas, C.A, "Leakage current attenuation of a three-phase cascaded inverter for transformer-less grid-connected PV systems," *IEEE Transactions on Industrial Electronics*, Vol.65,pp. 676–686, 2018.

[101] Jiang, T.; Zhang, J.; Wu, X.; Sheng, K.; Wang, Y, "A bidirectional three-level LLC resonant converter with PWAM control," *IEEE Transaction on Power Electronics*, Vol.31,pp. 2213–2225, 2016.

[102] Sha, D.; Lin, Q.; You, F.; Wang, X.; Xu, G.; Chen, H, "A ZVS bidirectional three-level dc–dc converter with direct current slew rate control of leakage inductance current," *IEEE Transaction on. Industrial Applications*, Vol.52, pp. 2368–2377, 2016.

[103] Jin, L.; Liu, B.; Duan, S, "ZVS operation range analysis of three-level dual active bridge dc-dc converter with phase-shift control," *IEEE Transaction on. Industrial Applications*, Vol.55, pp. 362–366, 2019.

[104] Filba-Martinez, A.; Busquets-Monge, S.; Nicolas-Apruzzese, J.; Bordonau, J, "Operating principle and performance optimization of a three-level NPC dual-active-bridge dc-dc converter," *IEEE Transaction on Power Electronics*, Vol.63, pp.678–690, 2016.

[105] Uno M, "High step-down converter integrating switched capacitor converter and PWM synchronous buck converter," *In Proceedings of the 35th International Telecommunications Energy Conference, SMART POWER AND EFFICIENCY*, Hamburg, Germany, 13–17 October 2013.

[106] Li, X.; Zhang, W.; Li, H.; Xie, R.; Xu, D, "Design and control of bi-directional dc/dc converter for 30kW fuel cell power system," *In Proceedings of the 8th International Conference on Power Electronics - ECCE Asia*, Jeju, South Korea, 30 May–3 June 2011; pp. 1024–1030.

[107] Jin, K.; Yang, M.; Ruan, X.; Xu, M, "Three-level bidirectional converter for fuel-cell/battery hybrid power system," *IEEE Transaction on Industrial Electronics*, Vol. 57, pp. 1976–1986. 2010.

Publications

Publications

A. Journals

Published

- Patil Mounica & S Srinivasa Rao (2021), "Bipolar Bidirectional DC-DC Converter for Bi-polar DC Micro-grids with Energy Storage Systems", ***International Journal of Electronics***, DOI: 10.1080/00207217.2021.1914184.

- Patil Mounica and S Srinivasa Rao, "Bipolar Bidirectional DC-DC Converter for Bi-polar DC Micro-grids with Energy Storage", ***Journal of Green Engineering***, Vol.11, no. 2, pp. 1060-1074, 2021.

Minor Revision Submitted

- Patil Mounica and S Srinivasa Rao, "Non-Isolated Bipolar Bidirectional Converter for DC Micro-grids ", to ***International Journal of Electronics.***

B. Conferences

Published

- Patil Mounica and S Srinivasa Rao, " Bipolar Bidirectional DC-DC Converter for Medium and High Voltage DC Micro grids", ***6th International Conference for Convergence in Technology (I2CT) Pune, India. April 02-04, 2021***